EXPERIMENTAL STUDY OF THE BRITTLE TO PLASTIC TRANSITION IN MARBLE AND DIABASE

BY

JOANNE THERESA FREDRICH

B.S. Geology
State University of New York at Stony Brook
(1985)

Submitted to the Department of Earth, Atmospheric,
and Planetary Sciences in Partial Fulfillment
of the Requirements for the Degree of

DOCTOR OF PHILOSOPHY

at the

MASSACHUSETTS INSTITUTE OF TECHNOLOGY

September 1990

Signature of Author_____
Department of Earth, Atmospheric, and Planetary Sciences
September 1990

Certified by_____
Brian Evans
Department of Earth, Atmospheric, and Planetary Sciences
Thesis Supervisor

Accepted by_____
Thomas H. Jordan
Department Chairman

Experimental Study of the Brittle to Plastic Transition in Marble and Diabase

by

Joanne Theresa Fredrich

Submitted to the Department of Earth, Atmospheric, and Planetary Sciences on August 31, 1990, in partial fulfillment of the requirements for the degree of Doctor of Philosophy in Geophysics

Abstract

The transition in failure mode from brittle fracture to plastic flow is important in understanding earthquake source mechanics, the rheology of the lithosphere, and the style of deformation at the field scale. We review previous experimental and theoretical studies relevant to the brittle to plastic transition in compression. Insight into the physics and mechanics of the brittle-plastic transition has been gained primarily through the acquisition of high quality mechanical data, the systematic observation of deformation microstructures, and the theoretical modeling of the failure of rocks in compression. Mechanical behavior over the brittle-plastic transition has been characterized for some rocks by measuring the pressure and temperature sensitivity of strength; particular advances have resulted from the measurement of volumetric strain. However, there have been few comprehensive studies of semibrittle flow in silicate rocks at high pressures and temperatures, or of the effect of variations of pore fluids, strain rate, and grain size on strength and rheology. The strengths at the transition from brittle fracture to semibrittle flow and from semibrittle flow to fully plastic flow are apparently linear functions of pressure, but the physical bases for the relations are not well established. Qualitative microstructural observations have provided information on the conditions under which various deformation mechanisms operate, estimates of strain partitioning, and identification of crack nucleation mechanisms. Microstructural data place important constraints on the micromechanics of deformation in the semibrittle field, but important gaps in our understanding remain. Theoretical treatments of rock failure based on bifurcation analyses and fracture mechanics model successfully only some of the experimental observations.

To study the micromechanics of the brittle to plastic transition, samples of Carrara marble were deformed at room temperature to varying strains at confining pressures spanning the range in mechanical behavior from brittle to plastic. Volumetric strain was measured during the experiments, and the stress-induced microstructure was characterized quantitatively using optical and transmission electron microscopy. The range of confining pressure over which transitional (or semibrittle) deformation occurs is 30-300 MPa. The macroscopic initial yield stress is constant for confining pressures greater than 85 MPa, whereas the differential stress at the onset of dilatancy increases with pressure up to 300 MPa. The dilatancy coefficient decreases rapidly with increasing pressure up to 100 MPa, and then asymptotically approaches zero for pressures up to 300 MPa. The work hardening coefficient increases with pressure up to 450 MPa; the pressure sensitivity is greatest for pressures up to 100 MPa. Active deformation mechanisms include microcracking, twinning, and dislocation glide.

Transmission electron microscopy observations indicate that dislocation glide occurs, at least on a local scale, in samples deformed in the semibrittle field at pressures as low as 50 MPa and applied differential stresses well below the critical resolved shear stress for glide on the easiest slip system. In the semibrittle field, the brittle and plastic deformation mechanisms sometimes interact: cracks and voids frequently nucleate at sites of stress concentration at twin boundaries, at twin terminations, and at the intersection of twin lamallae, and geometries suggestive of crack tip shielding by dislocations are also observed. Stereological measurements indicate that at constant strain in the semibrittle field, the stress-induced crack density and anisotropy decrease with increasing pressure. The mean dislocation density at constant differential stress increases significantly for samples deformed at pressures of 230 MPa and greater. We find that the transition from localized brittle fracture to nonlocalized semibrittle flow is not marked by drastic changes in either the density and anisotropy of stress-induced cracking or in the mean dislocation density; however, estimates of the ratio of brittle energy dissipation to total energy dissipation are significantly lower in the semibrittle field. Theoretical predictions of the critical hardening modulus required for localization based on Rudnicki and Rice's (1975) model suggest that localization is inhibited in the semibrittle field as long as the rocks work harden with strain; we consider that the transition from work softening to work hardening is due to dislocation "blunting" of microcracks, which limits the characteristic dimension of stress-induced cracks in the semibrittle field.

Grain size is one of the most important microstructural parameters affecting the mechanical properties of rocks. To determine the effect of grain size on strength and the brittle-plastic transition, and to test existing micromechanical models, triaxial experiments were performed at room temperature and confining pressures up to 450 MPa on four pure, dense calcite rocks whose average grain sizes range over four orders of magnitude. Volumetric strain was measured during some of the experiments and microstructural studies were conducted to identify the active deformation mechanisms. The brittle fracture strength and macroscopic initial "plastic" yield stress in the semibrittle field follow empirical Hall-Petch relations. The confining pressure at the brittle-ductile transition depends inversely on grain size, but the stress ratio σ_3/σ_1 at the transition is nearly the same for the different rocks. We assume that the initial flaw size scales with grain size and compare our experimental data to the fracture mechanics models of Ashby and Hallam (1986) for brittle fracture and Horii and Nemat-Nasser (1986) for the brittle-plastic transition in compression. The first model predicts that small confining pressures are sufficient to inhibit work softening behavior; however, our data indicate that localization occurs for significantly higher values of confining pressure than predicted. Furthermore, we find that localization is inhibited with increased confining pressure because of the increased activity of plastic flow mechanisms, rather than because of the increased difficulty of crack propagation alone. With certain assumptions, the model predicts the experimentally determined slope of the Hall-Petch relation in the brittle field, although it underestimates the compressive strength of the rocks. Nevertheless, we consider that, in addition to controlling the initial flaw size, grain size may have a more fundamental effect on brittle fracture. We suppose that the spatial heterogeneity of the local stress field scales inversely with grain size, and that this may be a more likely cause for the observed grain size effect. The second model predicts that the stress ratio σ_3/σ_1 at the brittle-plastic transition scales with the square root of the grain size; however, the experimental data do not corroborate the model unless the square of the ratio of the mode I fracture toughness to the plastic yield stress in shear scales with the grain size. This suggests that the structural complexity of polycrystalline aggregates influences significantly the nature of plastic flow and microcrack propagation; such considerations are probably necessary in order to model the

brittle-plastic transition more accurately. The stress ratio at the brittle-ductile transition is apparently a constant for many different rock types; we suggest that the physical basis for this relationship is that the ductility of most mineral aggregates falls within a small range.

The lack of a constitutive relation for the semibrittle flow of silicate rocks is one of the most significant factors contributing to uncertainties in the rheology and strength of the lithosphere. To investigate the mechanisms of fracture and semibrittle flow at high temperatures, samples of Maryland diabase were deformed in a triaxial apparatus at temperatures of 800 to 900°C and confining pressures of 100 to 400 MPa and examined using scanning and transmission electron microscopy. Small (< 1-2%) amounts of glass (melt) were identified in nearly all of the deformed samples. In contrast to Caristan's earlier results at 1000°C, our mechanical data exhibit a positive pressure dependency of strength. The basis for the "negative pressure effect" reported by Caristan may simply be the larger melt fractions present in his experiments. To test the effect of water content, some samples were subjected to a high-temperature heat treatment prior to deformation; their weight decreased by 0.02-0.03 wt% due to the decomposition of minor hydrous phases. These samples were found to contain no partial melt and are more brittle and markedly stronger than their untreated counterparts which contain melt. Additionally, the initial moduli of the stress-strain curves of the former samples are markedly greater than those of the latter, suggesting that even small melt fractions affect the deformation significantly. Thus, the data are consistent with either a partial melt effect or a hydrolytic weakening phenomenon, or possibly a combination of both. Under certain conditions, the properties of high temperature faults may differ markedly from their low temperature counterparts. One experiment suggests a low coefficient of friction at high temperatures ($\mu \approx 0.3$), whereas microscopy of another deformed sample suggests that frictional sliding may locally elevate temperatures to supra-solidus conditions and cause enhanced plasticity in the vicinity of faults. Stable work softening followed by a period of strength recovery was observed in two experiments and illustrates dramatically a cyclic link between the physical and mechanical properties of fault zones. One experiment exhibited two intervals of softening and recovery; correspondingly, two macroscopic faults were found to traverse the length of the sample. The stress-strain data for these two experiments suggest that mechanical effects associated with elevated pore pressures induced shear localization. Furthermore, both the level of strength recovery and electron microscopy suggest that physical "healing" of the fault occurred.

Thesis Supervisor: Dr. Brian Evans
Title: Professor of Geophysics

Biographical Note

1981 - 1985: Attended the State University of New York at Stony Brook, B.S. in Geology. Cum laude and Departmental Honors. Sigma Xi Excellence in Research Award, Stony Brook Foundation Award, Myron Fuller Award.

Summer 1985: Attended the University of Michigan at Ann Arbor (no degree).

PUBLICATIONS

Fredrich, J. T. and T.-f. Wong, Micromechanics of thermally induced cracking in three crustal rocks, *J. Geophys. Res.*, **91**, 12,743-12,764, 1986.

Fredrich, J., R. McCaffrey, and D. Denham, Source parameters of seven large Australian earthquakes determined by body waveform inversion, *Geophys. J.*, **95**, 1-13, 1988.

Fredrich, J. T., B. Evans, and T.-f. Wong, Micromechanics of the brittle to plastic transition in Carrara marble, *J. Geophys. Res.*, **94**, 4129-4145, 1989.

Wong, T.-f., J. T. Fredrich, and G. D. Gwanmesia, Crack aperture statistics and pore space fractal geometry of Westerly granite and Rutland quartzite: Implications for an elastic contact model of rock compressibility, *J. Geophys. Res.*, **94**, 10,267-10,278, 1989.

Evans, B., J. T. Fredrich, and T.-f. Wong, The brittle - ductile transition in rocks: Recent experimental and theoretical progress, in *The Brittle-Ductile Transition in Rocks (The Heard Volume)*, A. G. Duba, W. B. Durham, J. W. Handin, and H. F. Wang (Eds.), *Geophys. Monogr. Vol. 56*, pp. 1-20, AGU, Washington D.C., 1990.

Fredrich, J. T., B. Evans, and T.-f. Wong, Effect of grain size on brittle and semibrittle strength: Implications for micromechanical modelling of failure in compression, *J. Geophys. Res.*, **95**, 10,907-10,920, 1990.

Table of Contents

Chapter 1
Introduction

Although rock failure in compression has been studied extensively from both experimental and theoretical viewpoints, important gaps in understanding remain. In particular, it is recognized that with increasing depth, and concurrent increases in pressure and temperature, rocks undergo a transition in mechanical behavior from brittle to plastic. The vast majority of experimental rock deformation studies have generally focussed on either one or the other of these two end member rheologies. In recent years, however, it has become increasingly clear that a fundamental understanding of the brittle to plastic transition and semibrittle flow is important to a variety of problems in geophysics. This thesis represents an attempt to provide basic constraints on the physics and mechanics of the brittle to plastic transition and semibrittle flow in rocks.

For the convenience of the reader unfamiliar with the general subject matter, an extensive review of the relevant experimental and theoretical work is presented in Chapter 2. The geological and geophysical implications are briefly discussed, and areas where further work is likely to yield additional insight are suggested.

Results from an experimental study of the brittle to plastic transition in calcite aggregates are presented in Chapters 3 and 4. Calcite aggregates are a useful analog for the study of the deformation of silicate rocks at high temperatures. In calcite rocks, a transition in mechanical behavior from brittle fracture to plastic flow may be induced by deformation at sufficiently high confining pressures. In contrast, at confining pressures accessible in the laboratory, elevated temperatures are required to activate crystal-plastic processes in low porosity silicate rocks. In room temperature tests, recovery of the dislocation structure during unloading is negligible; moreover, no thermal cracks resulting from quenching are introduced. Thus, observed microstructures can be correlated to mechanical data with little or no ambiguity.

In all, 77 experiments on marble and limestone were performed at room temperature and confining pressures up to 500 MPa. The results of a systematic study of the brittle-plastic transition in Carrara marble are presented in Chapter 3. Mechanical measurements of axial stress and axial and volumetric strain are integrated with quantitative characterization of the microcrack and dislocation structures in samples deformed to varying strains at confining pressures spanning the range in mechanical behavior from brittle to plastic. The experimental results are interpreted in the context of bifurcation theory which models localization as an instability in the macroscopic constitutive description of the inelastic response.

In Chapter 4, the effect of grain size on compressive strength and the brittle to plastic transition is studied. Experiments were performed on four rocks whose average grain sizes span four orders of magnitude. The experimental data are compared to the theoretical predictions of linear elastic fracture mechanics models for the failure of rocks in compression. The models are evaluated critically and the geological implications are discussed briefly.

In Chapter 5, results from a study of the high temperature fracture and flow of Maryland diabase are presented. Nineteen triaxial experiments were performed at confining pressures up to 400 MPa and temperatures of 800-900°C. Certain aspects of faulting at high temperatures are studied and the effects of water and small amounts of partial melt on the deformation are evaluated.

The main chapters of the thesis are intended to be read separately.

Chapter 2
The Brittle-Ductile Transition in Rocks: A Review of Previous Work

INTRODUCTION

With increasing depth, and concurrent increases in pressure and temperature, rocks undergo a transition in failure mode from localized brittle fracture to nonlocalized plastic flow. This transition has important implications for various geophysical and geological problems. For example, the brittle-ductile transition may limit the maximum depth of seismicity [*Sibson*, 1977; 1982], and it is probable that the peak stresses in the lithosphere are supported by semibrittle deformation [*Goetze and Evans*, 1979; *Brace and Kohlstedt*, 1980; *Kirby*, 1980]. Rheological models of the lithosphere are important for a variety of geophysical problems, and the extrapolation of either brittle fracture or plastic flow laws into the semibrittle regime results in significant overestimates of strength [*Carter and Kirby*; 1978; *Kirby*, 1980; *Carter and Tsenn*, 1987]. The transition from brittle fracture to semibrittle flow may also have important implications for earthquake source mechanics and processes [e.g., *Tse and Rice*, 1986; *Hobbs et al.*, 1986; *Li and Rice*, 1987; *Scholz*, 1988].

Heard's [1960] study of the transition in Solnhofen limestone was seminal in demonstrating the effect of confining pressure, temperature, stress state, and pore fluid pressure on the rheology of rocks [see also *Paterson*, 1978]. Recent progress in understanding of the brittle-ductile transition in low-porosity intact rocks has occurred on three fronts: increased accuracy and quality of mechanical data [e.g., *Edmond and Paterson*, 1972]; systematic microstructural observations of experimentally deformed samples [e.g., *Tullis and Yund*, 1977]; and theoretical modeling of localization and failure [e.g., *Rudnicki and Rice*, 1975; *Nemat-Nasser and Horii*, 1982]. We review these topics below for the case of low-porosity intact samples. We do not discuss the phenomenology of the brittle-ductile transition as observed in porous rocks, as this subject is worthy of independent review (for example, see

the recent work by *Wong* [1989*a*]). Some aspects of the brittle-ductile transition in experiments utilizing "sawcut" samples are likely to be analogous to those occurring in low-porosity intact rocks [e.g., *Shimamoto and Logan*, 1986; *Chester*, 1988]; however, other elements are more likely to be akin to the deformation of porous rocks.

MECHANICAL BEHAVIOR

Early workers [*Adams*, 1910, 1912; *Von Karman*, 1911; *Griggs*, 1936] showed that rocks can sustain substantial strain before failure if tested at elevated pressure and/or temperature. *Heard*'s [1960] systematic investigation of the mechanical properties of Solnhofen limestone included more than 115 mechanical tests in both extension and compression and ranged over temperatures from 25 to 700°C and confining pressures up to 700 MPa, and varying pore pressures. He observed that, as pressure increased, there was a transition from axial splitting to faulting along a shear-oriented plane, and finally, to macroscopically homogeneous flow (see also *Griggs and Handin* [1960]). *Heard* [1960] defined the pressure for the brittle-ductile transition as that at which the rock can sustain axial strains of at least 5% before failure.

The macroscopic failure mode can be categorized as brittle, fully plastic, or semibrittle [*Paterson*, 1978; *Carter and Kirby*, 1978; *Rutter*, 1986]. During brittle fracture, strength shows little temperature and strain rate sensitivity, but substantial pressure sensitivity. Rocks failing by this mode dilate during deformation, and show strain softening and localization. During plastic flow, strength is pressure independent but highly strain rate and temperature dependent; deformation is not necessarily localized, and there is negligible volumetric strain. The predominant deformation mechanisms during brittle failure are cataclastic processes, including microfracturing and frictional sliding. Plastic flow may involve crystalline plasticity, twinning, or diffusional processes. Semibrittle flow involves macroscopically

distributed, dilatant deformation by both crystal plasticity and microcracking; the strength is, of course, pressure dependent.

Cataclastic flow, i.e., distributed deformation with microcracking as the predominant deformation mechanism, has been observed in high porosity basalts [*Mogi*, 1965; *Shimada*, 1986] and sandstone [e.g., *Hadizadeh and Rutter*, 1983; *Hirth and Tullis*, 1989]. Serpentine-bearing dunite and gabbro also undergo a transition to cataclastic flow at room temperature with increasing pressure [*Byerlee*, 1968*a*], probably due to the embrittlement of grain boundaries by the serpentine. Cataclastic flow has also been reported in low porosity feldspar aggregates deformed to relatively high strains without added water, at 300-650°C, and at pressures of 700-1500 MPa [*Tullis and Yund*, 1987]. At present, it is uncertain whether localization can be suppressed for arbitrarily large strains in low porosity rocks when only cataclastic processes operate (see later discussion).

When rocks are deformed at elevated temperature and pressures, optical and electron microscope observations of granites, feldspathic rocks, diabase, pyroxenites, marbles, and limestones indicate that ductile flow involves both crystal plasticity and cataclastic processes. With increased pressure or temperature, deformation may occur by fully plastic processes. Thus, two transitions in failure mode are encountered: the first, from brittle failure to semibrittle flow, can be recognized in experiments by the absence of strain localization and stress drops; the second, from semibrittle to plastic flow, can be recognized by the absence of dilatancy and the low pressure sensitivity of strength. Since both plastic and cataclastic deformation mechanisms may be involved during semibrittle flow, the transitions from brittle failure to semibrittle flow, and from semibrittle flow to fully plastic flow may depend on mineralogy, pressure, temperature, strain rate, grain size, and the presence of fluids.

Effect of Pressure

For a wide range of silicate and carbonate rocks, the transition from localized failure to nonlocalized flow occurs at pressures where the Coulomb criterion for brittle fracture intersects the failure curve for frictional sliding [*Mogi*, 1966; *Byerlee*, 1968*b*]. This bound can be rationalized qualitatively by noting that, for stress states where the curves coincide, sliding on an optimally oriented surface is as easy as producing a new fracture surface. However, the detailed relationship between the coefficient of sliding friction and the coefficient of internal friction of the Coulomb criterion is not well explained, especially near the brittle-ductile transition [*Handin*, 1969; *Mogi*, 1974]. Nevertheless, even an empirical relation, if confirmed, might be particularly useful in predicting rock deformation, because frictional strengths have been shown to be relatively insensitive to strain rate, rock type, and surface condition over the range of rates, temperatures, and sample sizes accessible to laboratory testing [*Byerlee*, 1978].

The failure strength in the brittle (localized) mode and the strength at a fixed strain for the ductile (nonlocalized) mode for limestone, marble, pyroxenite, and diabase are plotted in Figure 1. For most of the rocks, including silicates and carbonates at both high and low temperatures, the friction law bounds the brittle-ductile transition accurately. However, for Solnhofen limestone at elevated temperatures, the confining pressure necessary to cause nonlocalized flow is overpredicted. Collected fracture data for several rock types suggest that there is a weak tendency for the angle between the shear fracture plane and the principal stress axis to increase as temperature increases [*Paterson*, 1978]. If neither the coefficient of sliding friction nor the internal coefficient of friction are affected, this change will result in the intersection of the Coulomb failure curve and the frictional sliding law at lower pressure. Thus, the reduction of the transition pressure with increasing temperature may be due simply to a change in the inclination of the fracture zone, although similar reductions are not apparent in Carrara marble deformed at the same temperatures. Solnhofen limestone is also

more porous than Carrara marble, and it may be that stress concentrations around the pores tend to delocalize the deformation.

A bound for the second transition, i.e., from semibrittle flow, which is pressure sensitive and dilatant, to fully plastic flow, for which the pressure sensitivity is negligible, was suggested by Goetze [*Briegel and Goetze*, 1978], on the basis of *Edmond and Paterson's* [1972] results (see also *Kirby* [1980]). Goetze reasoned that crack extension would be suppressed when the least compressive stress and yield strength were of the same order. Under those conditions, the work to produce an element of shear strain via plastic flow is roughly equal to that necessary to produce a similar amount of volumetric strain.

The identification of fully plastic flow is usually based on the lack of pressure sensitivity of strength or on the examination of microstructures of deformed samples. Both criteria are helpful in constraining the pressure at which the second transition occurs (see Figures 1*a-d*). However, the former is subject to uncertainties in stress measurement, while the latter may easily overlook microcracks introduced during semibrittle flow. Direct measurements of dilatancy in the semibrittle regime have been made in a only a few studies [*Scholz*, 1968; *Edmond and Paterson*, 1972; *Fischer and Paterson*, 1989]; these are plotted in Figures 1*e* and 1*f*. The empirical criterion $\sigma=P_C$ also seems to overpredict the pressure necessary for the transition to fully plastic flow in Solnhofen limestone. However, the inelastic compaction that occurs at high pressures [*Edmond and Paterson,* 1972; *Fischer and Paterson*, 1989] may mask some residual local dilatancy, thus accounting for a lower apparent transition pressure in Solnhofen.

Although the failure mode may be predicted by the condition $\sigma=P_C$, the exact strength may depend on temperature, pressure, fluid conditions, and strain rate. In calcite rocks, enough plasticity can be induced at room temperature and elevated pressure so that a condition like the von Mises criterion may be fulfilled allowing the transition to fully plastic flow (see *Paterson* [1978] for a review). Similarly, the pressure sensitivity of flow strength in

polycrystalline magnesia at high temperatures disappears when the strength equals the yield stress necessary for slip on the [111] system in single crystal experiments. At this stress, slip on both the [100] and [111] systems could be activated, thus satisfying the von Mises criterion [*Paterson and Weaver*, 1970; *Paterson*, 1978]. However, using this criterion and single crystal data to predict polycrystalline flow will necessarily neglect any strengthening or weakening owing to grain boundary processes.

Negative Pressure Effect

In general, strength in the semibrittle regime is a monotonically increasing function of pressure, with pressure sensitivity that decreases as the steady-state plastic flow stress is approached (Figure 1). There are, however, some exceptions where rock strength has been found to decrease with increasing pressure: limestone at 400°C [*Heard*, 1960], diabase at 900-1000°C [*Caristan*, 1982], quartzite at 800-900°C [*Kronenberg and Tullis*, 1984], and granite, aplite, and albite above 900°C [*Tullis et al.*, 1979; *Shelton et al.*, 1981].

The reason for such an effect is obscure. *Tullis et al.* [1979], *Tullis and Yund* [1980], and *Kronenberg and Tullis* [1984] suggested that the negative pressure sensitivity in Westerly granite, Hale albite, Enfield aplite and several quartzites and novaculites might result from increased solubility of water and concomitant hydrolytic weakening at higher pressures. Indeed, increasing the amount of pore fluid does continue to weaken these rocks and seems to affect the microstructure (see later discussion). Additional fluid could also increase pore pressure and promote partial melting under some circumstances, although the previous workers did not observe any evidence of melting. *Caristan* [1982] suggested that the negative pressure sensitivity of strength might result from interactions between plastic flow processes and microcracking. In order to produce strengthening with decreasing pressure, this interaction would necessarily require that plastic flow be retarded by microcracking; *Caristan* [1982] did not discuss this point. Additionally, his experiments contained partial melt, which

may have had a significant effect on strength and fracture mode. *Heard's* [1960] observation of negative pressure sensitivity at 400°C is curious in that neither partial melting nor hydrolytic weakening have been observed in calcite at those temperatures. Experiments at similar effective pressures have not been duplicated, and other experiments at slightly higher pressures and similar temperatures do not show this effect.

Effect of Temperature and Strain Rate

For strain rates generally accessible in the laboratory, and pressures up to 3 GPa, silicate rocks fail by brittle fracture at room temperature [e.g., *Schock et al.*, 1973; *Schock and Heard*, 1974]. With increased temperature and pressure, semibrittle flow can be induced, and useful insight has been gained from macroscopic and microscopic observations of experimentally deformed rocks. *Tullis and Yund's* [1977] macroscopic observations indicate a temperature for the brittle-semibrittle transition similar to that obtained by plotting the intersection of the frictional sliding strength curve [*Stesky et al.*, 1974] with the Mohr failure envelope for intact granite [*Wong*, 1982]. However, the pressure predicted by the latter intersection is lower. Both studies suggest that the brittle-semibrittle transition in this rock is quite sensitive to temperature. Unfortunately, no direct measurements of dilatancy in granite have been made at high temperature. The extreme temperature sensitivity of the brittle-semibrittle transition in granite differs quite markedly from that in carbonates. For carbonates, the transition is much less sensitive to temperature than is the plastic flow strength. Observations at room temperature suggest that twinning is an important element in the initial yielding of Carrara marble; it is perhaps important that the stress to cause twinning is relatively insensitive to temperature.

There are few data that bear on the effect of variations in strain rate on the brittle-semibrittle transition. At temperatures less than 400°C, dry Solnhofen limestone and Carrara marble show small reductions in strength in the semibrittle regime when tested over strain

rates varying from 10^{-4}-10^{-8} [*Rutter*, 1974]. The pressure for the brittle-semibrittle transition in carbonates at a given strain rate also seems to be less sensitive to temperature than is the pressure at which full plasticity is achieved.

Effect of Fluids

Fluids may affect the mode of deformation by two general classes of mechanisms. The first is mechanical and occurs when effective pressure is reduced, as has been observed in serpentinite heated above its dehydration temperature [*Raleigh and Paterson*, 1965; *Paterson*, 1978], in limestone, marble, and sandstone with elevated pore fluid pressure [*Rutter*, 1974; *Fischer and Paterson*, 1989], in granite with melt [*van der Molen and Paterson*, 1979], and in olivine with added CO_2 [*Rovetta et al.*, 1987]. The second class includes chemical effects such as hydrolytic weakening in granites and feldspathic rocks [*Tullis and Yund*, 1980], embrittlement by discharge of water from Hale albite dried at high temperatures [*Shelton et al.*, 1981], and embrittlement of topaz by the presence of crystalline "water" [*Lee and Kirby*, 1984].

The common practice of using sample assemblies sealed with added fluid and tested at high temperatures renders the pore fluid pressure indeterminate. Since these tests are undrained, the actual pore fluid pressure depends critically on the amount of fluid added, on the integrity of the container, and on the porosity of the sample and its assembly. Both the failure mode and the deformation mechanisms are affected, and the results from such experiments are problematic. Thus, arguments concerning the contribution of hydrolytic weakening to strength reductions often rely heavily on interpretation of the microstructure.

For rocks with low porosity, permeability is also quite low, and therefore brittle strength may be sensitive to strain rate via mechanisms similar to dilatancy hardening [*Brace and Martin*, 1968]. Compaction softening owing to reduced permeability was suggested for Solnhofen limestone deformed in the semibrittle regime with aqueous pore fluid [*Rutter*,

1974]. Thus, the strain rate dependence of strength for Solnhofen limestone is much greater than that for Carrara marble, which was inferred to have larger permeability under the test conditions.

In a recent study that included experiments on Solnhofen limestone and Carrara marble with argon as pore fluid, *Fischer and Paterson* [1989] emphasized the interrelation between fluids, evolving porosity, and rock strength. The strength of Carrara with argon as pore fluid in their experiments is comparable to *Rutter*'s [1974] earlier measurements with added water; the comparison for Solnhofen is more difficult because both the wet and dry strength data of *Rutter* [1974] are systematically lower those of *Fischer and Paterson* [1989]. *Rovetta et al.* [1987] tested olivine in the semibrittle regime and concluded that the addition of CO_2 decreased the strength owing to a decrease in the effective pressure.

MICROSTRUCTURAL OBSERVATIONS

Systematic observations of the deformation microstructures in granite [*Tullis and Yund*, 1977, 1980], aplite [*Tullis and Yund*, 1980, 1987], diabase [*Kronenberg and Shelton*, 1980], and clinopyroxenite [*Kirby and Kronenberg*, 1984] have been made over a range of experimental conditions encompassing the brittle to ductile transition. Deformation microstructures formed under a more limited range of conditions in the semibrittle field have been observed in polycrystalline dunite [*Boland and Hobbs*, 1973; *Rovetta et al.*, 1987], diabase [*Caristan*, 1982], and clinopyroxenite [*Boland and Tullis*, 1986], and single crystals of feldspar [*Marshall and McLaren*, 1977]. A general conclusion of these studies is that the transition from brittle fracture to semibrittle flow with increasing pressure and/or temperature involves enhanced plastic flow (i.e., dislocation glide and twinning).

Three stages of microcracking occur during the failure of rocks deformed in compression: nucleation, propagation, and coalescence. Microstructural observations pertinent to the

nucleation and propagation of cracks in the brittle field have been reviewed recently by *Kranz* [1983]. Observations related to crack coalescence and localization have been summarized by *Evans and Wong* [1985]. Microstructures characteristic of the plastic deformation of minerals and rocks have been discussed thoroughly by *Nicolas and Poirier* [1976]. Here we focus on microstructural observations pertinent to the semibrittle deformation of rocks.

Microcracking in the Semibrittle Field

There are three relevant questions concerning microcracking in the semibrittle field. First, what are the mechanisms by which cracks nucleate? Second, is crack propagation stable or unstable; and what are the geometrical characteristics of the microcrack population in the semibrittle field? Finally, what mechanisms inhibit crack coalescence in the semibrittle field?

In the brittle field, microcracking may be induced by a variety of mechanisms, including local stress concentrations associated with grain boundaries, pre-existing pores and cracks, and elastic moduli mismatch at grain boundaries [e.g., *Paterson*, 1978; *Kranz*, 1983]. In the semibrittle field, when plastic deformation by dislocation glide and twinning occurs, additional crack nucleation mechanisms may operate [e.g., *Carter and Kirby*, 1978; *Kranz*, 1983]. At higher temperatures (or lower strain rates), these mechanisms will be less important since recovery by cross slip and climb may prevent the internal stresses from reaching the levels necessary for crack nucleation.

The tendency for voids to form at the intersection of twin lamellae in calcite was first noted by Rose in 1868 [see *Barber and Wenk*, 1979] and has been observed frequently in both experimentally and naturally deformed marble. Such voids are more common in marbles deformed at low temperatures [*Barber and Wenk*, 1979]. Microcracks may also nucleate at the intersection of twin lamallae with grain boundaries [*Olsson and Peng*, 1976]; conversely, *Marshall and McLaren* [1977] have suggested that the stress concentrations associated with

microcracks may nucleate twins. Microcracks have also been observed to nucleate at the boundaries of asymmetrical kink bands [e.g., *Christie et al.*, 1964; *Carter and Kirby*, 1978].

Stress concentrations induced when dislocations pileup at obstacles such as grain boundaries or precipitates may be sufficient to nucleate tensile microcracks [*Zener*, 1948; *Petch*, 1953; *Stroh*, 1954, 1955]. This mechanism has been cited in a number of microstructural studies [e.g., *Tullis and Yund*, 1977; *Mitra*, 1978; *Rovetta et al.*, 1986, 1987]; however, it should be noted that none of the above studies have actually observed dislocation pileups at grain boundaries or other obstacles. *Rovetta et al.* [1986, 1987] measured the crystallographic orientation of healed microcracks in naturally and experimentally deformed dunite and concluded that a significant percentage of the total crack population was oriented in a direction consistent with the Zener-Stroh mechanism. However, this interpretation is not unique since there are a number of possible geometries for cracks nucleated by this mechanism [e.g., *Lawn and Wilshaw*, 1975, Figure 2.7].

For materials deformed in tension, semibrittle crack propagation is generally unstable, and consequently, crack nucleation may lead directly to failure. However, in rocks deformed in compression, dilatant crack propagation is stable [*Brace et al.*, 1966]. Thus, semibrittle crack nucleation is not as significant to the macroscopic mechanical behavior as are the processes of crack propagation and interaction. Therefore, analyses that correlate ultimate rock strength to semibrittle crack nucleation are invalid [e.g., *Mitra*, 1978].

There are probably three parameters significant to the description of microcracks in rocks deformed in the semibrittle field: the crack density, anisotropy, and length. Owing to the tedious nature of the measurements, there have been only a few quantitative studies.

Boland and Tullis [1986] distinguished two microcrack populations in samples of polycrystalline clinopyroxenite deformed in the semibrittle field: high aspect ratio cracks whose orientation was isotropic, and low aspect ratio cracks, which occurred preferentially along grain boundaries and were oriented subparallel to the direction of the macroscopic

applied stress. Those authors concluded that the first set of cracks had formed during pressure and temperature changes at the beginning or end of the experiments, and that the grain boundary cracks had accommodated both shear and dilation during deformation. They did not make quantitative measurements of the latter crack type. Additionally, it is not clear that it is appropriate to distinguish different crack populations solely on the basis of aspect ratio.

Rovetta et al. [1987] measured the crack surface area per unit volume of healed microcracks in dunite deformed in the semibrittle field and found that it increased by factors of 2-7 in samples deformed to axial strains up to 11%. The healed cracks were preferentially oriented parallel to the applied stress direction. However, the data do not describe completely the crack structure because of the exclusion of cracks along grain boundaries and cracks less than 30 μm long.

Although high confining pressure certainly inhibits crack growth, it is not sufficient to suppress brittle fracture in most low porosity silicate rocks [e.g., *Shock and Heard*, 1974; *Shimada et al.*, 1983]. In marble the occurrence of twinning alone does not suppress crack coalescence and localization [*Olsson and Peng*, 1976]. *Tullis and Yund* [1987] observed that feldspar aggregates undergo an intermediate stage of cataclastic flow with no dislocation activity; however, they do not address the micromechanical basis for the stabilization of cracking. We discuss below the role of dislocation glide in stabilizing microcracking.

Dislocation Activity in the Semibrittle Field

Inhomogeneous plastic flow is characteristic of semibrittle flow in rocks and minerals at pressures and temperatures not greatly in excess of those at the brittle-semibrittle transition; dislocations often appear to be pinned and tangled, while microcracking remains an active deformation mechanism [*Tullis and Yund*, 1977, 1980, 1987; *Marshall and McLaren*, 1977; *Kronenberg and Shelton*, 1980]. In polycrystalline clinopyroxene, dislocations are active on only one slip system [*Kirby and Kronenberg*, 1984]. As temperature is raised, dislocation

densities become more homogeneous, tangles are observed less frequently, and microcracking is less pervasive. With further temperature increases, there is evidence for enhanced recovery and recrystallization [*Tullis and Yund*, 1977, 1980, 1987; *Kronenberg and Shelton*, 1980; *Kirby and Kronenberg*, 1984; *Boland and Tullis*, 1986].

The role of dislocations in stabilizing microcracking in the semibrittle field is not well documented, due in large part to the inherent difficulties associated with the deformation of polycrystalline aggregates. The interpretation of specific microstructures is often complicated, even in experiments carried out to axial strains as low as 1%. Nevertheless, some workers have observed microstructures strongly suggestive of crack tip blunting [*Boland and Hobbs*, 1973; *Carter et al.*, 1981; *Boland and Tullis*, 1986].

Strain Localization in the Semibrittle Field?

The question of when or whether strain localization will occur in the semibrittle field is complicated. For experiments performed at pressures and temperatures close to the brittle-ductile transition, axial stress-strain curves generally indicate work hardening. If microcracking is accommodating some amount of the imposed strain, it is possible that the deformation will localize at some higher strain. However, the evolution of strain partitioning between the brittle and plastic deformation mechanisms with strain is not understood.

Edmond and Paterson [1972] and *Fischer and Paterson* [1989] found that semibrittle deformation was stable in marble and limestone deformed to axial strains of 20%. Likewise, *Kirby and Kronenberg* [1984] associated the brittle-ductile transition in polycrystalline clinopyroxenite with the activity of plastic flow mechanisms; they did not observe localization in samples deformed in the semibrittle field to axial strains of 20-25%. *Tullis and Yund* [1987] found that the brittle-ductile transition in polycrystalline albite was not associated with the activity of plastic flow mechanisms, and that the albite deformed in a stable mode to axial strains of 50-60%.

The issue is difficult to investigate experimentally. Samples deformed to high strains deviate markedly from their initial cylindrical shape, and hence, stress states may differ significantly from the ideal triaxial state. Consequently, the interpretation of such experiments may be ambiguous.

In experiments on diabase, *Caristan* [1982] observed faulting in the transitional regime of negative pressure dependence. The fault formed in the transitional regime differed from that typically observed in rocks deformed in the brittle field. Dilatant cracks were absent, and material along the fault contained sintered grains with a high density of equidimensional pores. The structure is similar to that observed in metals deformed in tension which fail by void growth [cf. *Goods and Brown*, 1979]. This is the only evidence of which we are aware suggesting that similar micromechanical processes may operate in materials deformed in compression. It is important to note that partial melting may have occurred in *Caristan's* [1982] experiments, and it is possible that this condition favors the formation of such microstructures.

Tullis et al. [1977, 1980, 1981] observed faults in samples of granite and polycrystalline albite deformed at pressures and temperatures greater than those at which the deformation initially stabilized. The faults were typically sharp with little gouge and they suggested that some deformation in the vicinity of the fault had been accommodated by plastic flow. *Shelton et al.* [1981] suggested that the micromechanical processes leading to the formation of the high temperature and high pressure faults may differ from those associated with faulting at lower pressures and temperatures. However, detailed microstructural characterization of the anomalous faults was not performed, and so the interpretation is still unclear.

Polymineralllic Rocks

The deformation of polymineralllic rocks (e.g., granite and diabase) at conditions near the brittle-plastic transition is necessarily more complicated than that of monomineralllic

aggregates but is more relevant to deformation of the lower crust. Limited dislocation mobility occurred in quartz and feldspar grains in granite deformed at temperatures of 300-400°C and 550-650°C, respectively [*Tullis & Yund*, 1977; 1980]. The observation that semibrittle flow occurred at temperatures of 300°C and pressures of 1000 MPa suggests that plasticity in the quartz alone (representing 30% volume fraction) was sufficient to inhibit localization. *Kronenberg and Shelton* [1980] deformed diabase and concluded that the microstructures observed in the individual phases of the diabase agreed qualitatively with those observed in monominerallic aggregates of plagioclase and clinopyroxenite deformed at the same conditions.

Effect of Fluids on Semibrittle Deformation

The mechanical effect of pore fluids on brittle fracture of rock is well known and described approximately by the effective pressure law [e.g., *Paterson*, 1978]. The chemical effects of pore fluids in the brittle field through stress corrosion [e.g., *Atkinson and Meredith*, 1987*a*] and in the plastic field through hydrolytic weakening [e.g., *Paterson*, 1989] are less well known and are the subject of considerable research. The effect of pore fluids on the brittle to plastic transition is not well constrained, although several studies have demonstrated that water has a strong effect on the style of semibrittle deformation.

At pressures and temperatures close to the brittle-semibrittle transition, *Tullis and Yund* [1980] observed that the presence of water enhanced the inhomogeneous nature of the microscopic semibrittle deformation in both granite and polycrystalline albite. The presence of water also apparently enhances recovery and recrystallization in granite [*Tullis and Yund*, 1980; *Carter et al.*, 1981], polycrystalline albite [*Tullis and Yund*, 1980], and polycrystalline clinopyroxenite [*Boland and Tullis*, 1986] deformed in the semibrittle regime. Microcracking may also be increased at low strains in the wet experiments [*Tullis and Yund*, 1980; *Carter et al.*, 1981]. *Boland and Tullis* [1986] observed increased grain boundary mobility in samples

of clinopyroxenite deformed in the presence of water, although the interpretation of their experiments is complicated by the presence of partial melt. The above workers have generally interpreted their results in the general context of hydrolytic weakening; however, a detailed understanding of the micromechanisms for the weakening is still lacking.

THEORETICAL MODELING

The brittle to plastic transition is accomplished through fundamental changes in both the inelastic behavior and failure mode. The micromechanical processes are extremely complex, involving the interaction of a multiplicity of defects (e.g., microcracks, voids, dislocations, and mechanical twins). Although one cannot expect any theory to model quantitatively all facets of the mechanics, there are at least two first order questions which have to be addressed by theory. First, what causes microcracking to be distributed, thus inhibiting microcrack coalescence and shear localization and causing the transition from brittle fracture to semibrittle flow? Second, what mechanical processes are responsible for the complete suppression of microcracking and dilatancy, thus causing the transition from semibrittle flow to homogeneous plastic flow?

Development of Shear Localization

The first question regarding the development of shear localization can be tackled theoretically using two complementary approaches. From a continuum mechanics point of view, strain localization can be analyzed as an instability in the macroscopic constitutive description of inelastic deformation [*Rice*, 1976]. Alternatively, the micromechanics of crack coalescence can be analyzed as an instability in the propagation behavior of an ensemble of interacting microcracks [e.g., *Horii and Nemat-Nasser*, 1985].

Most of the recent localization analyses in rock mechanics and soil mechanics have been formulated in the spirit of a seminal study by *Rudnicki and Rice* [1975] (see the reviews by *Wong* [1985*a*] and *Evans and Wong* [1985]). *Rudnicki and Rice* [1975] formulated a constitutive relation to describe the pressure-sensitive, dilatant properties of geologic materials using three parameters: an internal friction coefficient (μ), a dilatancy factor (β), and a hardening modulus (h). For axisymmetric compressive loading, their bifurcation analysis predicts that decreases in μ and β result in an increase in the angle of the shear band to the maximum principal stress, with a maximum angle of 45°. Their analysis predicts the onset of shear localization only when the hardening coefficient h has attained a critical negative value h_{cr} given by [*Rudnicki and Rice*, 1975, equation (20)]

$$h'_{cr}/G = [(1+\nu)(\beta-\mu)^2/9(1-\nu)] - [(1+\nu)/2]\{N+[(\beta+\mu)/3]\}^2 \qquad (1)$$

where ν and G are the Poisson's ratio and shear modulus, respectively, and $N=1/\sqrt{3}$ for axisymmetric compression. Most of the laboratory observations on semibrittle behavior are in qualitative agreement with *Rudnicki and Rice's* [1975] model. The deformational behavior in the semibrittle regime is pressure-sensitive ($\mu>0$) with appreciable dilatancy ($\beta>0$), but shear localization does not occur since the inelastic deformation is attained through work hardening ($h>0>h_{cr}$).

Major advances have been made in the past decade in the theoretical understanding of the hardening and softening behavior of a cracked solid in compression using an alternative approach based on micromechanical models. Most of the studies focus on the sliding crack model, which was first proposed by *Brace et al.* [1966] as a mechanism for inelastic dilatancy in rocks (Figure 2). The application of a non-hydrostatic compressive load causes the shear traction along a "main crack" (of length $2c$ and at an angle γ to the maximum compressive stress direction) to exceed the frictional resistance; the enhancement in stress intensity factor resulting from slip along the main crack causes a "wing crack" to nucleate and extend to a length M. The wing crack initiates at an angle $\theta=70.5°$ ($=\cos^{-1}1/3$) to the main crack, and

propagates along a curved path, ultimately reaching a stable orientation parallel to the maximum compression direction (i.e., $\theta=\gamma$).

The qualitative behavior of such a sliding crack system was first studied by *Brace and Bombolakis* [1963] in photoelastic material and glass. A first order solution in closed form for the onset of crack kinking and the development of a wing crack was obtained by *Cotterell and Rice* [1980] using a perturbation technique. The exact formulation and solution of this fracture mechanics problem is very involved; the technical difficulties were reviewed by *Lo* [1978] who also presented one of the most thorough analyses. With applications to geologic materials in mind, *Nemat-Nasser and Horii* [1982] generalized *Lo's* [1978] approach to the case of compressive loading, and later extended the analysis to an array of interacting sliding cracks [*Horii and Nemat-Nasser*, 1985], and the crack-blunting process, which may be important in bringing about the brittle-plastic transition [*Horii and Nemat-Nasser*, 1986]. Guided by these rigorous numerical results, several groups recently developed approximate analytic solutions for the sliding crack model [*Steif*, 1984; *Nemat-Nasser*, 1985; *Ashby and Hallam*, 1986; *Kemeny and Cook*, 1987*a*,*b*].

The theoretical analyses all consider a two-dimensional configuration. If the remotely applied maximum compressive stress is σ_1 and the lateral confining stress is σ_2 $(=\lambda\sigma_1)$, then the main crack orientation most favorable for the nucleation of a wing crack is $\tan 2\gamma=1/\mu$, where μ is the friction coefficient along the main crack surface. The mode I stress intensity factor at the tip of such a wing crack is given by the following approximate expression [*Nemat-Nasser*, 1985; *Horii and Nemat-Nasser*, 1986]

$$K_1/\sigma_1\sqrt{(\pi c)}= [(1-\lambda)\sqrt{(1+\mu^2)}-(1+\lambda)\mu]/[\pi\sqrt{(L+L^*)}]\sin\theta - (\sqrt{L}/2)[(1+\lambda)-(1-\lambda)\cos 2(\theta-\gamma)] \quad (2)$$

where $L=\ell/c$, and $L^*=8/(3\pi^2)=0.27$. Crack propagation occurs when $K_1=K_c$, the mode I fracture toughness. By maximizing the above expression for K_1 with respect to θ, one can determine the orientation of the wing crack. The crack growth behavior of this model is shown in Figure 3, where we plot the above expression (for a fixed friction coefficient

μ=0.3) as a function of θ and L. The wing crack initiates at an angle of about 70.5° to the main crack; this angle decreases with increasing wing crack length, and asymptotically approaches the value of γ (=36.7° for μ=0.3) for very large L.

An important result is that under all-compressive loading ($\sigma_1 > 0$ and $\lambda > 0$), K_1 at the tip of a wing crack decreases with increasing L (Figure 3). In other words, wing crack growth is always stable: continuous crack growth is possible only if either σ_1 increases or λ decreases monotonically. Consequently, the overall deformation behavior will not show strain softening if the inelasticity results from the collective growth of an ensemble of such non-interacting wing cracks. In this sense, the sliding crack can be used to model rock deformation in the semibrittle field.

Under a relatively low confining pressure, the wing crack can extend to several times the main crack length (Figure 3*a*), and the expression for K_1 can be simplified by taking $\theta=\gamma$ [*Ashby and Hallam*, 1986; *Kemeny and Cook*, 1987*a*]. However, an additional complication due to crack interaction has to be considered. The rigorous treatment by *Horii and Nemat-Nasser* [1985] showed that the interaction results in overall strain softening and crack coalescence, which probably corresponds to the onset of shear localization. Approximate analytic estimates of the interaction effect were recently given by *Sammis and Ashby* [1986], *Ashby and Hallam* [1986], and *Kemeny and Cook* [1987*a*]. *Ashby and Hallam's* [1986] formulation is based on beam flexure analysis, and the crack interaction effect results in an enhancement of stress intensity factor given by

$$K_1/\sigma_1\sqrt{(\pi c)} = \sqrt{(2\epsilon_o/\pi)}(L+\alpha)^{1/2}[(1-8\epsilon_o\lambda(L+\alpha)^3)(1-2\epsilon_o\lambda(L+\alpha)^3)]^{1/2} \qquad (3)$$

where $\alpha=1/\sqrt{2}$ and $\epsilon_o=c^2N_A$. The stereological quantity N_A is the number of main sliding cracks per unit volume, and ϵ_o as defined here is the two-dimensional equivalent of the "crack density" parameter introduced by *Walsh* [1965] and *Budiansky and O'Connell* [1976] to analyze the effect of cracks on the elastic moduli.

In summary, the important physical quantities, which in the sliding crack model determine the onset of crack coalescence, strain softening, and shear localization, are λ, μ, K_c, and ϵ_o (Figure 4). Crack coalescence can be inhibited by either an increase in the confining pressure, friction coefficient or fracture toughness, or by a decrease in the crack density. Comparing Figures 3*a* and 3*b*, it can be seen that an increase in confining pressure (corresponding to an increase in λ) is very effective in suppressing wing crack extension. For example, for $\lambda = 1/3$ (corresponding to $(\sigma_1-\sigma_2)=2\sigma_2$), the model predicts that the wing crack can at most extend by about one-tenth of the main crack length (Figures 3*b* and 4).

The rock deformation data summarized above show that dilatancy and pressure-sensitivity are generally observed for $(\sigma_1-\sigma_2)>\sigma_2$ (i.e., $\lambda<0.5$). It can be seen from equation (2) above that if $\lambda=0.5$, then the friction coefficient must be ~ 0.2 or so for a wing crack to nucleate and extend to a very short distance (say, $\ell=0.03c$). A similar problem was encountered by *Nemat-Nasser and Obata* [1988]; they had to choose an extremely low coefficient of friction on the sliding crack ($\mu=0.1$) to match the experimental data for rock dilatancy. These results imply that the sliding crack model does not account for all of the grain-scale stress concentration effects. A number of alternative mechanisms have been proposed (see reviews by *Kranz* [1983] and *Wong* [1985*a*]). *Costin* [1985] recently formulated a damage mechanics model based on the elastic mismatch mechanism that considered crack interaction and strain softening behavior. *Nemat-Nasser* [1985] has also argued that the stress concentrations from elastic mismatch or equidimensional voids result in crack growth behavior qualitatively similar to that observed for the sliding crack model.

The important damage variable in most of the micromechanical models is the crack density ϵ. This is a quantity that is difficult to determine by quantitative microscopy [*Wong*, 1985*b*]. Careful measurements were conducted by *Hadley* [1976] who determined $\epsilon=0.25$ for an unstressed sample of Westerly granite. It is unclear whether the sliding cracks should be identified with all of the microcracks observed under the electron microscope. Nevertheless,

most of the recent theoretical calculations [e.g., *Kemeny and Cook*, 1987*b*; *Nemat-Nasser and Obata*, 1988] have assumed ϵ_o=0.2-0.3, as suggested by microscopy. According to *Madden's* [1983] analysis of rock fracture as a critical phenomenon using a renormalization group approach, the crack density ϵ has to attain a value of 1 at criticality (or about 0.8 if crack anisotropy is considered).

Semibrittle Crack Nucleation and Blunting

Rock deformation data summarized above suggest that pressure by itself is not sufficient to completely inhibit dilatancy and microcracking in low porosity crystalline rocks. In the semibrittle field, inelastic deformation is accommodated by a combination of microcracking and crystal plasticity processes (e.g., dislocation glide, mechanical twinning, diffusional mass transfer processes). The interaction of these defects may result in crack tip blunting. Dislocation pileups and mechanical twins may also enhance microcracking by providing additional crack nucleation mechanisms.

Fracture toughness and subcritical crack growth data for common minerals and rocks under room conditions are available [*Atkinson and Meredith*, 1987*b*]. However, few data are available at elevated pressures and temperatures. In the semibrittle field, the apparent toughness may be high due to crack tip shielding by dislocations and twins. Although such processes have been analyzed thoroughly in the engineering literature, most of the theoretical analyses are unlikely to be applicable to the compressive loading configuration relevant to geophysics. A more realistic model involving the interaction of a sliding crack with a wing crack and a dislocation pileup at each of the main crack tips was formulated recently by *Horii and Nemat-Nasser* [1986]. An important result is that the transition to fully plastic flow is dictated by the "ductility" $\Delta=K_c/\tau_y(\pi c)^{1/2}$, where τ_y is the plastic yield stress in shear. For a given Δ, there is a critical stress ratio λ^* above which wing crack growth is inhibited completely, so that the inelastic deformation is solely accommodated by dislocation activity.

This critical value λ^* increases with decreasing Δ; for rocks, Δ is relatively low. In the limit of Δ approaching 0, the critical stress ratio can be determined to be [*Horii and Nemat-Nasser*, 1986, equation (3.21)]

$$\lambda^* = (\sin 2\gamma - \mu + \mu\cos 2\gamma)/(\sin 2\gamma + \mu + \mu\cos 2\gamma) \quad (4)$$

with the angle γ as defined in Figure 2. It can be seen that the friction coefficient μ has to be relatively low (<0.3 or so) to satisfy the condition $\lambda^* > 0.5$, which is implied by the rock deformation data discussed above.

In the semibrittle field, crack density may be increased by the activity of semibrittle crack nucleation mechanisms involving dislocation pileups and twinning. *Wong* [1989*b*] analyzed the effect of compressive stress on the propagation behavior of a crack nucleated by a dislocation pile-up [*Stroh*, 1954]. In the case of compressive loading, failure is not nucleation controlled (unlike the case of tensile loading). In fact, the Stroh crack propagates in a stable manner and its length depends on the stress ratio λ and the fracture toughness K_c in a manner similar to the sliding crack discussed above (equation (2)). For the sliding crack model, the wing crack length ℓ scales as the main crack length c, whereas the Stroh crack length scales as the dislocation pile up length $\mathcal{L} = G/[\pi(1-\nu)\tau^*]nb$ (where n is the number of dislocations in the pileup, τ^* is the difference between the shear stress resolved on the slip plane and the Peierls stress, b is the Burgers vector, G is the shear modulus, and ν is Poisson's ratio).

Discussion

Geological Implications

Deformation style. Widespread evidence of strain localization is one of the most striking aspects of natural deformation as observed in the field. Careful examinations at microscopic, outcrop, and map scales frequently indicate complex spatial and temporal relations between the dominant deformation mechanisms, failure modes, and loading conditions [e.g., *Segall*

and Pollard, 1983; *Simpson,* 1986; *Hobbs et al.,* 1986; *Groshong,* 1988]. Although details of the loading conditions for naturally deformed rocks are rarely known, analyses such as that of *Rudnicki and Rice* [1975] are still helpful for assessing the development of localization and fault zones [e.g., *Aydin and Johnson,* 1983]. Experiments and theory suggest that, besides the obvious influence of mineralogy, small changes in porosity, grain size, and second phase content might also influence the occurrence of localized shear zones.

Experiments indicate that dilatancy persists during deformation over a broad range of pressure and temperature conditions, and that even small amounts of dilatancy are associated with significant variations in strength. Likewise, microscopy on experimentally deformed samples indicates that significant changes in strength and failure mode are not necessarily linked to conspicuous changes in the deformation microstructure. Thus, distinguishing between brittle, semibrittle, and plastic flow requires thorough microstructural analysis.

The fact that dilatancy persists during deformation at quite high pressures and temperatures suggests that potential sites for fluid transport may exist at depth in the crust. Of course it must be kept in mind that crack healing processes [e.g., *Smith and Evans,* 1984] are enhanced at high temperatures and will tend to reduce porosity. Whether net porosity is created or destroyed will depend upon the stress level and the relative rates of deformation and crack healing.

Strength of the lithosphere. Brace and Kohlstedt [1980] suggested a conceptual framework for evaluating the strength of the lithosphere and provided quantitative profiles using laboratory derived laws for frictional sliding and plastic flow. However, as *Kirby* [1980] and *Carter and Tsenn* [1987] have emphasized, the transition from brittle failure to fully plastic flow does not occur abruptly; rather, the rheology evolves gradually over a transitional, semibrittle regime. Further, extrapolations of either the brittle or plastic strengths into the semibrittle regime result in significant overestimates of strength. More realistic estimates of crustal strength requires quantitative constitutive relations for semibrittle flow. Increased

knowledge of alternative deformation mechanisms, such as pressure solution, and of the effect of fluids are also needed to construct more accurate models [*Sibson*, 1983].

Seismicity. In continental crust, earthquake foci are typically concentrated in the upper 10-15 km; the lower crust is generally considered aseismic [*Chen and Molnar*, 1983; *Strehlau*, 1986]. The depth extent of the seismogenic layer and the seismic-aseismic transition have been interpreted to be a consequence of the brittle-ductile transition [e.g., *Sibson*, 1982]. However, *Tse and Rice* [1986] have pointed out that frictional sliding may be either stable or unstable, and that the seismogenic layer should be identified only with that portion of the brittle layer within which frictional instabilities can nucleate.

Seismologic observations suggest that significant healing may occur along faults at depth during the postseismic stage [*Scholz et al.*, 1986]. The structure of faults in the earth may therefore differ from those in laboratory frictional tests. Natural fault rocks in the earth may, in fact, have structures intermediate between the end member categories of intact and "sawcut" rocks studied presently in the laboratory. *Andrews* [1989] suggested recently that the rupture of fresh material may also be an important mechanism for nucleating instabilities at fault junctions.

During large earthquakes, ruptures may propagate into the semibrittle region [*Strehlau*, 1986; *Hobbs et al.*, 1986; *Scholz*, 1988; *Jackson and White*, 1989]. Strain rates may increase by as much as 10 orders of magnitude during the coseismic stage, and thus rocks which deform plastically during the preseismic stage may deform in either a brittle or semibrittle manner during the rupture phase. At present, it is unclear how far below the seismogenic layer the ruptures may extend. Technical problems related to the interpretation of seismological data were discussed by *Jackson and White* [1989]. Based on a compilation of focal depths for 36 continental earthquakes and their aftershocks, *Strehlau* [1986] concluded that the deepest aftershock locations are about 5 ± 2 km below the hypocentral depth of the main shock. Thus, rupture may have propagated to comparable depth below the seismogenic

layer. A better understanding of the physics of semibrittle deformation is essential for improving theoretical modelling of the dynamics of earthquake rupture [e.g., *Das*, 1982].

Suggestions for Further Work

The present ensemble of experimental data suffers from deficiencies in three areas: a lack of data on the semibrittle rheology of silicates and polyphase aggregates at high temperatures, and, perhaps most significantly, a lack of knowledge of the influence of fluids and melts on semibrittle rheology.

Fluids, in particular water, have a profound effect on strength and rheology. In order to separate the mechanical and chemical effects, future studies need to control fluid pressure and water fugacity. An effective way to accomplish this is through the use of drained experiments in which the pore fluid pressure is maintained separately [e.g., *Fischer and Paterson*, 1989]. As pointed out by these workers, it is important to understand the interrelationship between the deformation and permeability of rocks. Relatively little attention has been paid to incorporating the processes of stress corrosion and pressure solution into the description of semibrittle deformation [e.g., *Rutter and Mainprice*, 1978; *Sibson*, 1983]. Effort also needs to be devoted towards constraining the influence of small amounts of melt on semibrittle rheology.

Localization is strongly influenced by loading conditions and geometry [e.g., *Rudnicki and Rice*, 1975]. Experiments designed to observe localization and macroscopic failure mode must have carefully controlled stress states and well-characterized machine stiffness. In particular, caution must be applied in the interpretation of high-strain experiments. In addition, the effects of pressurization, heating, quenching, and unloading on the microstructure must be carefully characterized in order to interpret accurately the experimentally produced deformation textures.

Theoretical modeling of the brittle to plastic transition in compression is presently limited by the lack of detailed microstructural observations of rocks deformed in the semibrittle regime. Semibrittle deformation, even in the relatively simple configuration of laboratory experiments, involves complex interactions among several deformation mechanisms. Attempting to predict the strength of polyphase rocks in the presence of circulating pore fluids, and possibly while undergoing chemical reactions, presents additional difficulties. To be tractable, individual models can only focus on the most important aspects of the overall process; the data with which to make such critical judgements must necessarily come from carefully conceived experimental studies.

Detailed microstructural observations, concerning, for example, crack-tip blunting by dislocations, are needed to motivate the development of more realistic theoretical models for crack propagation in the semibrittle regime. Careful stereological characterization of the stress-induced crack structure is necessary for the quantitative testing of theoretical models, and such data also provide insight into the micromechanics of deformation. Systematic studies that isolate the effect of one parameter on the deformation mode and strength may also be useful for testing the theoretical models and revealing their deficiencies.

Field studies often present complex polyphase deformation histories, which are difficult to interpret quantitatively; however, field observations are indispensable to workers in experimental rock mechanics as paradigms of natural deformation modes. Conversely, in some field studies, workers have been able to apply the information derived from experimental and theoretical investigations to gain substantial insight toward the understanding of tectonic processes [e.g., *Segall and Simpson*, 1986].

To apply laboratory results to natural deformation requires extrapolation of data to very slow strain rates and large scales; some of the problems inherent in the extrapolation of experimental data for plastic flow have been discussed by *Paterson* [1987]. Similar problems will arise when applying laboratory data for semibrittle deformation to natural situations. The

issue of strain localization is particularly important to the field geologist; unfortunately, localization in the semibrittle field is still not understood well.

With present understanding and current technical competence, many useful experiments are yet to be performed. Experiments documenting the effect of pressure, temperature, and strain rate on semibrittle flow are necessary before accurate constitutive laws for semibrittle deformation may be derived. The development of such constitutive relations is critical for the construction of more accurate strength profiles for the lithosphere. There is still much to be learned from the quantitative characterization of stress-induced microstructures in rocks deformed experimentally in the semibrittle regime. It may also be fruitful to investigate the interaction between propagating cracks and dislocations using single crystal experiments in carefully controlled environments. Another area where data are lacking is the characterization of fracture strength and toughness at high temperatures and pressures.

REFERENCES

Adams, F. D., An experimental investigation into the action of differential pressure on certain minerals and rocks, employing the process suggested by Professor Kick, J. Geol., 18, 489-525, 1910.

Adams, F. D., An experimental contribution to the question of the depth of the zone of flow in the earth's crust, *J. Geol.*, *20*, 97-118, 1912.

Andrews, D. J., Mechanics of fault junctions, *J. Geophys. Res.*, *94*, 9389-9397, 1989.

Ashby, M. F., and S. D. Hallam, The failure of brittle solids containing small cracks under compressive stress states, *Acta Metall.*, *34*, 497-510, 1986.

Atkinson, B. K., and P. G. Meredith, Theory of subcritical crack growth with applications to minerals and rocks, in *Fracture Mechanics of Rock,* edited by B. K. Atkinson, pp. 111-166, Academic Press, London, 1987*a*.

Atkinson, B. K., and P. G. Meredith, Experimental fracture mechanics data for rocks and minerals, in *Fracture Mechanics of Rock,* edited by B. K. Atkinson, pp. 477-525, Academic Press, London, 1987*b*.

Aydin, A., and A. M. Johnson, Analysis of faulting in porous sandstones, *J. Struct. Geol.*, *5*, 19-31, 1983.

Barber, D. J., and H.-R. Wenk, Deformation twinning in calcite, dolomite, and other rhombohedral carbonates, *Phys. Chem. Mineral.*, *5*, 141-165, 1979.

Boland, J. N., and B. E. Hobbs, Microfracturing processes in experimentally deformed peridotite, *Int. J. Rock Mech. Min. Sci. Geomech. Abstr.*, *10*, 623-626, 1973.

Boland, J. N., and T. E. Tullis, Deformation behavior of wet and dry clinopyroxenite in the brittle to ductile transition region, in *Mineral and Rock Deformation: Laboratory Studies*, *Geophys. Monogr. Ser.*, vol. 36, edited by B. E. Hobbs and H. C. Heard, pp. 35-50, AGU, Washington, D.C., 1986.

Brace, W. F., and E. G. Bombolakis, A note on brittle crack growth in compression, *J. Geophys. Res.*, *68*, 3709-3713, 1963.

Brace, W. F., B. Paulding, and C. H. Scholz, Dilatancy in the fracture of crystalline rocks, *J. Geophys. Res.*, *71*, 3939-3954, 1966.

Brace, W. F., and R. J. Martin, A test of the law of effective stress for crystalline rocks of low porosity, *Int. J. Rock Mech. Min. Sci. Geomech. Abst.*, *5*, 415-426, 1968.

Brace, W. F., and D. L. Kohlstedt, Limits on lithospheric stress imposed by laboratory experiments, *J. Geophys. Res.*, *85*, 6248-6252, 1980.

Briegel, U., and C. Goetze, Estimates of differential stress recorded in the dislocation structure of Lochseiten limestone (Switzerland), *Tectonophys.*, *48*, 61-76, 1978.

Budiansky, B., and R. J. O'Connell, Elastic moduli of a cracked solid, *Int. J. Solids Struct.*, *12*, 81-97, 1976.

Byerlee, J. D., Brittle-ductile transition in rocks, *J. Geophys. Res.*, *73*, 4741-4750, 1968*a*.

Byerlee, J. D., Frictional characteristics of granite under high confining pressure, *J. Geophys. Res.*, *72*, 4741-4750, 1968*b*.

Byerlee, J. D., Friction of rocks, *Pure Appl. Geophys.*, *116*, 615-626, 1978.

Caristan, Y., The transition from high temperature creep to fracture in Maryland diabase, *J. Geophys. Res.*, *87*, 6781-6790, 1982.

Carter, N. L., and S. H. Kirby, Transient creep and semibrittle behavior of crystalline rocks, *Pure Appl. Geophys.*, *116*, 807-839, 1978.

Carter, N. L., D. A. Anderson, F. D. Hansen, and R. L. Kranz, Creep and creep rupture of granitic rocks, in *Mechanical Behavior of Crustal Rocks*, *Geophys. Monogr. Ser.*, vol. 24, edited by N. L. Carter, M. Friedman, J. M. Logan, and D. W. Stearns, pp. 61-82, AGU, Washington, D.C., 1981.

Carter, N. L., and M. C. Tsenn, Flow properties of continental lithosphere, *Tectonophys.*, *136*, 27-63, 1987.

Chen, W. P., and P. Molnar, Focal depths of intracontinental and intraplate earthquakes and their implications for the thermal and mechanical properties of the lithosphere, *J. Geophys. Res.*, *88*, 4183-4214, 1983.

Chester, F. M., The brittle-ductile transition in a deformation-mechanism map for halite, *Tectonophys.*, *154*, 125-136, 1988.

Christie, J. M., D. T. Griggs, and N. L. Carter, Experimental evidence of basal slip in quartz, *J. Geol.*, *72*, 734-756, 1964.

Costin, L., Damage mechanics in the post-failure regime, *Mech. Mat.*, *4*, 149-160, 1985.

Cotterell, B., and J. R. Rice, Slightly curved or kinked cracks, *Int. J. Fracture*, *16*, 155-169, 1980.

Das, S., Appropriate boundary conditions for modelling very long earthquakes and physical consequences, *Bull. Seismol. Soc. Am.*, *72*, 1911-1926, 1982.

Edmond, J. M., and M. S. Paterson, Volume changes during the deformation of rocks at high pressures, *Int. J. Rock Mech. Min. Sci. Geomech. Abstr.*, *9*, 161-182, 1972.

Evans, B., and T.-f. Wong, Shear localization in rocks induced by tectonic deformation, in *Mechanics of Geomaterials*, edited by Z. Bazant, pp. 189-210, John Wiley, New York, 1985.

Fischer, G. J., and M. S. Paterson, Dilatancy during the deformation of rocks at high temperatures and pressures, *J. Geophys. Res.*, *94*, 17607-17617, 1989.

Goetze, C., and B. Evans, Stress and temperature in the bending lithosphere as constrained by experimental rock mechanics, *Geophys. J. R. astr. Soc.*, *59*, 463-478, 1979.

Goods, S. H., and L. M. Brown, The nucleation of cavities by plastic deformation, *Acta Metall.*, *27*, 1-15, 1979.

Griggs, D. T., Deformation of rocks under high confining pressure, *J. Geol.*, *47*, 225-251, 1936.

Griggs, D. T., and J. Handin, Observations on fracture and a hypothesis of earthquakes, in *Rock Deformation, Mem. Geol. Soc. Am., 79,* edited by D. T. Griggs and J. Handin, pp. 347-364, Geol. Soc. Am., NY, 1960.

Groshong, R. H., Low-temperature deformation mechanisms and their interpretation, *Geol. Soc. Amer. Bull.*, *100*, 1329-1360, 1988.

Hadizadeh, J., and E. H. Rutter, The low temperature brittle-ductile transition in a quartzite and the occurrence of cataclastic flow in nature, *Geol. Rund.*, *72*, 493-509, 1983.

Hadley, K., Comparison of calculated and observed crack seismic velocities in Westerly granite, *J. Geophys. Res.*, *81*, 3484-3494, 1976.

Handin, J., On the Coulomb-Mohr failure criterion, *J. Geophys. Res.*, *74*, 5343-5348, 1969.

Heard, H. C., Transition from brittle fracture to ductile flow in Solnhofen limestone as a function of temperature, confining pressure and interstitial fluid pressure, in *Rock Deformation, Mem. Geol. Soc. Am., 79,* edited by D. T. Griggs and J. Handin, pp. 193-226, Geol. Soc. Am., New York, 1960.

Hirth, G. and J. Tullis, The effects of pressure and porosity on the micromechanics of the brittle-ductile transition in quartzite, *J. Geophys. Res.*, *94*, 17825-17838, 1989.

Hobbs, B. E., A. Ord, and C. Teyssier, Earthquakes in the ductile regime?, *Pure Appl. Geophys.*, *124*, 309-336, 1986.

Horii, H., and S. Nemat-Nasser, Compression-induced microcrack growth in brittle solids: Axial splitting and shear failure, *J. Geophys. Res.*, *90*, 3105-3125, 1985.

Horii, H., and S. Nemat-Nasser, Brittle failure in compression: Splitting, faulting and brittle-ductile transition, *Phil. Trans. Royal Soc. London, 319*, 337-374, 1986.

Jackson, J. A., and N. J. White, Normal faulting in the upper continental crust: Observations from regions of active extension, *J. Struct. Geol., 11*, 15-36, 1989.

Kemeny, J. M., and N. G. W. Cook, Crack models for the failure of rocks in compression, *Proc. Int. Conf. on Const. Laws for Eng. Mat., 2*, 879-887, 1987*a*.

Kemeny, J. M., and N. G. W. Cook, Determination of rock fracture parameters from crack models for failure in compression, *Proc. U.S. Symposium on Rock Mechanics, 28th*, 367-374, 1987*b*.

Kirby, S. H., Tectonic stresses in the lithosphere: Constraints provided by experimental deformation of rocks, *J. Geophys. Res., 89*, 6353-6363, 1980.

Kirby, S. H., and A. K. Kronenberg, Deformation of clinopyroxenite: Evidence for a transition in flow mechanisms and semibrittle behavior, *J. Geophys. Res., 85*, 3177-3192, 1984.

Kranz, R. L., Microcracks in rocks, a review, *Tectonophys., 100*, 449-480, 1983.

Kronenberg, A. K., and G. L. Shelton, Deformation microstructures in experimentally deformed Maryland diabase, *J. Struct. Geol., 2*, 341-353, 1980.

Kronenberg, A. K., and J. Tullis, Flow strengths of quartz aggregates: Grain size and pressure effects due to hydrolytic weakening, *J. Geophys. Res., 89*, 4281-4197, 1984.

Lawn, B. R., and T. R. Wilshaw, *Fracture of Brittle Solids*, 204 pp.,Cambridge University Press, London, 1975.

Lee, R. W., and S. H. Kirby, Experimental deformation of topaz crystals: Possible embrittlement by intracrystalline water, *J. Geophys. Res., 89*, 4161-4166, 1984.

Li, V. C., and J. R. Rice, Crustal deformation in great California earthquake cycles, *J. Geophys. Res., 92*, 11,533-11,551, 1987.

Lo, K. K., Analysis of branched cracks, *J. Appl. Mech., 45*, 797-802, 1978.

Madden, T. R., Microcrack connectivity in rocks: A renormalization group approach to the critical phenomena of conduction and failure in crystalline rocks, *J. Geophys. Res., 88*, 585-592, 1983.

Marshall, D. B., and A. C. McLaren, Deformation mechanisms in experimentally deformed plagioclase feldspars, *Phys. Chem. Miner., 1*, 351-370, 1977.

Mitra, G., Ductile deformation zones and mylonites: The mechanical processes involved in the deformation of crystalline basement rocks, *Amer. J. Sci., 278*, 1057-1084, 1978.

Mogi, K., Deformation and fracture of rocks under confining pressure (2), Elasticity and plasticity of some rocks, *Bull. Earthquake Res. Inst., Tokyo Univ., 43*, 349-374, 1965.

Mogi, K., Pressure dependence of rock strength and transition from brittle to ductile flow, *Bull. Earthquake Res. Inst., Tokyo Univ., 44,* 215-232,1966.

Mogi, K., On the pressure dependence of strength of rocks and the Coulomb fracture criterion, *Tectonophys., 21,* 273-285, 1974.

Nemat-Nasser, S., and H. Horii, Compression-induced nonplanar crack extension with application to splitting, exfoliation, and rock burst, *J. Geophys. Res., 87,* 6805-6822, 1982.

Nemat-Nasser, S., and M. Obata, A microcrack model of dilatancy in brittle materials, *J. Appl. Mech., 55,* 24-35, 1988.

Nemat-Nasser, S., Discussion of "Geometric probability approach to the characterization and analysis of microcracking in rocks" by Teng-fong Wong, *Mech. Mat., 4,* 277-281, 1985.

Nicolas, A., and J. P. Poirier, *Crystalline Plasticity and Solid State Flow in Metamorphic Rocks,* 444 pp., John Wiley, New York, 1976.

Olsson, W. A., and S. S. Peng, Microcrack nucleation in marble, *Int. J. Rock Mech. Min. Sci. Geomech. Abstr., 13,* 53-59, 1976.

Paterson, M. S., *Experimental Rock Deformation-the Brittle Field,* 254 pp., Springer-Verlag, New York, 1978.

Paterson, M. S., Problems in the extrapolation of laboratory rheological data, *Tectonophys., 133,* 33-43, 1987.

Paterson, M. S., The interaction of water with quartz and its influence in dislocation flow: An overview, in *Rheology of Solids and of the Earth,* edited by S. Karato and M. Toriumi, pp. 107-142, Oxford University Press, London, 1989.

Paterson, M. S., and C. W. Weaver, Deformation of polycrystalline MgO under pressure, *J. Am. Cer. Soc., 53,* 463-471, 1970.

Petch, N. J., The cleavage strength of polycrystals, *J. Iron. Steel. Inst., 173,* 25, 1953.

Raleigh, C. B., and M. S. Paterson, Experimental deformation of serpentinite and its tectonic implications, *J. Geophys. Res., 70,* 3965-3985, 1965.

Rice, J. R., The localization of plastic deformation, in *Proc. Int. Cong. Theor. Appl. Mech., 14th,* edited by W. T. Koiter, pp. 207-220, North-Holland, Amsterdam, 1976.

Rovetta, M. R., J. R. Delaney, and J. D. Blacic, A record of high-temperature embrittlement of peridotite in CO_2 permeated xenoliths from basalt, *J. Geophys. Res., 91,* 3841-3848, 1986.

Rovetta, M. R., J. D. Blacic, and J. R. Delaney, Microfracture and crack healing in experimentally deformed peridotite, *J. Geophys. Res., 92,* 12,902-12,910, 1987.

Rudnicki, J. W., and J. R. Rice, Conditions for the localization of deformation in pressure sensitive dilatant materials, *J. Mech. Phys. Solids*, *23*, 371-394, 1975.

Rutter, E. H., The influence of interstitial water on the rheological behavior of calcite rocks, *Tectonophys.*, *14*, 13-33, 1972*a*.

Rutter, E. H., The effects of strain-rate changes on the strength and ductility of Solnhofen limestone at low temperatures and confining pressures, *Int. J. Rock Mech. Min. Sci. Geomech. Abstr.*, *9*, 183-189, 1972*b*.

Rutter, E. H., The influence of temperature, strain rate and interstitial water in the experimental deformation of calcite rocks, *Tectonophys.*, *22*, 311-334, 1974.

Rutter, E. H., On the nomenclature of mode of failure transitions in rocks, *Tectonophys.*, *122*, 381-387, 1986.

Rutter, E. H., and D. M. Mainprice, The effect of water on stress relaxation of faulted and unfaulted sandstone, *Pure Appl. Geophys.*, *116*, 634-654, 1978.

Sammis, C. G., and M. F. Ashby, The failure of brittle porous solids under compressive stress states, *Acta Metall.*, *34*, 511-526, 1986.

Schmid, S. M., R. Pannozo, and S. Bauer, Simple shear experiments on calcite rocks: Rheology and microfabric, *J. Struct. Geol.*, *9*, 747-778, 1987.

Schock, R. N., H. C. Heard, and D. R. Stephens, Stress-strain behavior of a granodiorite and two graywackes on compression to 20 kilobars, *J. Geophys. Res.*, *78*, 5922-5941, 1973.

Schock, R. N., and H. C. Heard, Static mechanical properties and shock loading response of granite, *J. Geophys. Res.*, *79*, 1662-1666, 1974.

Scholz, C. H., Microfracturing and the inelastic deformation of rock in compression, *J. Geophys. Res.*, *73*, 1417-1432, 1968.

Scholz, C. H., The brittle-plastic transition and the depth of seismic faulting, *Geol. Rund.*, *77*, 319-328, 1988.

Scholz, C. H., C. A. Aviles, and S. G. Wesnousky, Scaling differences between large interplate and intraplate earthquakes, *Bull. Seism. Soc. Am.*, *76*, 65-70, 1986.

Segall, P., and D. D. Pollard, Nucleation and growth of strike-slip faults in granite, *J. Geophys. Res.*, *88*, 555-568, 1983.

Segall, P., and C. Simpson, Nucleation of ductile shear zones on dilatant fractures, *Geol.*, *14*, 56-59, 1986.

Shelton, G. L., J. Tullis, and R. A. Yund, Experimental high temperature and high pressure faults, *Geophys. Res. Lett.*, *8*, 55-58, 1981.

Shimada, M., Mechanism of deformation in a dry porous basalt at high pressure, *Tectonophys.*, *121*, 153-173, 1986.

Shimada, M., A. Cho, and H. Yukatake, Fracture strength of dry silicate rocks at high confining pressures and activity of acoustic emission, *Tectonophys.*, *96*, 159-172, 1983.

Shimamoto, T., and J. M. Logan, Velocity-dependent behavior of simulated halite shear zones: An analogue for silicates, in *Earthquake Source Mechanics, Geophys. Mono. Ser.*, vol 37, edited by S. Das and C. H. Scholz, pp. 49-63, AGU, Washington, D.C., 1986.

Sibson, R. H., Fault rocks and fault mechanism, *J. Geol. Soc. Lond.*, *133*, 191-213, 1977.

Sibson, R. H., Fault zone models, heat flow, and the depth distribution of earthquakes in the continental crust of the United States, *Bull. Seismol. Soc. Am.*, *72*, 151-163, 1982.

Sibson, R. H., Continental fault structure and the shallow earthquake source, *J. Geol. Soc. Lond.*, *140*, 741-767, 1983.

Simpson, C., Fabric development in brittle-to-ductile shear zones, *Pure Appl. Geophys.*, *124*, 269-288, 1986.

Smith, D., and B. Evans, Diffusional crack healing in quartz, *J. Geophys. Res.*, *89*, 4125-4135, 1984.

Stesky, R. M., W. F. Brace, D. K. Riley, and P.-Y. F. Robin, Friction in faulted rock at high temperature and pressure, *Tectonophys.*, *23*, 177-203, 1974.

Steif, P. S., Crack extension under compressive loading, *Eng. Fracture Mech.*, *20*, 463-473, 1984.

Strehlau, J., A discussion of the depth extent of rupture in large continental earthquakes, in *Earthquake Source Mechanics, Geophys. Mono. Ser.*, vol 37, edited by S. Das and C. H. Scholz, pp. 131-146, AGU, Washington, D.C., 1986.

Stroh, A. N., The formation of cracks as a result of plastic flow, *Proc. Roy. Soc. Lond.*, *A223*, 404-414, 1954.

Stroh, A. N., The formation of cracks in plastic flow II, *Proc. Roy. Soc. Lond.*, *A232*, 548-560, 1955.

Tse, S. T., and J. R. Rice, Crustal earthquake instability in relation to the depth variation of frictional properties, *J. Geophys. Res.*, *91*, 9452-9472, 1986.

Tullis, J., and R. A. Yund, Experimental deformation of dry Westerly granite, *J. Geophys. Res.*, *82*, 5705-5718, 1977.

Tullis, J., G. L. Shelton, and R. A. Yund, Pressure dependence of rock strength: Implications for hydrolytic weakening, *Bull. Mineral.*, *102*, 110-114, 1979.

Tullis, J., and R. A. Yund, Hydrolytic weakening of experimentally deformed Westerly granite and Hale albite rock, *J. Struct. Geol.*, *2*, 439-451, 1980.

Tullis, J., and R. A. Yund, Transition from cataclastic flow to dislocation creep of feldspar: Mechanisms and microstructures, *Geology*, *15*, 606-609, 1987.

van der Molen, I., and M. S. Paterson, Experimental deformation of partially-melted granite, *Contrib. Mineral. Petrol.*, *70*, 299-318, 1979.

von Karman, T., Festigkeitsversuche unter allseitigem druck, *Zeitschr. Ver. deutsch. Ingenieure*, *55*, 1749-1757, 1911.

Walsh, J. B., The effect of cracks on the compressibility of rocks, *J. Geophys. Res.*, *70*, 381-389, 1965.

Wong, T.-f., Effects of temperature and pressure on failure and post-failure behavior of Westerly granite, *Mech. Mater.*, *1*, 3-17, 1982.

Wong, T.-f., Development of stress-induced anisotropy and localized deformation in brittle rock, in *Plastic Behavior of Anisotropic Solids*, edited by J. P. Bochler, pp. 321-339, 1985*a*.

Wong, T.-f., Geometric probability approach to the characterization and analysis of microcracking in rocks, *Mech. Mat.*, *4*, 261-276, 1985*b*.

Wong, T.-f., Mechanical compaction and brittle-ductile transition in porous sandstones, in *Deformation Mechanisms, Rheology and Tectonics*, edited by R. S. Knipe, Spec. Pub., Geol. Soc. London, in press, 1989*a*.

Wong, T.-f., A note on the propagation behavior of a crack nucleated by a dislocation pileup, in press, *J. Geophys. Res.*, 1989*b*.

Zener, C., The micro-mechanism of fracture, in *Fracturing of Metals*, edited by F. Johnson, W. P. Roop, and R. T. Bayles, pp. 3-31, ASM, Cleveland, Ohio, 1948.

FIGURE CAPTIONS

Figure 1. Strength and failure mode versus confining pressure for (*a*) Solnhofen limestone at room temperature and (*b*) elevated temperatures, (*c*) Carrara marble, and (*d*) pyroxenite and diabase. In Figures 1*a-d*, the transition from localized, brittle fracture to nonlocalized semibrittle flow is plotted. For comparison the differential stress necessary to cause frictional sliding on a fault inclined at 30° (and at 45° in Figure 1*b*) is shown by a dotted line. In Figures 1*e* and 1*f* the transition from semibrittle (nonlocalized dilatant deformation) to fully plastic flow (nonlocalized, nondilatant deformation) is shown for Solnhofen limestone and Carrara marble, respectively. Localized brittle fracture is denoted by circles, nonlocalized semibrittle flow by triangles, and nonlocalized, nondilatant, fully plastic flow by squares. Temperatures are indicated in Figures 1*b-f*. Symbols for the sources of data are as follows: Figures 1*a*, 1*c*, 1*e*, and 1*f*: B, *Byerlee* [1968*b*]; F, *Fischer and Paterson* [1989]; E, *Edmond and Paterson* [1972]; H, *Heard* [1960]; R, *Rutter* [1972*a*,*b*, 1974]. Figure 1*b*: SPB, *Schmid et al.* [1987], other symbols as above. Figure 1*d*: K, *Kirby and Kronenberg* [1984]; B, *Boland and Tullis* [1986]; C, *Caristan* [1982].

Figure 2. The propagation of a wing crack (of length ℓ) from the tip of a main crack (of length 2*c*) in the sliding crack model [from *Horii and Nemat-Nasser*, 1986]. The maximum compressive stress is σ_1 and the lateral compressive stress is σ_2. The main crack is at an angle γ with respect to the σ_1 direction. The angle between the wing crack and the main crack is θ.

Figure 3. The normalized stress intensity factor and the wing crack orientation as functions of the normalized wing crack extension for stress ratios λ of (*a*) 0.005 and (*b*) 1/3. The computation uses equation (1), which is for an isolated sliding crack with a friction coefficient of 0.3.

Figure 4. The normalized stress necessary for wing crack growth plotted as a function of the normalized crack length. Crack interaction is taken into account by combining the two components of stress intensity factor from equations (1) and (2), and wing crack propagation

occurs if $K_1 = K_c$. The calculation is for a friction coefficient of 0.3 and a crack density of 0.2. Note that for a stress ratio $\lambda < 0.01$, crack growth is unstable and may lead to crack coalescence and overall strain softening behavior.

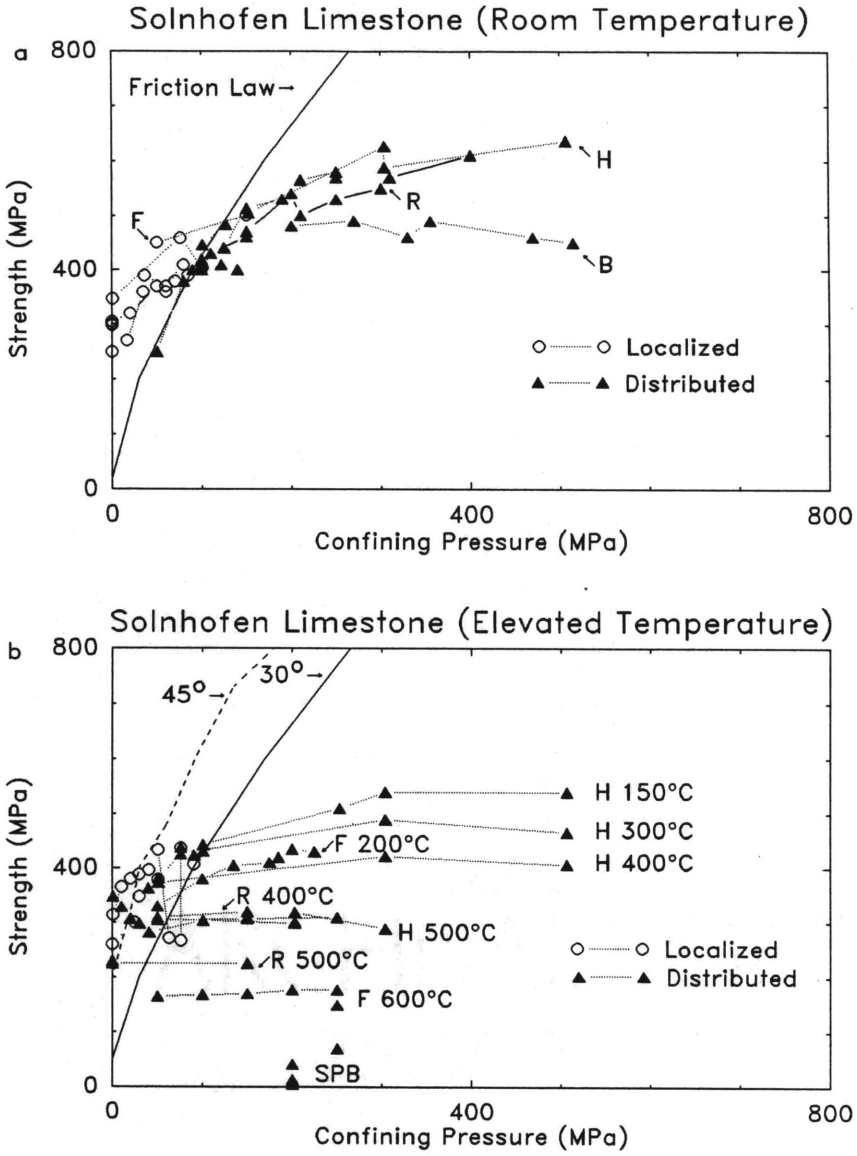
Solnhofen Limestone (Room Temperature)
a
800
400
0
Friction Law→
F
H
R
B
Localized
Distributed
Strength (MPa)
0
400
800
Confining Pressure (MPa)
Solnhofen Limestone (Elevated Temperature)
b
800
400
0
45°→
30°→
H 150°C
H 300°C
F 200°C
H 400°C
R 400°C
H 500°C
R 500°C
F 600°C
SPB
Localized
Distributed
Strength (MPa)
0
400
800
Confining Pressure (MPa)

Figure 1*a,b*

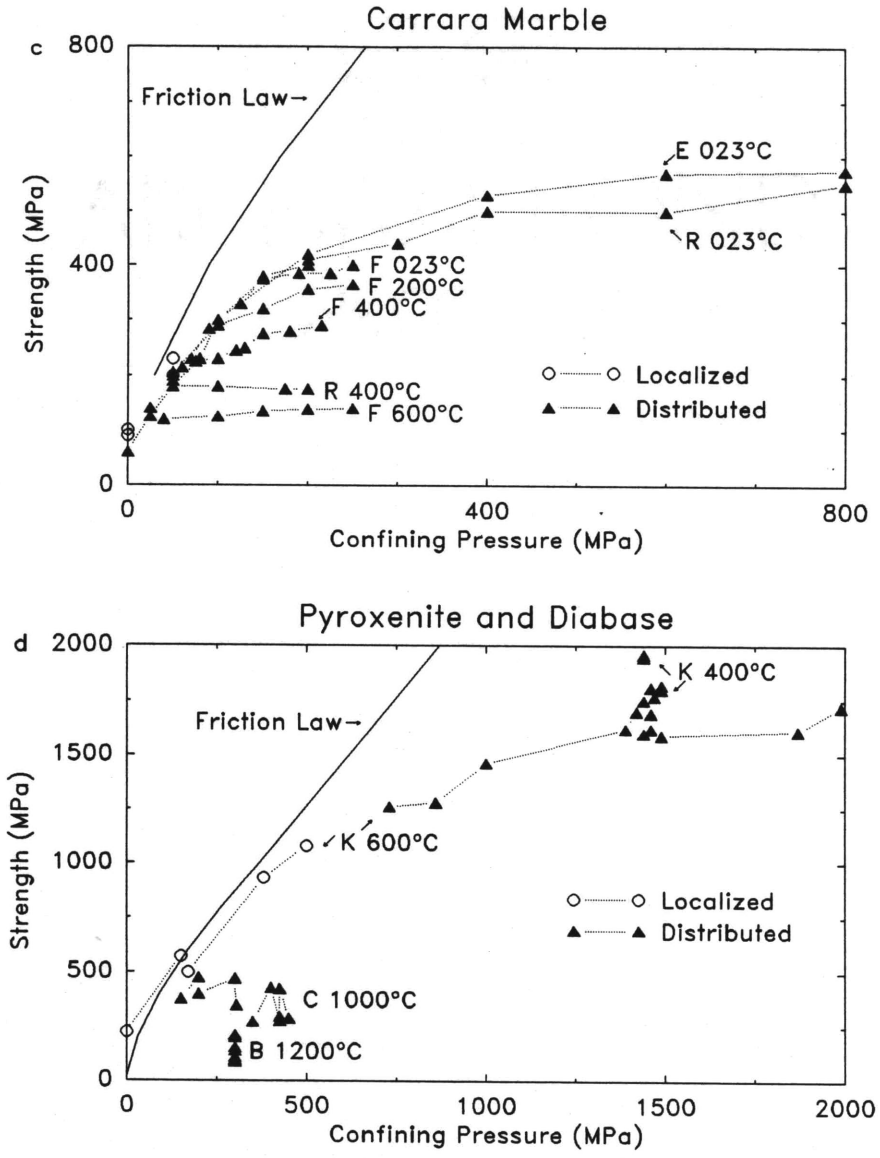
Carrara Marble
c
800
400
0
Strength (MPa)
Friction Law→
E 023°C
R 023°C
F 023°C
F 200°C
F 400°C
R 400°C
F 600°C
Localized
Distributed
0
400
800
Confining Pressure (MPa)
Pyroxenite and Diabase
d
2000
1500
1000
500
0
Strength (MPa)
Friction Law→
K 400°C
K 600°C
Localized
Distributed
C 1000°C
B 1200°C
0
500
1000
1500
2000
Confining Pressure (MPa)

Figure 1*c,d*

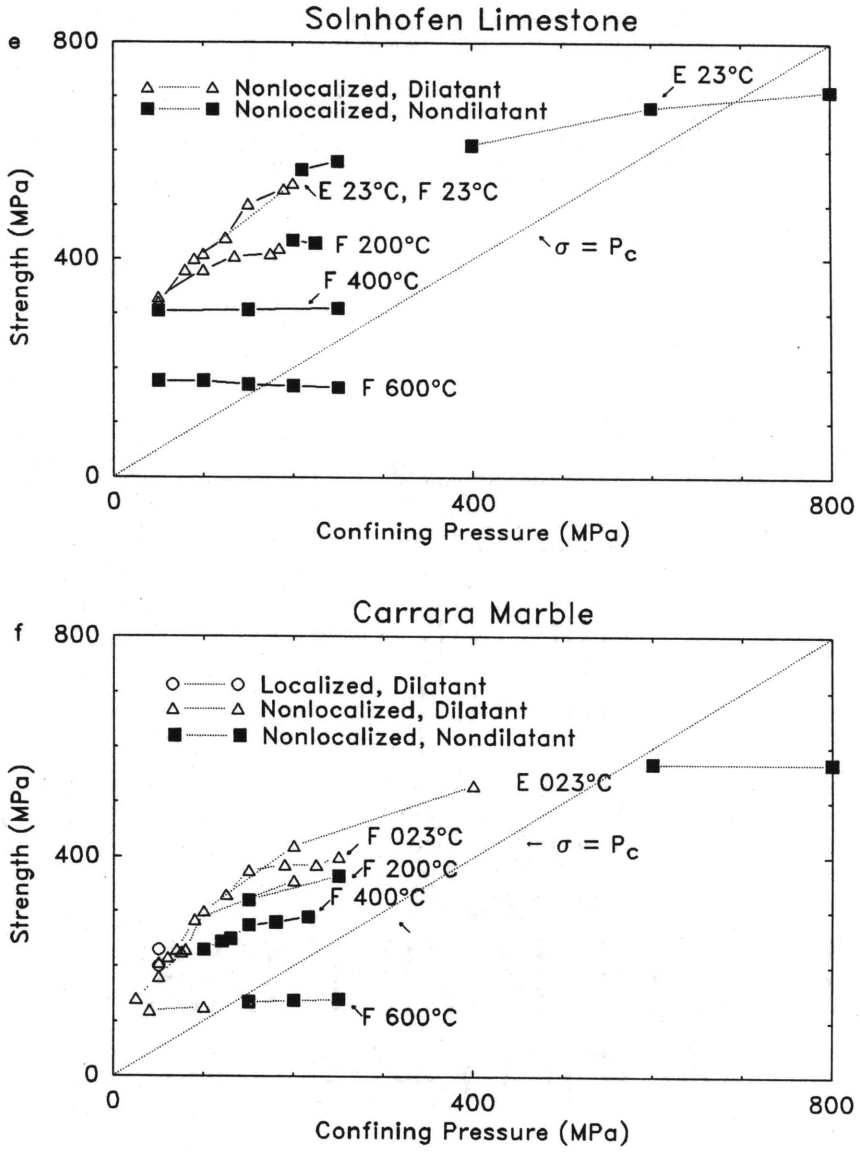
e
Solnhofen Limestone
Nonlocalized, Dilatant
Nonlocalized, Nondilatant
E 23°C
E 23°C, F 23°C
F 200°C
F 400°C
F 600°C
σ = Pc
Strength (MPa)
Confining Pressure (MPa)
0
400
800
f
Carrara Marble
Localized, Dilatant
Nonlocalized, Dilatant
Nonlocalized, Nondilatant
E 023°C
F 023°C
F 200°C
F 400°C
F 600°C
σ = Pc
Strength (MPa)
Confining Pressure (MPa)

Figure 1*e,f*

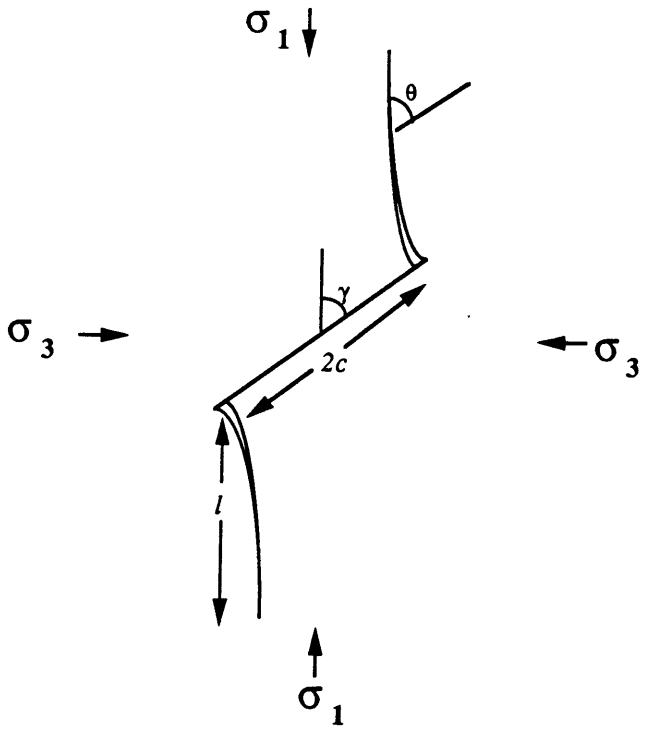

Figure 2

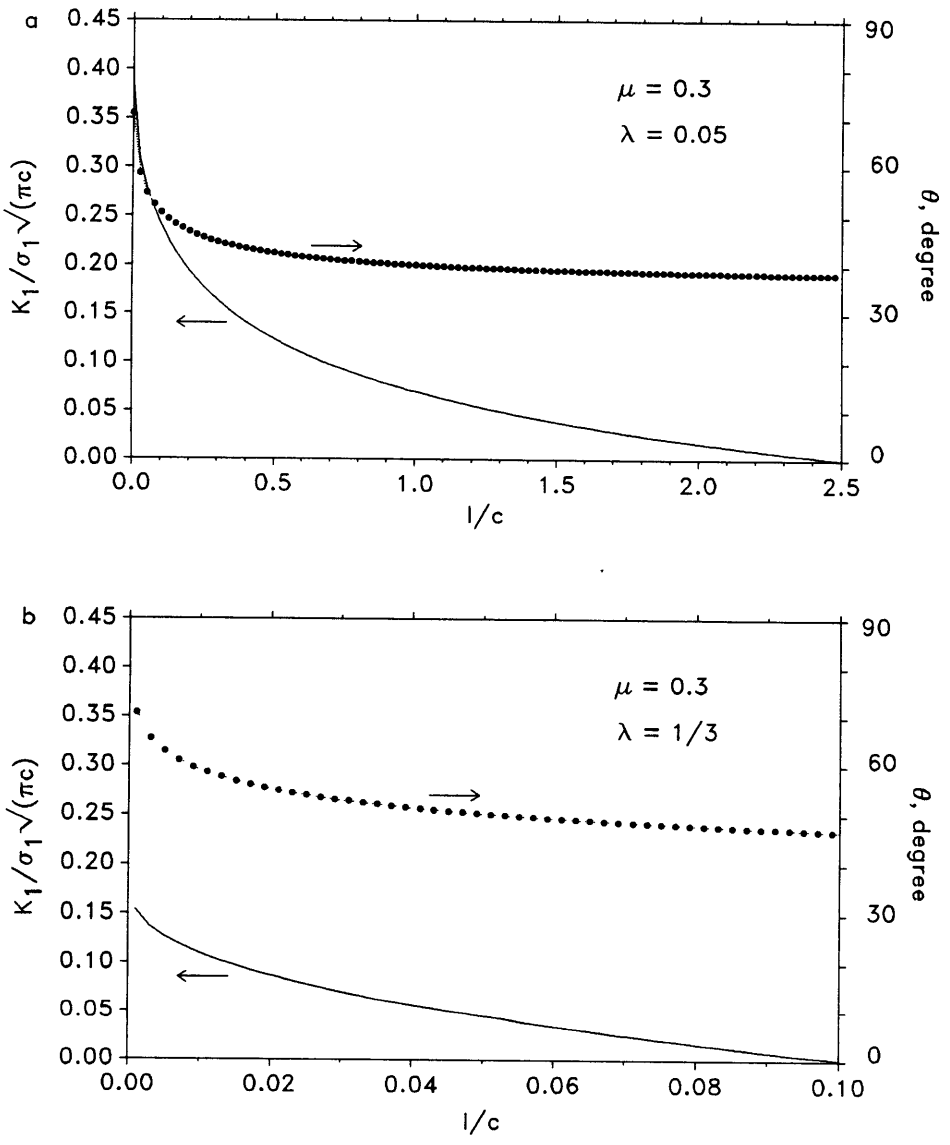
a
b
μ = 0.3
λ = 0.05
μ = 0.3
λ = 1/3
$K_1/\sigma_1\sqrt{(\pi c)}$
θ, degree
l/c

Figure 3*a,b*

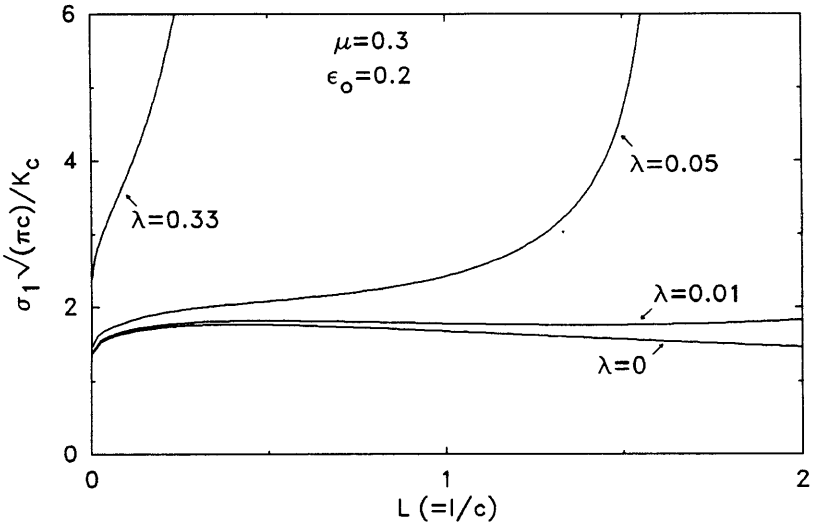

Figure 4

Chapter 3
Micromechanics of the Brittle to Plastic Transition in Carrara Marble

INTRODUCTION

Interest in the brittle-ductile transition has increased considerably in recent years, in large part due to the suggestion by *Sibson* [1982] that the maximum depth of seismicity is limited by a transition in deformation mechanism from localized brittle fracture to homogeneous plastic flow. The maximum stresses in the Earth are likely to be supported by semibrittle deformation [e.g., *Brace and Kohlstedt*, 1980], and various investigators have suggested that this is perhaps the most prevalent deformation mode in the lower crust and upper mantle [*Carter and Kirby*, 1978; *Kirby*, 1980; *Carter and Tsenn*, 1987].

A transition in mechanical behavior from localized brittle deformation to distributed flow may occur in two different ways, depending on rock type, effective pressure, temperature, and strain rate. In porous sandstone [*Handin and Hager*, 1957], quartzite [*Hadizadeh and Rutter*, 1983], and basalt [*Shimada*, 1986], a transition from localized brittle fracture to homogeneously distributed microcracking (e.g., cataclastic flow) can be induced at room temperature by an increase in effective pressure alone. Serpentine-bearing dunite and gabbro also undergo a brittle to ductile transition [*Byerlee*, 1968], probably due to the embrittlement of grain boundaries by the serpentine. *Shimada et al.* [1983] found that nonporous granite, gabbro, dunite, and eclogite remained in the brittle field when tested at room temperature and confining pressures up to 3 GPa. For confining pressures accessible in the laboratory, an increase in both temperature and pressure is necessary to activate crystal plasticity processes (and likewise to promote a brittle to plastic transition) in granite [*Tullis and Yund*, 1977], diabase [*Kronenberg and Shelton*, 1980; *Caristan*, 1982], clinopyroxenite [*Kirby and Kronenberg*, 1984; *Boland and Tullis*, 1986], and quartzite [*Hirth and Tullis*, 1986]. Marbles and limestones undergo a brittle-plastic transition at room temperature with increasing

confining pressure [*Robertson*, 1955; *Paterson*, 1958; *Heard*, 1960; *Rutter*, 1974], probably due to the relatively low shear stresses required to initiate twinning and slip in calcite at room temperature [*Turner et al.*, 1954; *Griggs et al.*, 1960].

Most experimental studies of the brittle to plastic transition have focused on macroscopic measurements of axial stress and strain and qualitative descriptions of the microstructural deformation mechanisms. Exceptions are studies by *Edmond and Paterson* [1972], *Schrodt and Holder* [1983], and *Fischer and Paterson* [1989]; these workers measured volumetric strain during semibrittle deformation and showed that dilatancy persists well into the "ductile" field. Although these studies have been useful in elucidating the general nature of the brittle-plastic transition, a number of fundamental questions remain unanswered. First, the mechanism by which localization is inhibited is poorly understood [e.g., *Paterson*, 1978]. *Wong and Biegel* [1985] have suggested that as confining pressure increases, microcracking ultimately may be isotropically distributed, implying a mechanism for the stabilization of cracking. *Tullis and Yund* [1987] have recently suggested that with increasing pressure and temperature, nonporous feldspar aggregates undergo an intermediate stage of cataclastic flow with no dislocation activity, although they did not address the micromechanical basis for the stabilization of cracking. Second, the issue of strain partitioning between the brittle and plastic flow mechanisms has been largely unaddressed, mainly because there have been no studies integrating macroscopic measurements of volumetric strain with quantitative microstructural characterization. Finally, interaction between the brittle and plastic flow processes is poorly understood (see reviews by *Carter and Kirby* [1978] and *Kranz* [1983]). Many of the studies documenting interactions between microcracks, dislocations, and twins have been on highly strained samples in which it is difficult to identify crack nucleation mechanisms or to determine spatial and temporal relationships between microcracks, dislocations, and twins.

In this study we investigate the micromechanics of the brittle-plastic transition with the aim of addressing the above three questions. We chose Carrara marble because it is a pure, crystalline, monominerallic, isotropic aggregate of low porosity [*Ramez and Murrell*, 1964; *Edmond and Paterson*, 1972]. In addition, the slip systems in calcite are well known [*Turner et al.*, 1954; *Griggs et al.*, 1960], and calcite is capable of being deformed plastically at room temperature. The latter characteristic is significant, since discriminating between deformation-induced microcracks and cracks caused by quenching has been a problem in previous studies [e.g., *Boland and Tullis*, 1986]. We integrate mechanical measurements of axial stress, axial strain, volumetric strain, and quantitative stereological characterization of the stress-induced microstructure using optical and transmission electron microscopy (TEM) on samples deformed to varying strains at confining pressures spanning the range in mechanical behavior from localized brittle fracture to fully plastic flow.

Experimental Procedures

Deformation Experiments

Precision ground cylindrical samples 15.88 mm in diameter and 38.10 mm in height were cored from two optically similar blocks of Carrara marble. The samples were predried in vacuo at 40°C, jacketed with either polyolefin heat shrink tubing or copper foil (see below), and deformed in the standard triaxial configuration at room temperature and confining pressures ranging from 5 to 450 MPa (Table 1). The confining medium was petroleum ether, except at 450 MPa, where argon gas was used, and samples were not vented to the atmosphere. Pressure was monitored with a Heise gauge and generally maintained constant to within 1 MPa. The axial load was provided by a piston driven at a constant displacement rate by a ball-screw mechanism and was measured with an external load cell; stresses calculated from the load are corrected for friction at the piston but refer to the original cross-sectional

area of the sample at room pressure. Displacement was measured with a differential transformer (DCDT) mounted between the moving piston and fixed lower platen. The stiffness of the loading system was 0.18 GN m^{-1} and was subtracted from the apparent displacement measured by the DCDT for calculation of axial strain. Axial strains are referred to the initial sample length at room pressure. The strain rate was 10^{-5} s^{-1}, and maximum axial strain was less than 6% for all experiments.

In some experiments, volumetric strain was measured with electric resistance strain gauges attached to thin foils of copper. Before attaching the strain gauges, samples were pressurized to the run pressure in order to collapse the jacket onto the sample. Gauges were then mounted onto the jacket parallel and perpendicular to the sample axis. For small strains, volumetric strain ϵ_V is given by

$$\epsilon_V = \epsilon_1 + 2\epsilon_r \tag{1}$$

where ϵ_1 and ϵ_r are the strains measured in the axial and radial directions, respectively. In order to ensure that the presence of the copper jacket was not affecting the strain measurements, two experiments were performed on hardened steel samples. Measurements made with gauges mounted on the copper-jacketed sample were identical (within experimental resolution) to those made with gauges mounted directly on the sample, indicating that the jacket had no appreciable effect on the strain measurements.

The load, displacement, and strain gauge signals were sampled by a 14-bit A/D converter at 1/s with resolutions of 3 bars, 1 μm, and 0.01 mstrain, respectively. Due to electrical noise and sample shortening, however, actual uncertainty in strain is 0.2% (when calculated from the DCDT signal) and 0.01% (when measured directly with strain gauges). Uncertainty in axial stress arises primarily from changes in cross-sectional area and is less than 8%. With one exception, the strength at 2% strain was reproducible to better than 20 MPa.

Optical and Transmission Electron Microscopy

Deformed samples selected for microscopy were impregnated with low viscosity epoxy and cut in half along a plane parallel to the axis of the sample. In cases where micrometer measurements indicated azimuthal variation in radial strain, samples were cut along the plane containing the maximum diameter.

Standard thin sections for transmitted optical microscopy, ultrathin sections for TEM, and thick (1-2 mm) polished sections for reflected optical microscopy were prepared from each half of the sample. Areas for TEM study were chosen at random; samples were not oriented. Ion-milled TEM samples were examined in bright-field in either a Philips EM300 or EM400 operating at 100 or 120 keV, respectively.

Quantitative Stereology

The stress-induced crack density and anisotropy were characterized quantitatively using standard stereological techniques [*Underwood*, 1970]. For reflected light microscopy, samples were coated with a thin layer of carbon to enhance the contrast from cracks and decrease that due to changes in crystallographic orientation at grain and twin boundaries. Although, in theory, spatial resolution in the scanning electron microscope (SEM) is much greater, we found that for cracks in marble, better contrast was obtained with the optical microscope (see *Nolen-Hoeksema and Gordon* [1987] for discussion of a similar phenomenon in a dolomitic marble).

Measurements were made at a magnification of x320 directly on the microscope as the sample was displaced in a fixed direction. Our test grid consisted of 20 parallel lines of length 2.0 mm and spaced by 0.2 mm. The number of crack intersections for each line was determined, and a set of 20 such measurements was then statistically analyzed to determine the mean and standard deviation. Crack densities were measured in two orthogonal directions,

with the mean number of cracks per unit length measured in a set of traverses parallel to σ_1 denoted by $P_L\|$ and that measured in a set of traverses perpendicular to σ_1 by $P_L{}^{\perp}$.

For a partially oriented system the total crack surface area per unit volume, S_V, is related to P_L (measured in a plane containing the axis of symmetry) by the relation [*Underwood*, 1970]

$$S_V = (\pi/2)P_L{}^{\perp} + (2 - (\pi/2)P_L\| \tag{2}$$

The degree of anisotropy is given by

$$\Omega_{12} = [P_L{}^{\perp} - P_L\|] \,/\, [P_L{}^{\perp} + ((\pi/2) - 1)P_L\|] \tag{3}$$

$$\Omega_{23} = [\pi/2(P_L{}^{\perp} - P_L\|)] \,/\, [(\pi/2)P_L{}^{\perp} + (2 - (\pi/2))P_L\|] \tag{4}$$

Physically, Ω_{12} represents the ratio of the length of cracks parallel to σ_1 to the total length of all cracks and Ω_{23} the ratio of crack surface area parallel to σ_1 to the total surface area of all cracks. Note that in the use of the above relations, we assume that the total crack population can be divided into two subpopulations: a set of cracks whose surfaces are randomly oriented and a set of cracks whose normals are aligned perpendicular to σ_1. This assumption has previously been shown to be valid for samples stressed in compression in the standard triaxial configuration [e.g., *Wong*, 1985].

For selected samples, approximately 15-20 TEM plates were exposed to obtain estimates of dislocation density. Dislocation line length per unit volume is equal to the number of dislocation endpoints divided by the area of the projection [*Underwood*, 1970].

Data Analysis

Using the axial stress-strain data, the volumetric strain measurements, and the stereological crack density data, we can analyze quantitatively the energetics of deformation. In a triaxial test with $\sigma_2 = \sigma_3 = \text{const}$, the energy input per unit volume (dW) for an increment of inelastic axial strain ($d\epsilon_1$) is given by [*Edmond and Paterson*, 1972]

$$dW = (\sigma_1 - \sigma_3)d\epsilon_1 + P_C(d\epsilon_V) \tag{5}$$

where $(\sigma_1 - \sigma_3)$ is the differential stress, P_C is the confining pressure, and $d\epsilon_V$ is an increment in inelastic volumetric strain (note the convention that compressive stresses and strains are positive). The total energy input per unit volume W during an experiment is thus given by

$$W = P_C(\epsilon_V) + \int (\sigma_1 - \sigma_3)d\epsilon_1 \quad (6)$$

The first term represents the work done against the confining pressure and is negative for dilation; ϵ_V is the inelastic dilation measured after unloading but before the release of confining pressure. The second term is the area under the complete axial stress-strain curve (i.e., loading and unloading portions) and can be calculated by numerical integration. Calculated values of W were reproducible to within 5%.

A lower bound on the energy dissipation per unit volume (M) by microcracking may be determined from the stereological crack density data using the relation [*Wong*, 1982*a*]

$$M = 2(S_V - S_V^0)\gamma = (S_V - S_V^0)G_{IC} \quad (7)$$

where S_V and S_V^0 are the crack surface area per unit volume in the stressed and unstressed sample determined from the stereological data with equation (2). G_{IC} is the critical energy release rate for mode I cracking and is equal to twice the specific surface energy γ. Numerous SEM studies have demonstrated that most microcracks formed under deviatoric compressive stresses open in mode I [e.g., *Tapponier and Brace*, 1976; *Wong*, 1982*b*; *Kranz*, 1983].

RESULTS

Mechanical Data

The axial stress-strain data (Figure 1*a*) show a transition in mechanical behavior with increasing confining pressure (P_C), similar to that previously observed for other marbles and limestones [e.g., *Paterson*, 1978]. Briefly, at low P_C (5-10 MPa), samples soften with strain, and deformation is localized on a single macroscopic shear fault. For $P_C \approx$ 30-450 MPa, the overall level of the axial stress-strain curve increases with P_C and shows work hardening.

Samples deformed at P_C of 30-50 MPa are barrelled, with numerous conjugate shear cracks visible on the sample surface. Samples deformed at larger P_C are more nearly cylindrical. At 450 MPa, strength is only 5% greater than that at 300 MPa (Table 1), and it is likely that at this pressure, the behavior is nearly fully plastic (due to strain gauge failure during this experiment, we cannot say with certainty that the sample did not dilate during deformation). Our results are comparable to those of *Edmond and Paterson* [1972] and *Fischer and Paterson* [1989], who performed similar experiments on Carrara marble.

In Figure 2 we plot the macroscopic initial yield stress (σ_Y), defined as the differential stress at which the axial stress-strain curve deviates from linearity, the differential stress at the onset of dilatancy (C') [e.g., *Brace et al.*, 1966], and the strength at 2% strain ($\sigma_{2\%}$) as a function of P_C. At room temperature, calcite deforms plastically by twinning on the e={0112} planes and glide on the r={1011} planes, and for comparison, the applied differential stresses necessary for e^- twinning and r^- slip on optimally oriented planes are also shown (single crystal data of *Turner et al.* [1954] and *Griggs et al.* [1960]). At low P_C, microcracking is clearly significant in controlling the initial yielding as well the strength. For P_C greater than 85 MPa, σ_Y is constant, whereas C' increases continually with P_C and is significantly greater than σ_Y, suggesting that constant-volume deformation mechanisms (i.e., twinning or dislocation glide) are responsible for the initial yield. At higher P_C the macroscopic applied differential stresses are beginning to reach those required for r^- slip and dislocation glide is probably occurring in an increasing number of grains.

The slope of the volumetric strain-axial strain curve m (dimensionless) (Figure 1*c*) and the postyield slope of the axial stress-axial strain curve h (units of stress) (Figure 1*a*) were estimated by visually fitting a straight line to the data. The "dilatancy coefficient" m plotted as a function of P_C (Figure 3*a*) shows that the contribution of microcracking to the imposed deformation decreases continuously with increasing confining pressure (a slope of zero corresponds to plastic flow), particularly over the pressure ranges of 5-85 MPa. The

"hardening coefficient" h (Figure 3*b*) increases with P_C for pressures up to 450 MPa. It should be pointed out that our estimates of h are averages, since for pressures greater than 85 MPa, the axial stress-strain curve deviates slightly from linearity and has a finite concave curvature. Also, h may be overestimated by up to 8% due to the increase in cross-sectional area with axial strain (which is neglected in the calculation for axial stress).

Optical and Transmission Electron Microscopy Observations

Starting material. The optical microstructure of the unstressed material is characterized by a low density of twins (Figure 4*a*) and microcracks (Table 2). Grains are generally equiaxed (grain size = 0.23 ± 0.04 mm) and occasionally show blocky undulatory extinction. TEM observation indicates a free dislocation density of (9.18 ± 4.72) x 10^8 cm^{-2} (Table 3), in good agreement with the range of (1-13) x 10^8 cm^{-2} given by *Schmid et al.* [1980] for the same rock. Free dislocations are gently curved and there is a high density of loops, sometimes forming trails (Figure 5*a*). Dislocations are sometimes organized into networks forming low-angle subgrain boundaries.

Brittle samples. As stated previously, observations of microcrack structure were not performed with the SEM, and so only the gross features of the crack structure were resolved optically. At a confining pressure of 5 MPa, the axial stress-strain curve shows work softening, although macroscopic faulting is only associated with the large stress drop at 1-1.5% strain (Figure 1*a*); we will refer to samples CM24 and CM21 as prefailure and postfailure (Table 1 and Figure 1*a*). Both the prefailure and postfailure samples exhibit significantly higher crack densities than the unstressed sample, with the postfailure sample having the larger increase. A large proportion of the cracks are aligned parallel to σ_1 (Figure

4*b*); cracking occurs along grain boundaries, intragranularly, and intergranularly. Intergranular cracks extending over three or four grains are common in both the prefailure and postfailure samples. The localized zone in the postfailure sample is typically about two to three grain diameters wide. In both samples, some grains exhibit a high density of mechanical twins.

Semibrittle samples. Optical and TEM observations indicate that deformation mechanisms active in this regime include microcracking, twinning, and dislocation glide. Optically, the deformation microstructure is quite heterogeneous, even on the intragranular scale.

At constant P_C microcrack density increases with increasing differential stress and axial strain. At constant strain the density of microcracks decreases with increasing P_C. As observed in the brittle field (Figure 4*b*), microcracking occurs predominantly in directions subparallel to σ_1 (Figure 4*c*). Besides the decreased density of microcracking, the most obvious difference between crack structures in the brittle and semibrittle samples is the absence of intergranular cracks extending over three to four grains in the latter (compare Figures 4*b* and 4*c*). For samples deformed at $P_C > 300$ MPa, the microcrack density is comparable to that in the starting material.

Mechanical twins are present in all of the deformed samples. Sample CM11 was stressed to σ_Y at a pressure of 120 MPa and then unloaded. Optical examination indicates a slight increase in the density of twins (Figure 4*d*) and suggests that in the semibrittle field, twinning is the dominant element for the initial yield (see previous discussion). The density of twins increases with axial strain at constant P_C (Figures 4*e* and 4*f*). Twin geometries are quite complex, with two and sometimes three sets of twins active in a single grain. Bent and kinked twins are also common.

In samples deformed at pressures as low as 50 MPa, some grains exhibit structures indicative of dislocation glide (Figure 5*b*). Dislocation loops are common in some grains and appear to form from the breakdown of dislocation dipoles (Figure 5*b*), although other

mechanisms are possible. Twin boundaries sometimes appear to act as barriers to dislocation glide (Figure 5*c*). The irregular distribution of dislocations in the vicinity of the twin boundary suggests that these are not twinning dislocations, but rather dislocations whose glide has been hindered due to the change in crystallographic orientation at the twin boundary. Dislocation structures which suggest tangling and pinning were frequently observed (Figures 5*b*, 5*c*, and 5*d*), suggesting that (thermally activated) recovery is limited.

Geometries strongly suggestive of interaction between the brittle and plastic deformation mechanisms were sometimes observed, with the association of twins and microcracks most common. Figure 6*a* shows a microcrack which appears to have nucleated at a twin boundary. The twin width is different above and below the microcrack, suggesting that as the twin expanded laterally, it encountered an obstacle which impeded its propagation, and the resulting stress concentration nucleated a microcrack. This association was frequently observed in TEM, and similar features were observed optically (although the inhomogeneity in twin thickness at the nucleation site is not resolvable optically). Cracks nucleated in this way generally propagated for only very short distances (i.e., $<<$ grain diameter). In another example, the stress concentration at the end of a twin has apparently nucleated a void (Figure 6*b*). The dislocation density is high in the vicinity of the void, and it is possible that the void has grown by emitting dislocations. Intersections of twin lamallae (Figure 6*c*) were frequently observed to be the site of void formation. This latter mechanism of crack nucleation has previously been observed in experimentally deformed iron [*Hull*, 1960] and marble [*Olsson and Peng*, 1976], and naturally deformed calcite [e.g., *Barber and Wenk*, 1979].

Another possible example of dislocation-microcrack interaction is shown in Figure 6*d* and is suggestive of crack blunting [e.g., *Rice and Thompson*, 1974]. This crack appeared to nucleate in a manner identical to that shown in Figure 6*a* (this part of the crack is not shown in the micrograph), reinforcing our interpretation that the twin nucleated the microcrack, rather than vice versa [e.g., *Marshall and McLaren*, 1977]. It is possible that the crack

initially propagated at too high a velocity for the continuous laying down of a trail of dislocations but that as the crack grew away from the local stress concentration, it slowed down and catastrophically blunted [e.g., *Argon*, 1987]. Cleavage cracks associated with high dislocation densities were also observed (Figure 6*e*).

Quantitative Microstructural Data

The stereological crack density data indicate that in the semibrittle field, stress-induced crack density (Figures 7*a* and 7*b* and Table 2) and anisotropy (Figure 7*d* and Table 2) at constant strain decrease with increasing P_C. At constant P_C, stress-induced crack area increases with axial strain (Figure 7*c*), whereas crack anisotropy either increases or remains approximately constant (Figure 7*d*). In contrast, in the brittle field, the prefailure crack density increases whereas the crack anisotropy decreases with increasing confining pressure [e.g., *Wawersik and Brace*, 1971; *Kranz*, 1980; *Wong and Biegel*, 1985].

Stress-induced crack anisotropy is significant at pressures up to 190 MPa, and, in fact, some semibrittle samples deformed to axial strains of 2.8-4.6% are approximately as anisotropic as the prefailure brittle sample deformed to 1% strain (Figure 7*d* and Table 2). This suggests that the microcrack structure in the semibrittle field is dominated by propagation effects, rather than by the details of the nucleation mechanism (i.e., whether cracks are nucleated as "wing" cracks or from dislocation pileups).

It is worthwhile to consider the extent to which the crack density measurements reflect the microcrack population induced during deformation, since this question has been raised previously. In particular, during the release of pressure after plastic deformation of marble and limestone, *Paterson* [1963] observed "secondary" changes in length in excess of the normal elastic changes expected. He postulated that residual stresses resulting from the anisotropy of yield stress in calcite caused extensive microfracturing during depressurization. We do not think that such effects were significant in our experiments for the following

reasons: Measurements of axial strain made at room pressure generally agreed within a few tenths of a percent with the strain measured after unloading but before depressurization (allowing for elastic decompression of the sample). In Paterson's case the observed secondary strains were of the order of a few percent. Second, dilatancy (measured during straining) scales directly with crack density (measured at room pressure after the experiment). Finally, residual stresses induced during unloading and depressurization should scale with P_C and differential stress. Therefore samples deformed at higher P_C and differential stresses are more likely to have cracking induced by residual stresses. Our data (Table 2), however, show that the stress-induced crack density (measured optically) decreases with increasing pressure and, in fact, is negligible for $P_C \geq 300$ MPa. Thus we conclude that our crack density measurements are a reasonable measure of the microcrack population induced during deformation. *Paterson* [1963] noted that such effects depended on total strain and were more significant in the coarse-grained Wombeyan marble than in the fine-grained Solnhofen limestone. In our experiments, axial strains were $<6\%$ (as compared to 18% for Paterson's experiments), and the grain size of Carrara marble is intermediate between those of the two carbonate rocks in Paterson's study.

An additional point which is difficult to resolve definitively is whether the majority of the crack surface area is resolved optically. There undoubtedly is pore surface of dimension less than the resolution of the optical microscope; however, the relative significance of our measurements (i.e., from sample to sample) will not be affected as long as the density of the unresolvable crack surface area does not increase in the deformed samples as compared to the unstressed sample. Whether or not this is the case is difficult to ascertain; however, we note that our TEM observation of the deformed samples did not seem to indicate a preponderance of cracks of dimension < 1 μm. Furthermore, the density of these small cracks did not appear to vary noticeably with confining pressure.

Dislocation densities were measured in samples deformed at confining pressures of 120-450 MPa and differential stresses up to 320-330 MPa (Table 3). Since in a polycrystalline sample, the shear stress resolved on any particular slip system varies from grain to grain (depending on orientation), dislocation density is expected to be quite variable. The data at $P_C = 120$ MPa show small increases in mean density and standard deviation (Table 3); however, it is not clear whether or not the changes are significant. For $P_C \geq 230$ MPa, the increases in mean density and standard deviation are large (Table 3), indicating that a statistically significant proportion of the grains are deforming plastically. Our qualitative observations of changing dislocation structure indicate that at least on a local scale, dislocation glide is occurring in some grains at pressures as low as 50 MPa (Figure 5*b*).

Discussion

Energetics of Brittle and Semibrittle Deformation

Our microscopy observations indicate that deformation in the brittle field is accommodated by microcracking and twinning and, in the semibrittle field, by microcracking, twinning, and dislocation glide. A basic question concerning the deformation is: what is the difference in strain partitioning between the brittle and plastic mechanisms in the brittle and semibrittle fields? A partial answer to this question can be obtained by considering the energetics of inelastic deformation.

For the deformation considered here, energy sinks include microcracking, crystal-plastic processes, production of heat, and acoustic emission. A minimum bound on the energy dissipation due to microcracking (M) is given by equation (7). The total work done on the sample during deformation (W) may be calculated with equation (8) (see Table 4). The ratio M/W is the ratio of brittle energy dissipation to total energy dissipation during deformation.

A necessary input parameter for the calculation of M/W is the tensile fracture energy G_{IC} (equation (7)). Typically, there is an order-of-magnitude difference between G_{IC} measured for a cleavage crack in a single crystal and that for a macrocrack propagating through a polycrystalline sample of the same material [*Friedman et al.*, 1972; *Atkinson*, 1984; *Swanson*, 1987]. The use of G_{IC}=0.54-0.70 J m^{-2} measured for (1011) cleavage cracks in single crystals of calcite [*Atkinson*, 1984] will lead to an underestimation of M since a significant proportion of the stress-induced microcracks are not cleavage cracks and thus necessarily lie along higher energy paths (see Figures 4*b* and 4*c*). Conversely, the use of G_{IC}=6.9 J m^{-2} for a macrocrack in Carrara marble [*Atkinson*, 1984] may lead to an overestimation of M since the process zone for a macrocrack is undoubtedly larger than that for a microcrack. We expect that the appropriate G_{IC} for our calculation actually lies between these two bounds. An additional complication is that G_{IC} may actually be a function of confining pressure. With increasing confining pressure, deviatoric stresses increase and dislocations become increasingly mobile. Thus plastic blunting of microcracks may occur, thereby decreasing the effective stress intensity factor K_I at the crack tip. In fact, our TEM observations of crack-dislocation interactions suggest that such effects may be significant as confining pressure increases (see Figures 4*d*, 5*b*, and 5*d*). In addition, *Swanson* [1987] suggested that frictional tractions along mode I macrocracks can lead to large apparent increases in fracture toughness. Such effects will become increasingly significant with increasing confining pressure. At present, however, there are no quantitative data with which we can assess the significance of these effects, and so we will assume that γ is constant with pressure.

In Figure 8 we plot the ratio M/W as a function of confining pressure. As an approximation, we use G_{IC}=3.8 J m^{-2} (the average of the measurements for a single-crystal cleavage crack in calcite and that for a macrocrack in Carrara marble). The point which we emphasize is that the energy budget for microcracking is clearly a decreasing function of confining pressure and, in the semibrittle field, is at least 66% lower than that at the

prefailure stage in the brittle regime. This conclusion remains valid for any choice of G_{IC}, as long as G_{IC} is approximately constant with confining pressure. Within the pressure range of 5-85 MPa, *M/W* decreases sharply with pressure, whereas at pressures greater than about 85 MPa, the data suggest an almost asymptotic approach to fully plastic flow. For pressures greater than about 300 MPa, when energy dissipation due to production of crack surface area is nearly negligible, the applied differential stresses are beginning to reach those necessary to activate r⁻ slip in an optimally oriented grain (Figure 2) (the Von Mises criterion requires the activation of both e⁻ twinning and r⁻ slip for homogeneous, fully plastic flow in polycrystalline calcite [*Paterson*, 1969]).

In the brittle field, increases in surface area caused by stress-induced microcracking can account for only about 12% of the total energy dissipation in the prefailure sample (Figure 8). Although the stress-induced crack surface area may be underestimated due to the resolution limit of the microscope, it seems unlikely that the stereological measurements could be off by more than a factor of 2. Acoustic emission is unlikely to account for significant energy dissipation. *Wong* [1985] observed a similar phenomenon for samples of San Marcos gabbro deformed in the brittle field and attributed the difference to energy dissipation through frictional sliding and plastic kinking of biotite. Frictional sliding undoubtedly accounts for some of the energy dissipation in our experiments and, indeed, is an essential element in models of brittle fracture in compression [e.g., *Kachanov*, 1982; *Horii and Nemat-Nasser*, 1985; *Ashby and Hallam*, 1986]. Energy dissipation through frictional sliding should follow a trend similar to that in Figure 8 since the amount of sliding accomplished is directly related to the amount of crack surface available for sliding, which decreases with increasing confining pressure (Figures 7*a* and 7*b*). The decrease in the dilatancy coefficient as a function of confining pressure (Figure 3*a*) may be indirect evidence of the decreasing contribution of frictional sliding with increasing pressure, since frictional sliding on shear cracks nucleates dilatant "wing" cracks [e.g., *Brace et al.*, 1966]. Other workers have shown that in the

brittle field, volumetric strain prior to failure increases with increasing pressure [*Kranz*, 1980; *Blacic et al.*, 1981].

In the semibrittle field, work done during shear to create twins is probably mainly dissipated as heat and can account for up to 20% of the total energy dissipated during deformation (W), assuming as an upper bound that about 25% of the volume fraction is twinned (Figures 3*e* and 3*f*), and that the twinning stress is 10 MPa. Twin boundary energies in calcite are of the order of 10^{-2} J m^{-2} [*Klassen-Neklyudova*, 1964] and, for our purposes, consume negligible amounts of energy. The remaining energy is undoubtedly dissipated through lattice friction resistance to dislocation glide (Figures 5*b*-5*d* and 6) and increases in dislocation line length/volume (Table 3).

Development of Shear Localization in the Brittle Field

The mode of inelastic deformation and failure of our samples deformed at a confining pressure of 5 MPa have all the attributes of brittle behavior. Dilatancy (Figure 1*b*) and the development of a stress-induced crack anisotropy (Figure 7*d*) are appreciable. Beyond peak stress, strength decreases (Figure 1*a*) and is accompanied by shear localization at an angle of about 30° to the maximum differential stress.

As was pointed out by *Olsson and Peng* [1976], some of the micromechanical processes causing dilatancy in calcite rocks deformed in the brittle field are different from those observed in low- porosity silicate rocks. Olsson and Peng emphasized the role of mechanical twinning in nucleating microcracks, whereas microcracking in silicate rocks is generally attributed to stress concentrations at grain boundaries, cracks and pores, and elastic mismatch between neighboring grains [e.g., *Kranz*, 1983].

Whereas we also observe that stress concentrations due to mechanical twins do nucleate microcracks, we find that most microcracks in our prefailure and postfailure samples deformed in the brittle field do not show any clear association with twinning. Our microscopy

observations indicate that a significant proportion of the stress-induced microcracks are oriented parallel to the maximum stress direction. The micromechanical processes leading to shear localization in Carrara marble seem to be similar to those observed in low-porosity silicate rocks [e.g., *Evans and Wong*, 1985].

A significant question concerning the development of shear localization in both Carrara marble and silicate rocks is whether localization occurs in the work softening or work hardening stage. As previously noted, localization in samples deformed at 5 MPa does not occur until well into the softening stage at about 1-1.5% axial strain, as was also observed by *Wawersik and Fairhurst* [1970] in experiments on Tennessee marble. Although *Wawersik and Brace* [1971] observed localization in the softening stage in experiments on granite and diabase, most studies of brittle fracture in silicate rocks have found that localization typically occurs in the hardening stage in the immediate vicinity of peak stress (see summary of experimental observations by *Evans and Wong* [1985]). This disparity, however, is unlikely to be attributable to any basic difference between carbonate and silicate rocks, since shear localization and failure in the finer-grained Saillon marble and Solnhofen limestone occur in a manner similar to that typically observed in silicate rocks [see Chapter 3].

Deformation in the Semibrittle Field

The transition between brittle failure and plastic flow spans a range of confining pressures of 30-300 MPa in Carrara marble [*Edmond and Paterson*, 1972; *Rutter*, 1974; this study, *Fischer and Paterson*, 1989]. In this regime, deformation is accommodated by a combination of microcracking, twinning, and dislocation glide. For confining pressures up to about 100 MPa, the strength (Figure 2), dilatancy coefficient (Figure 3*a*), and hardening coefficient (Figure 3*b*) are highly pressure-sensitive. For pressures of 100-300 MPa, $\sigma_{2\%}$, m, and h are less pressure-sensitive and tend to level off asymptotically.

Our stereological data indicate that the development of a stress-induced crack density and anisotropy is significant in the semibrittle field for confining pressures up to 190 MPa (Table 2). Specifically, the data show that semibrittle samples deformed to axial strains of 2.8 and 4.6% at confining pressures of 40 and 85 MPa develop a crack anisotropy and density almost identical to the prefailure brittle sample deformed to 1% strain at 5 MPa (Table 2 and Figures 7*c* and 7*d*). Similarly, semibrittle samples deformed to axial strains >3% at pressures up to 120 MPa have crack densities significantly greater than that of the prefailure brittle sample (Table 2 and Figures 7*a* and 7*b*). Certainly, a fundamental question is: given the high stress-induced crack density and anisotropy in some of the semibrittle samples, why does shear localization not develop?

From a continuum mechanics point of view, strain localization can be analyzed as an instability in the macroscopic constitutive description of inelastic deformation. *Rudnicki and Rice* [1975] formulated a constitutive relation for pressure-sensitive, dilatant materials involving three parameters: an internal friction coefficient (μ), a dilatancy factor (β), and a hardening modulus (h'). Note that the parameters β and h' differ slightly from our definitions of m and h (see Table 5). For axisymmetric compressive loading, their bifurcation analysis predicts that decreases in μ and β result in an increase in the angle of the shear zone to the maximum differential stress, with a maximum angle of 45°. For a wide range in values of the parameters μ and β appropriate for brittle rocks, Rudnicki and Rice's analysis predicts the onset of shear localization only when the hardening coefficient h' has attained a critical negative value h'_{cr}.

In Table 5 we list the values of the parameters μ, β, and h' determined from our experimental data [see *Rudnicki*, 1977*a*]. Also given is the incremental Poisson's ratio ν, as defined by the slope $-\epsilon_r/\epsilon_1$. We find that in the semibrittle field, h' increases, whereas β and ν decrease with increasing confining pressure. The slope μ is equal to 0.5 for pressures less than 120 MPa and 0.2 for pressures of 120-300 MPa. Our estimates of μ are consistent with

those calculated by *Rudnicki and Rice* [1975] from experimental data in the literature, whereas our values of β tend to be slightly higher, particularly at low pressures. Conjugate shear cracks observed on the surfaces of semibrittle samples deformed at 30 and 50 MPa may be related to the decrease in β with confining pressure.

The critical hardening modulus h'_{cr} normalized by the incremental shear modulus G necessary for localization is given by (equation 20 of *Rudnicki and Rice* [1975])

$$h'_{cr}/G = [(1+\nu)(\beta-\mu)^2/9(1-\nu)] - [(1+\nu)/2]\{N+[(\beta+\mu)/3]\}^2 \quad (8)$$

where N is equal to $1/\sqrt{3}$ for axisymmetric compression. For the values of μ, β, and ν found in all of our experiments, Rudnicki and Rice's analysis predicts the onset of shear localization only when the hardening modulus h' is negative, a condition which is realized only in the experiment at 5 MPa (Table 5). As was noted by Rudnicki and Rice, their model predicts overly negative slopes, in that unrealistically high reductions in the incremental shear modulus are required to match the hardening rates typically observed prior to localization. For example, to match the observed hardening rate prior to localization in the experiment at 5 MPa, a reduction of $\approx 5 \times 10^2$ in the shear modulus would have been required over the course of the experiment. However, the predicted slopes are more realistic if the effects of yield vertices [*Rudnicki and Rice*, 1975] and stress-induced anisotropy [*Cleary and Rudnicki*, 1976; *Rudnicki*, 1977*b*] are considered. For the experiments at 40 MPa and greater, the observed hardening rates are positive, whereas the theoretical hardening rates required for localization are negative (Table 5). Rudnicki and Rice's model thus suggests that shear localization is inhibited in the semibrittle field as long as the samples continue to work harden.

Our microscopy observations can, in part, explain the transition in mechanical behavior from work softening to work hardening. We observe a qualitative difference in the characteristic dimensions of stress-induced cracks in the brittle and semibrittle samples. In the prefailure brittle sample there are many relatively long intergranular cracks which propagate through as many as three or four grains (Figure 4*b*). In the semibrittle field, however, cracks

are significantly shorter and generally only propagate along grain boundaries or intragranularly (Figure 4*c*). In the semibrittle field, intergranular cracking and crack coalescence (and therefore strain softening and localization) are undoubtedly inhibited, in part, by the stabilizing effect of increased confining pressure on crack propagation [e.g., *Francois and Wilshaw*, 1968]. Our microscopy observations, however, suggest that dislocations might also aid intragranular crack arrest (Figures 6*b* and 6*d*) and that intergranular cracking is probably inhibited by the increased density of plastically "soft" grains with increased confining pressure and differential stress (Figures 5*b* and 5*c*). Cracks impinging on such grains are probably more likely to induce slip rather than continued crack propagation.

In fact, the parameter $\mathbf{M}<a>^2$, where $\mathbf{M}$ is the number of cracks per unit area and $<a>$ is the average crack length, is central to *Madden's* [1983] analysis of rock fracture as a critical phenomenon using a renormalization group approach. The same parameter enters into the theoretical calculation of the elastic moduli of a cracked solid [*Budiansky and O'Connell*, 1976], where their "crack density" ϵ is proportional to $\mathbf{M}<a>^2$, assuming that crack lengths are distributed over a relatively narrow range [e.g., *Abdel-Gawad et al.*, 1987]. In Madden's analysis, ϵ attains a value of 1 at criticality (or 0.8 if crack anisotropy is considered). It can be shown that $\mathbf{M}<a>^2$ is proportional to $P_L<a>$ [e.g., *Wong*, 1985], and so an increase in ϵ can come about through an increase in either the number or length of cracks. Our qualitative observations indicate that cracks are shorter in the semibrittle field; thus, although P_L in the semibrittle samples is similar to that observed in the brittle samples, ϵ is smaller.

An interesting implication of the above is that work softening and localization should still occur at some point, given our observations that P_L increases with strain at constant confining pressure. Although our experiments were only carried out to axial strains of $<6\%$, similar experiments on Carrara marble by *Edmond and Paterson* [1972] and *Fischer and Paterson* [1989] show that semibrittle deformation is stable for axial strains of 20%. Our analysis of the energetics of inelastic deformation suggested that although the stress-induced crack surface

area and anisotropy in some of the semibrittle samples is comparable to that observed in the prefailure brittle samples, the ratio of brittle energy dissipation to total energy dissipation is actually significantly lower in the semibrittle field (Figure 8). It is likely that a more detailed understanding of the interactions between microcracks, dislocations, and twins is necessary before we can more fully understand the stability of deformation in the semibrittle field.

Work Hardening at High Pressures

Our data for the pressure dependence of M/W (Figure 8), the dilatancy coefficient (Figure 3*a*), and dislocation density (Table 3) suggest that plastic flow accommodates increasing amounts of the imposed deformation with increasing confining pressure. These observations, coupled with the observed positive pressure dependence of the hardening coefficient (Figure 3*b*), suggest that the observed work hardening over the pressure range of 120-450 MPa is strongly influenced by plastic flow processes.

Work hardening during plastic flow has been studied extensively [e.g., *Hirth and Weertman*, 1968] and is attributable to a variety of mechanisms, including glide-dislocation interaction with forest dislocations and accumulated dislocation loops (see review by *Nabarro et al.* [1964]). The back stress exerted by pinned dislocations inhibits the glide of free dislocations, and thus an increase in the applied differential stress is necessary for additional increments in strain. Our TEM observations indicate that both mechanisms may contribute to the observed hardening rates (Figures 5*b*, 5*c*, and 5*d*). An additional mechanism for hardening in polycrystals is the back stress caused by dislocation pileups at grain and twin boundaries (Figure 5*b*). If the work hardening in the marble is caused by such mechanisms, then as dislocation motion accommodates increasing amounts of the deformation (and as dislocation density increases), the hardening coefficient should increase as well.

The hardening coefficient may be expressed as

$$h = d\sigma/d\epsilon_1 = (d\sigma/d\rho)(d\rho/d\epsilon_1) \quad (9)$$

where ρ is dislocation density. The $d\sigma/d\rho$ may be found from the well-established relation between dislocation density and stress [e.g., *Takeuchi and Argon*, 1976]

$$\sigma=\alpha G b \rho^{0.5} \tag{10}$$

where α is an experimentally determined constant, G is the shear modulus, and b is the Burgers vector. An approximate bound on $d\rho/d\epsilon_1$ may be obtained from the experimental data (Table 3). Since our hardening coefficient is in terms of differential stress (not resolved shear stress), and the dislocation densities are averages obtained from different grains, we use the value of α determined for polycrystalline calcite. Taking α=2.24 and b=6.35 x 10^{-10} m [*Goetze and Kohlstedt*, 1977] and G=32.7 GPa (the average of the Voight and Reuss bounds at room temperature [*Simmons and Wang*, 1971]) and using our dislocation density data for pressures of 300 and 450 MPa (Table 3), the predicted hardening rates are 2.4 and 3.5 GPa, as compared with the observed rates of 3.1 and 3.6 GPa, respectively. Given the intrinsic uncertainties in the calculation and the fact that the measured dislocation densities are not steady state densities, we find the agreement between the predicted and observed hardening coefficients (Figure 3*b*) to be quite reasonable, thus supporting our contention that deformation is accommodated almost exclusively by plastic flow at confining pressures of 300 MPa and greater.

Conclusions

When loaded in axisymmetric compression, at room temperature, strain rates of 10^{-5} s^{-1}, and in the absence of pore fluids, Carrara marble deforms by brittle fracture at pressures less than 30 MPa, plastically at pressures greater than 300 MPa, and in a stable, semibrittle mode at intermediate pressures. In agreement with earlier studies [*Edmond and Paterson*, 1972 and *Schrodt and Holder*, 1983] we find that dilatancy persists to quite high pressures, indicating that small amounts of volume producing processes (i.e., microcracking) are necessary for

deformation. In order to extend these and other laboratory results to predict semibrittle deformation in the Earth, constitutive laws must be formulated which incorporate accurate models of the micromechanical processes. Our experimental data and microstructural observations provide new insights into the details of the localization process and the micromechanics of semibrittle flow.

The transition from localized brittle fracture to nonlocalized semibrittle flow is not marked by drastic changes in either the density or the anisotropy of stress-induced cracks or in the mean dislocation density. For example, samples deformed to the prefailure stage in the brittle field have crack densities and anisotropies quite similar to that developed in samples deformed in the semibrittle regime at pressures up to 120 MPa (but to higher strains). Nor are there striking differences in the relative proportions of grain boundary versus intragranular cracking in the two fields (although we have not quantified this observation). We do, however, detect a qualitative difference in the characteristic length of cracks in the brittle and semibrittle fields. The effect of crack length on localization can be rationalized using *Madden's* [1983] analysis of rock fracture as a critical phenomenon. Likewise, elastic analyses of cracks [e.g. *Horii & Nemat-Nasser*, 1985] predict that interactions between cracks are increased for cracks which are either longer or more closely spaced. Thus measurements of crack density and anisotropy alone may not be sufficient to characterize the damage structure necessary for localization; future microstructural studies should attempt quantitative characterizations of crack length as well.

Our results are consistent with the notion that localization in marble is inhibited with increased confining pressure by the enhanced plasticity of the rock matrix coupled with the increased difficulty of crack propagation. Microstructural observations suggest that above 85 MPa twinning is responsible for the initial yield. There is also qualitative evidence of local dislocation glide in semibrittle samples deformed at pressures as low as 50 MPa. As suggested by *Edmond and Paterson* [1972], it seems likely that at lower pressures, crystal plasticity

does not supply sufficient independent strain elements to satisfy a Von Mises-type criterion, and thus continued microcracking is necessary until the strength reaches levels sufficient to activate dislocation glide on a large scale.

The microstructural observations imply that brittle and plastic deformation mechanisms interact in a variety of ways. Cracks and voids appear to nucleate at sites of stress concentration at twin boundaries, at twin terminations, and at the intersection of twin lamallae. Geometries suggestive of crack tip shielding by dislocations are also observed. The pronounced anisotropy of microcracking in the semibrittle regime and the observed decrease in crack length at a given strain with increasing pressure suggest that the overall microcrack structure is controlled by propagation effects, rather than by the details of the nucleation mechanism. The role of dislocations in "blunting" microcracks or otherwise limiting void growth or crack propagation is likely to be significant in determining the deformation style and the inhibition of localization.

Estimates of strain partitioning between the brittle and plastic deformation mechanisms suggest that the energy dissipated through microcracking normalized by the total work done during deformation is at least 60% lower in the semibrittle field than in the brittle field. The most marked changes in strain partitioning occur over a range in pressure which is relatively small compared to the range over which the deformation is semibrittle. Because the strain contributions of microcracking may be relatively small for a large range of pressure, qualitative observations at the outcrop scale, for example, may not be sensitive indicators of the extent to which rocks are, or are not, deforming by pressure-sensitive processes.

Phenomenologically similar transitions are likely to occur in nonporous silicate rocks with increasing pressure and temperature, although we note that it has been suggested that the activation of plastic deformation mechanisms may not be a necessary requirement for the inhibition of localization [e.g., *Tullis and Yund*, 1987].

REFERENCES

Abdel-Gawad, M., J. Bulau, and B. Tittman, Quantitative characterization of microcracks at elevated pressure, *J. Geophys. Res.*, *92*, 12,911-12,916, 1987.

Argon, A. S., Brittle to ductile transition in cleavage fracture, *Acta Metall.*, *35*, 185-196, 1987.

Ashby, M. F., and S. D. Hallam, The failure of brittle solids containing small cracks under compressive stress states, *Acta Metall.*, *34*, 497-510, 1986.

Atkinson, B. K., Subcritical crack growth in geological materials, *J. Geophys. Res.*, *89*, 4077-4114, 1984.

Barber, D. J., and H.-R. Wenk, Deformation twinning in calcite, dolomite and other rhombohedral carbonates, *Phys. Chem. Miner.*, *5*, 141-165, 1979.

Blacic, J. D., P. H. Halleck, P. D'Onfro, and R. E. Riecker, Thermomechanical properties of Galesville sandstone, in *Mechanical Behavior of Crustal Rocks*, *Geophys. Monogr. Ser.*, vol. 24, edited by N. L. Carter, M. Friedman, J. M. Logan, and D. W. Stearns, pp. 153-159, AGU, Washington, D. C., 1981.

Boland, J. N., and B. E. Hobbs, Microfracturing processes in experimentally deformed peridotite, *Int. J. Rock Mech. Min. Sci. Geomech. Abstr.*, *10*, 623-626, 1973.

Boland, J. N., and T. E. Tullis, Deformation behavior of wet and dry clinopyroxenite in the brittle to ductile transition region, in *Mineral and Rock Deformation: Laboratory Studies*, *Geophys. Monogr. Ser.*, vol. 36, edited by B. E. Hobbs and H. C. Heard, pp. 35-50, AGU, Washington, D. C., 1986.

Brace, W. F., B. W. Paulding, and C. H. Scholz, Dilatancy in the fracture of crystalline rocks, *J. Geophys. Res.*, *71*, 3939-3953, 1966.

Brace, W. F., and D. L. Kohlstedt, Limits on lithospheric stress imposed by laboratory experiments, *J. Geophys. Res.*, *85*, 6248-6252, 1980.

Budiansky, B., and R. J. O'Connell, Elastic moduli of a cracked solid, *Int. J. Solids Struct.*, *12*, 81-97, 1976.

Byerlee, J. D., Brittle-ductile transition in rocks, *J. Geophys. Res.*, *73*, 4741-4750, 1968.

Caristan, Y., The transition from high temperature creep to fracture in Maryland diabase, *J. Geophys. Res.*, *87*, 6781-6790, 1982.

Carter, N. L., and S. H. Kirby, Transient creep and semi-brittle behavior of crystalline rocks, *Pure Appl. Geophys.*, *116*, 807-839, 1978.

Carter, N. L., and M. C. Tsenn, Flow properties of continental lithosphere, *Tectonophysics*, *136*, 27-63, 1987.

Cleary, M. P., and J. W. Rudnicki, The initiation and propagation of dilatant rupture zones in geological materials, in *The Effects of Voids on Material Deformation*, edited by S. C. Cowin, pp. 13-30, American Society of Mechanical Engineers, New York, 1976.

Devore, J. L., *Probability and Statistics for Engineering and the Sciences*, Brooks/Cole, Monterey, Calif., 1982.

Edmond, J. M., and M. S. Paterson, Volume changes during the deformation of rocks at high pressures, *Int. J. Rock Mech. Min. Sci. Geomech. Abstr.*, *9*, 161-182, 1972.

Evans, B., and T.-f. Wong, Shear localization in rocks induced by tectonic deformation, in *Mechanics of Geomaterials*, edited by Z. Bazant, John Wiley, pp. 189-210, New York, 1985.

Fischer, G. J., and M. S. Paterson, Dilatancy during rock deformation at high temperatures and pressures, *J. Geophys. Res.*, *94*, 17607-17618, 1989.

Francois, D., and T. R. Wilshaw, The effect of hydrostatic pressure on the cleavage fracture of polycrystalline materials, *J. Appl. Phys.*, *39*, 4170-4177, 1968.

Friedman, M., J. Handin, and J. Alani, Fracture surface energy of rocks, *Int. J. Rock Mech. Min. Sci. Geomech. Abstr.*, *9*, 757-766, 1972.

Goetze, C., and D. L. Kohlstedt, The dislocation structure of experimentally deformed marble, *Contrib. Mineral. Petrol.*, *59*, 293-306, 1977.

Griggs, D. T., F. J. Turner, and H. C. Heard, Deformation of rocks at 500° to 800°C, in Rock Deformation, edited by D. T. Griggs and J. Handin, *Mem. Geol. Soc. Am.*, *79*, 39-104, 1960.

Hadizadeh, J., and E. H. Rutter, The low temperature brittle-ductile transition in a quartzite and the occurrence of cataclastic flow in nature, *Geol. Rundsch.*, *72*, 493-509, 1983.

Heard, H. C., Transition from brittle fracture to ductile flow in Solenhofen limestone as a function of temperature, confining pressure and interstitial fluid pressure, in Rock Deformation, edited by D. T. Griggs and J. Handin, *Mem. Geol. Soc. Am.*, *79*, 193-226, 1960.

Hirth, G., and J. Tullis, Cataclastic flow of dry non-porous quartzite (abstr.), *Eos Trans. AGU*, *67*, 1186, 1986.

Hirth, J. P., and J. Weertman, *Work Hardening*, Gordon and Breach, New York, 1968.

Horii, H., and S. Nemat-Nasser, Compression-induced microcrack growth in brittle solids: axial splitting and shear failure, *J. Geophys. Res.*, *90*, 3105-3125, 1985.

Hull, D., Twinning and fracture of single crystals of 3% silicon iron, *Acta Metall.*, *8*, 11-18, 1960.

Kachanov, M. L., A microcrack model of rock inelasticity, part I, Frictional sliding on microcracks, *Mech. Mater.*, *1*, 19-27, 1982.

Kirby, S. H., Tectonic stresses in the lithosphere: Constraints provided by experimental deformation of rocks, *J. Geophys. Res.*, *85*, 6353-6363, 1980.

Kirby, S. H., and A. K. Kronenberg, Deformation of clinopyroxenite: Evidence for a transition in flow mechanisms and semibrittle behavior, *J. Geophys. Res.*, *89*, 3177-3192, 1984.

Klassen-Neklyudova, M. V., *Mechanical Twinning of Crystals*, Consultants Bureau, New York, 1964.

Kranz, R. L., The effects of confining pressure and stress difference on static fatigue of granite, *J. Geophys. Res.*, *85*, 1854-1866, 1980.

Kranz, R. L., Microcracking in rocks, a review, *Tectonophysics*, *100*, 449-480, 1983.

Kronenberg, A. K., and G. L. Shelton, Deformation microstructures in experimentally deformed Maryland diabase, *J. Struct. Geol.*, *2*, 341-353, 1980.

Madden, T. R., Microcrack connectivity in rocks: a renormalization group approach to the critical phenomena of conduction and failure in crystalline rocks, *J. Geophys. Res.*, *88*, 585-592, 1983.

Marshall, D. B., and A. C. McLaren, Deformation mechanisms in experimentally deformed plagioclase feldspars, *Phys. Chem. Miner.*, *1*, 351-370, 1977.

Nabarro, F. R. N., Z. S. Basinski, and D. B. Holt, The plasticity of pure single crystals, *Adv. Phys.*, *13*, 193-323, 1964.

Nolen-Hoeksema, R. C., and R. B. Gordon, Optical detection of crack patterns in the opening-mode fracture of marble, *Int. J. Rock Mech. Min. Sci. Geomech. Abstr.*, *24*, 135-144, 1987.

Olsson, W. A., and S. S. Peng, Microcrack nucleation in marble, *Int. J. Rock Mech. Min. Sci. Geomech. Abstr.*, *13*, 53-59, 1976.

Paterson, M. S., Experimental deformation and faulting in Wombeyan marble, *Geol. Soc. Am. Bull.*, *69*, 465-476, 1958.

Paterson, M. S., Secondary changes of length with pressure in experimentally deformed rocks, *Proc. R. Soc. London Ser. A*, *271*, 57-87, 1963.

Paterson, M. S., The ductility of rocks, in *Physics of Strength and Plasticity*, edited by A. S. Argon, pp. 379-392, M.I.T. Press, Cambridge, Mass., 1969.

Paterson, M. S., *Experimental Rock Deformation-the Brittle Field*, Springer-Verlag, New York, 1978.

Ramez, M. R. H., and S. A. F. Murrell, A petrofabric analysis of Carrara marble, *Int. J. Rock Mech. Min. Sci. Geomech. Abstr.*, *1*, 217-229, 1964.

Rice, J. R., and R. Thomson, Ductile versus brittle behavior of crystals, *Phil. Mag.*, *29*, 73-97, 1974.

Robertson, E. C., Experimental study of the strength of rocks, *Geol. Soc. Am. Bull.*, *66*, 1275-1314, 1955.

Rudnicki, J. W., The inception of faulting in a rock mass with a weakened zone, *J. Geophys. Res.*, *82*, 844-854, 1977*a*.

Rudnicki, J. W., The effect of stress-induced anisotropy on a model of brittle rock failure as localization of deformation, *Proc. U.S. Symp. Rock Mech.*, *18th*, 3B41-3B48, 1977*b*.

Rudnicki, J. W., and J. R. Rice, Conditions for the localization of deformation in pressure-sensitive dilatant materials, *J. Mech. Phys. Solids*, *23*, 371-394, 1975.

Rutter, E. H., The influence of temperature, strain rate and interstitial water in the experimental deformation of calcite rocks, *Tectonophysics*, *22*, 331-334, 1974.

Schmid, S. M., M. S. Paterson, and J. N. Boland, High temperature flow and dynamic recrystallization in Carrara marble, *Tectonophysics*, *65*, 245-280, 1980.

Schrodt, J. K., and J. T. Holder, Temperature and strain rate effects on micromechanical behavior in triaxially compressed marbles, *Proc. U.S. Symposium on Rock Mechanics*, *24th*, 449-468, 1983.

Shimada, M., A. Cho, and H. Yukatake, Fracture strength of dry silicate rocks at high confining pressures and activity of acoustic emission, *Tectonophysics*, *22*, 331-334, 1983.

Shimada, M., Mechanism of deformation in a dry porous basalt at high pressures, *Tectonophysics*, *121*, 153-173, 1986.

Sibson, R. H., Fault zone models, heat flow, and the depth distribution of earthquakes in the continental crust of the United States, *Bull. Seismol. Soc. Am.*, *72*, 151-163, 1982.

Simmons, G., and H. Wang, *Single Crystal Elastic Constants and Calculated Aggregate Properties*, M.I.T. Press, Cambridge, Mass., 1971.

Swanson, P. L., Tensile fracture resistance mechanisms in brittle polycrystals: An ultrasonics and insitu microscopy investigation, *J. Geophys. Res.*, *92*, 8015-8036, 1987.

Takeuchi, S., and A. S. Argon, Steady state creep of single-phase crystalline matter at high temperature, *J. Mater. Sci.*, *11*, 1542-1566, 1976.

Tapponnier, P., and W. F. Brace, Development of stress-induced microcracks in Westerly granite, *Int. J. Rock Mech. Min. Sci. Geomech. Abstr.*, *13*, 103-113, 1976.

Tullis, J., and R. A. Yund, Experimental deformation of dry Westerly granite, *J. Geophys. Res.*, *82*, 5705-5718, 1977.

Tullis, J., and R. A. Yund, Transition from cataclastic flow to dislocation creep of feldspar: Mechanisms and microstructures, *Geology*, *15*, 606-609, 1987.

Turner, F. J., D. T. Griggs, and H. C. Heard, Experimental deformation of calcite crystals, *Geol. Soc. Am. Bull.*, *65*, 883-934, 1954.

Underwood, E. E., *Quantitative Stereology*, Addison-Wesley, Reading, Mass., 1970.

Wawersik, W. R., and C. Fairhurst, A study of brittle rock fracture in laboratory compression experiments, *Int. J. Rock Mech. Min. Sci. Geomech. Abstr.*, *7*, 561-575, 1970.

Wawersik, W. R., and W. F. Brace, Post-failure behavior of a granite and diabase, *Rock Mech.*, *3*, 61-85, 1971.

Wong, T.-f., Shear fracture energy of Westerly granite from post-failure behavior, *J. Geophys. Res.*, *87*, 990-1000, 1982*a*.

Wong, T.-f., Micromechanics of faulting in Westerly granite, *Int. J. Rock Mech. Min. Sci. Geomech. Abstr.*, *19*, 49-64, 1982*b*.

Wong, T.-f., Geometric probability approach to the characterization and analysis of microcracking in rocks, *Mech. Mater.*, *4*, 261-276, 1985.

Wong, T.-f. and R. Biegel, Effects of pressure on the micromechanics of faulting in San Marcos gabbro, *J. Struct. Geol.*, *7*, 737-749, 1985.

TABLE 1. Deformation History of Samples

Sample	P_C, MPa	$(\sigma_1-\sigma_3)_{max}$, MPa	ϵ_1[a], %	C'[b], MPa	σ_Y[c], MPa	$\sigma_{2\%}$[d], MPa
CM1	85	257	4.64	*	*	232
CM2	150	331	5.16	*	*	268
CM3	50	195	4.85	*	*	190
CM4	30	150	4.21	*	*	158
CM5	120	319	5.36	*	*	267
CM6	10	108	5.16	*	*	97
CM7	190	349	5.46	*	*	272
CM11	120	195	0.71	*	*	*
CM12	120	219	0.90	*	*	*
CM13	50	209	2.38	*	*	207
CM14	120	267	2.99	*	*	246
CM16	230	319	3.63	*	*	284
CM20	85	224	1.45	*	*	*
CM21	5	95	1.88	*	*	*
CM22	190	275	1.35	*	*	*
CM24	5	95	0.95	62	77	*
CM25	85	249	4.91	159	110	220
CM26	120	299	5.55	178	118	242
CM27	120	293	5.34	171	110	244
CM28	190	299	3.45	203	115	270
CM29	190	333	5.14	212	112	265
CM30	300	329	3.00	247	130	296
CM31	40	173	2.81	99	88	172
CM32	120	283	5.28	150	122	234
CM33	450	320	2.20	*	*	312

[a]Total axial strain (elastic + permanent).

[b]Differential stress at the onset of dilatancy.

[c]Differential stress at the onset of nonlinearity in the axial stress-strain curve. Data only reported for cases where C' was measured.

[d]Differential stress at 2% axial strain.

TABLE 2. Stereological Crack Density Data

Sample	$P_L^{\perp}$, mm^{-1}	$P_L\|\|$, mm^{-1}	S_V, mm^2/mm^3	Ω_{12}	Ω_{23}
CM0	2.10±1.00	1.48±0.92	3.93	*	*
CM1	20.50±2.41	12.40±1.94	37.52	0.29	0.34
CM5	14.30±2.18	9.95±1.73	26.73	0.22	0.26
CM7	4.80±1.45	3.53±1.63	9.05	0.19	0.22
CM12	9.75±2.40	6.73±1.12	18.20	0.22	0.26
CM14	11.55±2.79	7.68±1.20	21.44	0.24	0.28
CM20	8.53±1.98	6.43±1.24	16.15	0.17	0.20
CM22	1.95±1.10	2.60±1.13	4.18	*	*
CM24	9.10±2.65	5.45±1.86	16.63	0.30	0.35
CM30	2.75±1.15	3.20±1.80	5.69	*	*
CM31	17.53±5.31	10.30±2.97	31.95	0.31	0.36

*Statistical analysis using the Smith-Satterthwaite test [*Devore*, 1982] indicated that the difference between $P_L\|$ and $P_L^{\perp}$ was not significant at the 99% confidence level.

TABLE 3. Dislocation Density Measurements

Sample	P_C, MPa	$(\sigma_1-\sigma_3)_{max}$, MPa	ρ_{max}[a]	ρ_{min}[a]	ρ_{ave}[a]
CM0	*	*	17	3	9.2±4.7
CM5	120	319	22	4	12.0±5.4
CM16	230	319	49	7	14.9±10.1
CM30	300	329	50	6	20.9±10.6
CM33	450	320	46	9	22.4±10.1

[a]Dislocation density in units of 10^8 cm^{-2}.

TABLE 4. Energy Input During Deformation

Sample	P_C, MPa	$\epsilon_V{}^a$, %	$P_C(\epsilon_V)^b$, 10^4 J m^{-3}	W^c, 10^4 J m^{-3}
CM24	5	3.10	15.5	39.9
CM31	40	3.90	156.0	221.6
CM25	85	2.15	182.8	800.3
CM27	120	2.75	330.0	903.0
CM32	120	2.22	266.4	891.5
CM29	190	0.60	114.0	1164.7
CM30	300	0.11	33.6	666.7

[a]Permanent volumetric strain measured after unloading but before release of P_C.

[b]The first term on the right-hand side of equation (6).

[c]Equation (6).

TABLE 5. Constitutive Parameters and Hardening Rates

Sample	P_C, MPa	β^a	μ^b	ν^c	$h'_{cr}{}^d$	$h'_{tan}{}^e$, MPa
CM24	5	1.20	0.51	1.05	$-3.39G$	-184.8
CM31	40	0.76	0.51	1.76	$-1.41G$	≈ 0
CM25	85	0.29	0.51	0.80	$-0.60G$	264.1
CM27	120	0.23	0.36	0.73	$-0.50G$	368.2
CM32	120	0.26	0.36	0.80	$-0.54G$	411.1
CM29	190	0.06	0.21	0.55	$-0.34G$	768.0
CM30	300	0.03	0.21	0.38	$-0.29G$	947.7

[a]Dilatancy factor (dimensionless). Similar to our dilatancy coefficient m expressed in terms of shear strain [see *Rudnicki*, 1977*a*].

[b]Coefficient of friction (dimensionless). This parameter is equal to the slope of a plot of C' (expressed in terms of shear stress) versus mean stress [see *Rudnicki*, 1977*a*].

[c]Incremental Poisson's ratio, defined by the slope $-\epsilon_r/\epsilon_1$.

[d]Predicted critical hardening modulus for the inception of localization (equation (8)). Expressed in terms of the incremental shear modulus G.

[e]Observed hardening modulus h'_{tan}. This parameter is equal to h' for $h'/G << 1$. Similar to our hardening coefficient h expressed in terms of shear stress and shear strain [see *Rudnicki*, 1977*a*].

FIGURE CAPTIONS

Figure 1. Representative sampling of (*a*) axial stress-axial strain, (*b*) axial stress-volumetric strain, and (*c*) volumetric strain-axial strain curves for samples deformed at the indicated confining pressures. Note that dilatancy is defined as negative and compaction as positive. In Figures 1*b* and 1*c* data are not shown for P_C=40 MPa past 4% volumetric strain due to a problem with the gain setting used during data acquisition. The jumpiness in the curves at 85 and 300 MPa was caused by a small leak in the pressure vessel during these runs. Corresponding experiments are (*a*) CM24 and (*b* and *c*) CM21 (50 MPa); CM31 (400 MPa); CM25 (85 MPa); (*a* and *b*) CM27 and (*c*) CM32 (120 MPa); CM29 (190 MPa); and CM30 (300 MPa).

Figure 2. Macroscopic initial yield stress (triangles), differential stress at the onset of dilatancy (squares), and strength at 2% strain (circles) versus confining pressure; σ_Y is constant at pressures greater than about 100 MPa, whereas C' increases with pressure for pressures up to 300 MPa. The pressure sensitivity of $\sigma_{2\%}$ is greatest over the interval 5-100 MPa. For comparison, the applied differential stresses necessary for e^- twinning and r^- slip on optimally oriented planes are shown [*Turner et al.*, 1954; *Griggs et al.*, 1960].

Figure 3. (*a*) The dilatancy coefficient m and (*b*) hardening coefficient h versus confining pressure (see text for definitions). The pressure sensitivity of both m and h is greatest for pressures up to 100 MPa.

Figure 4. Optical micrographs of (*a*) the starting material and (*b-f*) deformed samples. All micrographs are 1.25 mm across. Figures 4*b* and 4*c* are of samples CM24 and CM5, respectively, and are reflected light micrographs of thick sections; the rest are transmitted light micrographs of samples CM0 (Figure 4*a*), CM11 (Figure 4*d*), CM14 (Figure 4*e*), and CM5 (Figure 4*f*). (*a*) The virgin rock has a low density of twins; some grains show blocky undulatory extinction. (*b*) In a prefailure sample deformed in the brittle field there is a high density of microcracks, a large portion of which are aligned parallel to σ_1 (oriented horizontal

and in the plane of the section). (*c*) Microcracking in a sample deformed in the semibrittle field is strongly anisotropic (same orientation as in Figure 4*b*). In the semibrittle field, microcracks are shorter than those observed in the prefailure brittle sample (Figure 4*b*), and generally only propagate intragranularly and along grain boundaries. (*d*) There is a noticeable increase in the twin density in a sample stressed to σ_Y and then unloaded. (*e*) and (*f*) The density of twins increases with strain and twinning is complex. Single grains often twin on more than one system.

Figure 5. TEM micrographs of the (*a*) starting and (*b-d*) stressed samples. All micrographs were taken in bright-field and are of samples CM0 (Figure 5*a*), CM13 (Figure 5*b*), and CM5 (Figures 5*c* and 5*d*). (*a*) The dislocation density in the starting material is high. Dislocations are gently curved, and there is a high density of loops, sometimes forming trails. (*b*) Dislocation glide apparently occurs in some grains in samples deformed at pressures as low as 50 MPa. Note the high density of loops (L) which may form from the breakdown of dislocation dipoles (D). (*c*) The high density and irregular distribution of dislocations in the vicinity of twin boundaries suggest that twins were sometimes obstacles to dislocation glide (the twin (T) is out of contrast and oriented NW-SE). Also note the apparent pinning of dislocations by other dislocations. (*d*) Intersecting dislocations frequently formed attractive and repulsive junctions.

Figure 6. TEM micrographs showing interactions between the brittle and plastic deformation mechanisms. All micrographs were taken in bright-field and are of samples CM14 (Figures 6*a* and 6*c*)), CM5 (Figure 6*b*), CM16 (Figure 6*d*), and CM2 (Figure 6*e*). (*a*) A crack (C) appears to have nucleated at a point in the twin (T) boundary where there is an inhomogeneity in twin thickness (see text for details). (*b*) A void (V) has apparently grown near the tip of a twin (T) (out of contrast) which terminated within a grain. A high density of dislocations (in contrast) is evident and it is possible that the void has grown by emitting dislocations. (*c*) Voids (V) were frequently observed at the intersection of twin lamallae. (*d*)

A string of dislocations appears to emanate from the tip of a crack (C) which nucleated in a manner identical to that shown in (Figure 6*a*). The dark speckling in the background is due to beam damage which occurs quite rapidly for some crystallographic orientations. (*e*) Cleavage cracks are sometimes associated with high dislocation densities. The two cracks (oriented NE-SW) are linked by a third crack (oriented NW-SE) which is oblique to the plane of the micrograph. A line of dislocations is colinear (although not necessarily coplanar) with the lower crack.

Figure 7. The stereological parameters $P_L\|$ (solid symbols) and $P_L{}^{\perp}$ (open symbols) versus axial strain for samples deformed at pressures of (*a*) 5 MPa (circles), 40 MPa (squares), and 85 MPa (triangles) and (*b*) 120 MPa (circles), 190 MPa (squares), and 300 MPa (triangles). The data at 0% strain (diamonds) are for the unstressed sample. For clarity, $P_L\|$ and $P_L{}^{\perp}$ are offset. (*c*) The stress-induced crack surface area S_V-$S_V{}^0$ (equation (2)) versus confining pressure. (*d*) Crack anisotropy Ω_{23} (equation (3)) versus confining pressure. In Figures 7*c* and 7*d*, data are shown at different axial strains, which are indicated next to each data point.

Figure 8. Energy dissipation through increase in crack surface area (M) normalized by the total work input during deformation (W) versus confining pressure. The data point at 5 MPa is for a prefailure sample deformed in the brittle field, and the rest are for samples deformed in the semibrittle field. Note that, in general, samples were not deformed to the same axial strain (strains are indicated next to each data point). Also, in some cases M and W were not measured on the same sample. For the data points at 85 and 190 MPa, S_V-$S_V{}^0$ was extrapolated to the required strain by assuming that S_V-$S_V{}^0$ increased linearly with strain (for both cases, two sets of measurements of crack density existed for samples stressed to different strains, and this slope was used for the extrapolation).

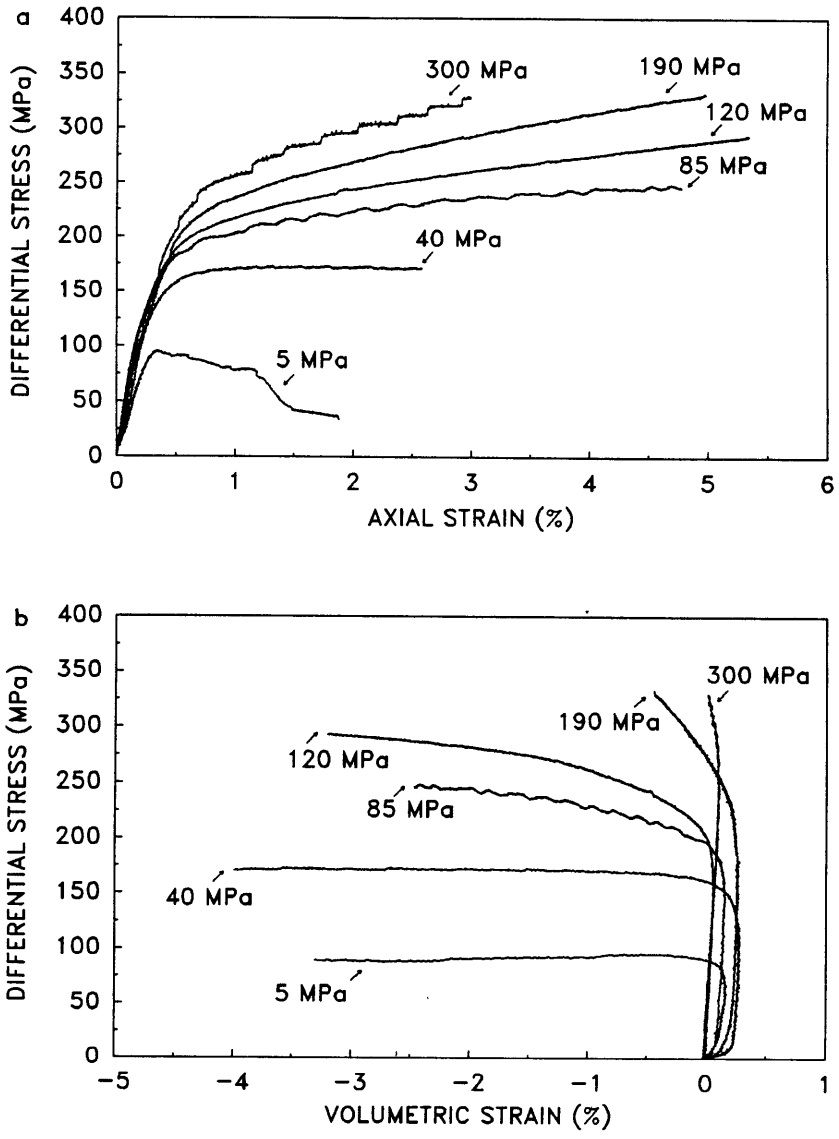
a
DIFFERENTIAL STRESS (MPa)
AXIAL STRAIN (%)
300 MPa
190 MPa
120 MPa
85 MPa
40 MPa
5 MPa
b
DIFFERENTIAL STRESS (MPa)
VOLUMETRIC STRAIN (%)
300 MPa
190 MPa
120 MPa
85 MPa
40 MPa
5 MPa

Figure 1*a,b*

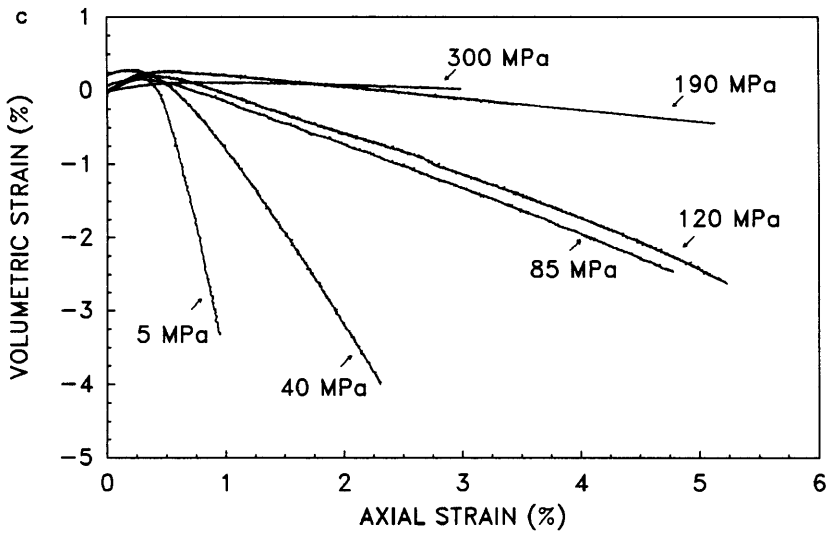
c
1
0
−1
−2
−3
−4
−5
VOLUMETRIC STRAIN (%)
0
1
2
3
4
5
6
AXIAL STRAIN (%)
300 MPa
190 MPa
120 MPa
85 MPa
5 MPa
40 MPa

Figure 1*c*

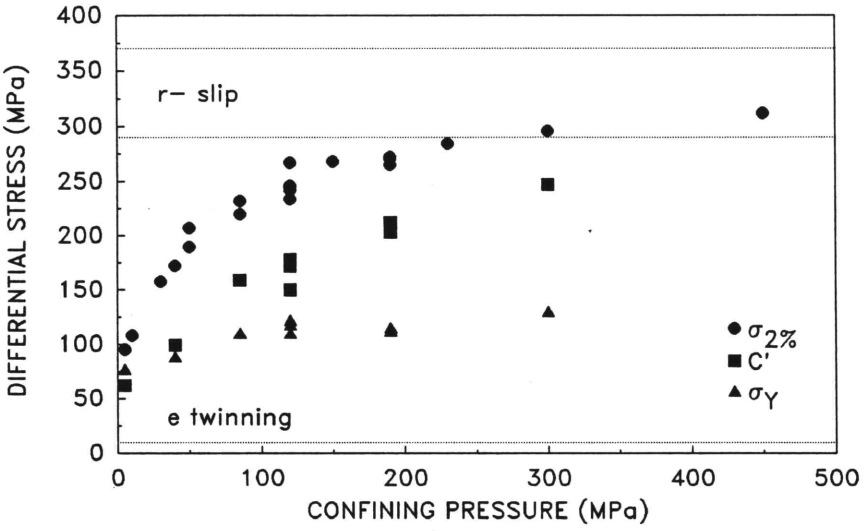
400
350
300
250
200
150
100
50
0
DIFFERENTIAL STRESS (MPa)
r− slip
e twinning
σ2%
C'
σY
0
100
200
300
400
500
CONFINING PRESSURE (MPa)

Figure 2

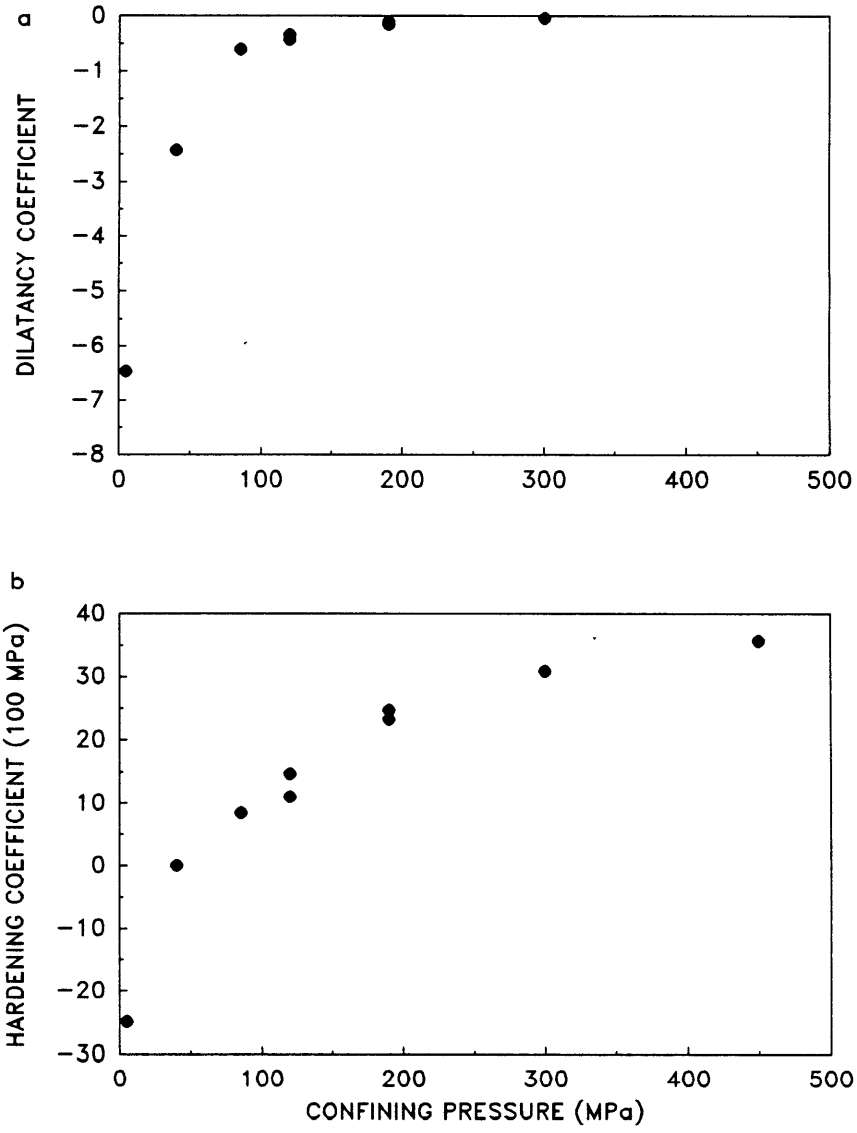
a
DILATANCY COEFFICIENT
0
−1
−2
−3
−4
−5
−6
−7
−8
0
100
200
300
400
500
b
HARDENING COEFFICIENT (100 MPa)
40
30
20
10
0
−10
−20
−30
0
100
200
300
400
500
CONFINING PRESSURE (MPa)

Figure 3*a*,*b*

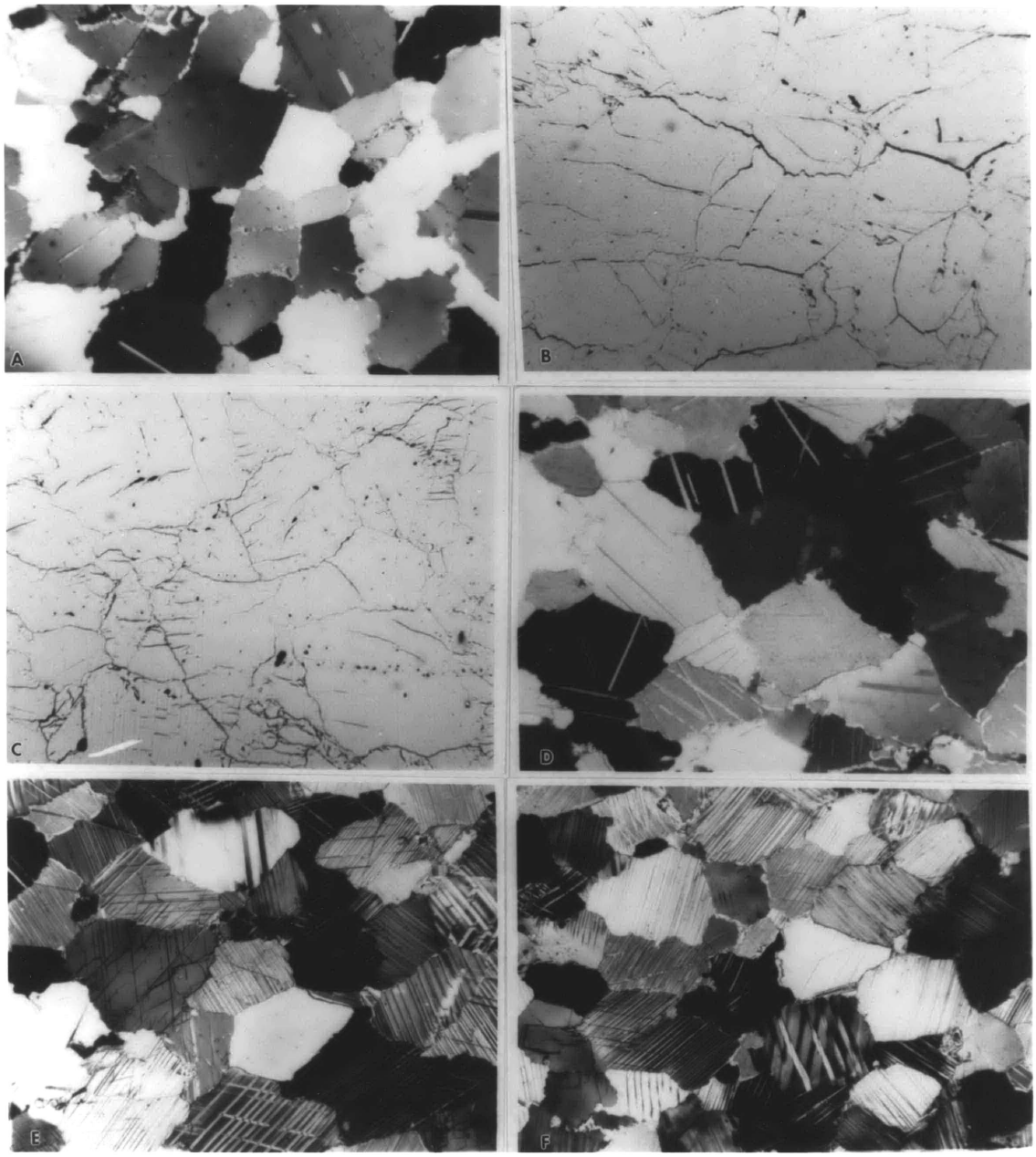

Figure 4

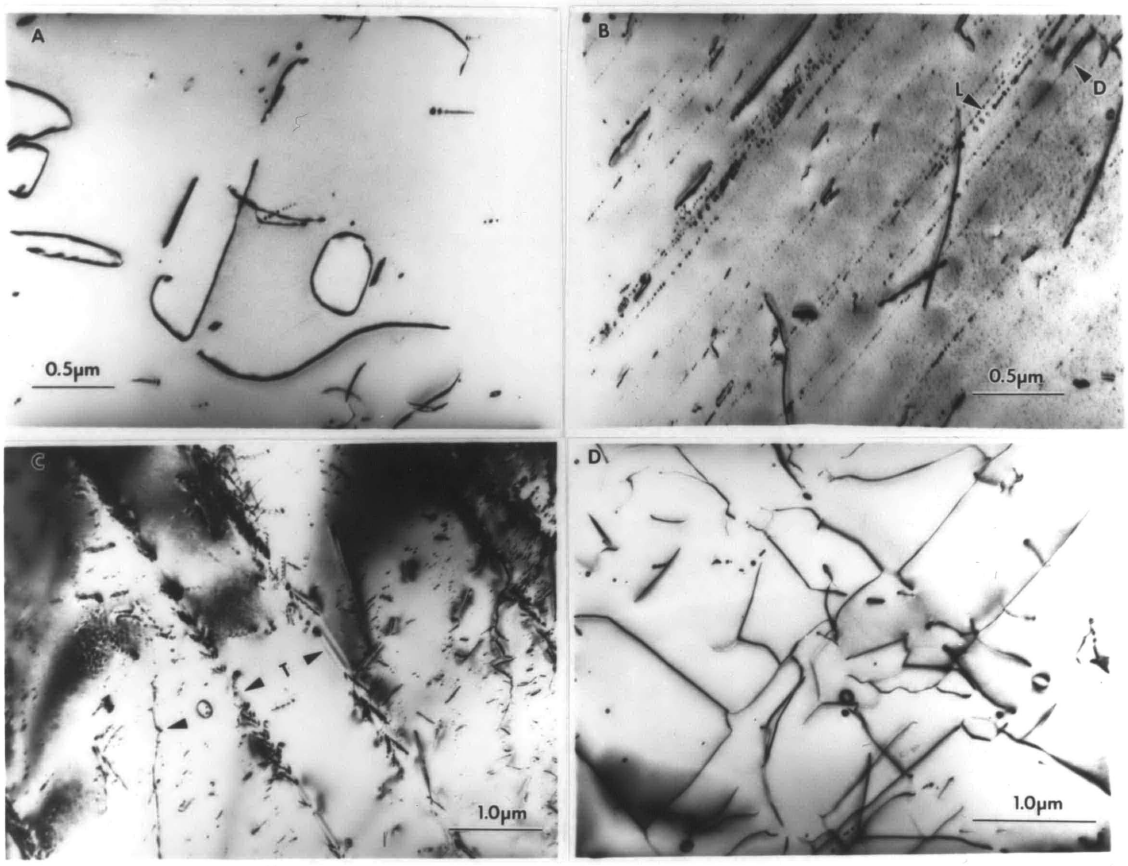

Figure 5

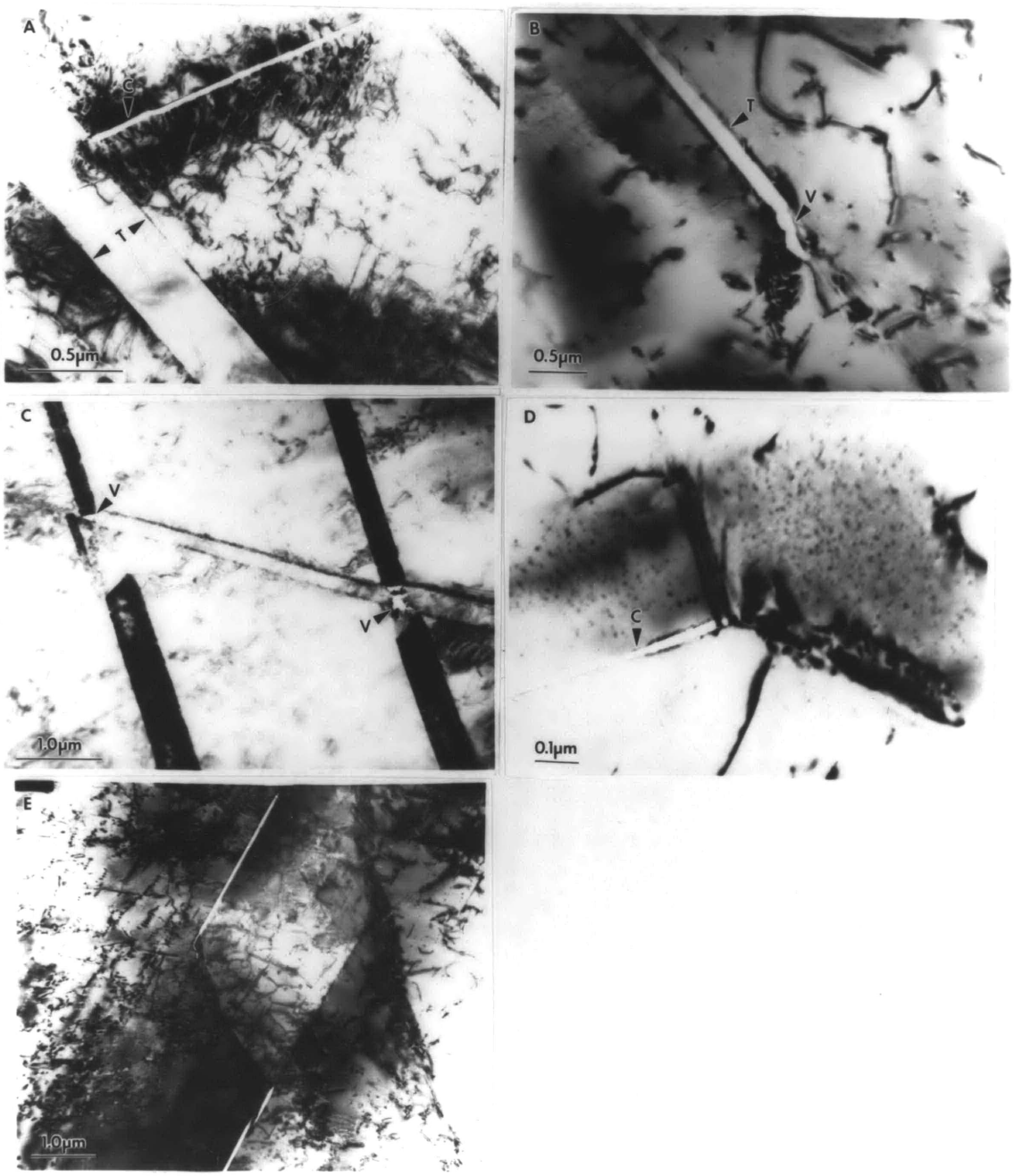

Figure 6

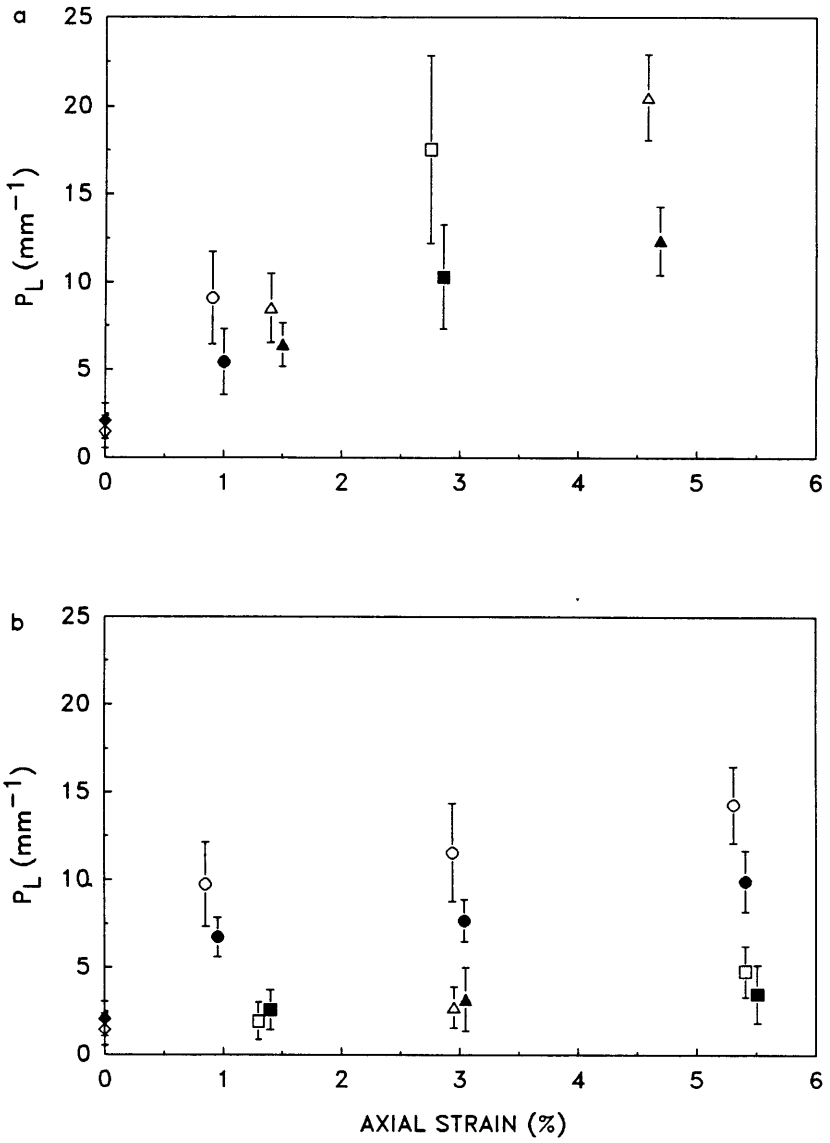

Figure 7*a,b*

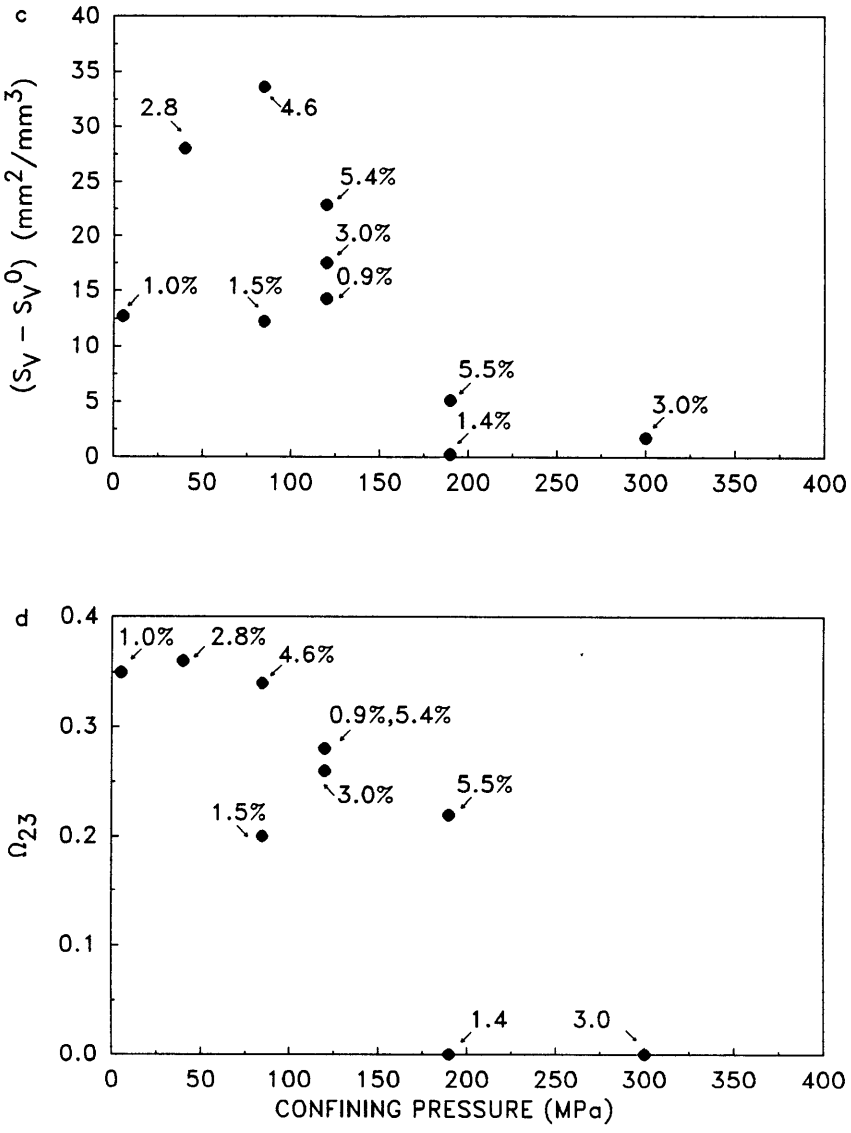
c
$(S_V - S_V^0)$ (mm^2/mm^3)
2.8
4.6
5.4%
3.0%
1.0%
1.5%
0.9%
5.5%
3.0%
1.4%
d
Ω_{23}
1.0%
2.8%
4.6%
0.9%,5.4%
3.0%
5.5%
1.5%
1.4
3.0
CONFINING PRESSURE (MPa)

Figure 7*c,d*

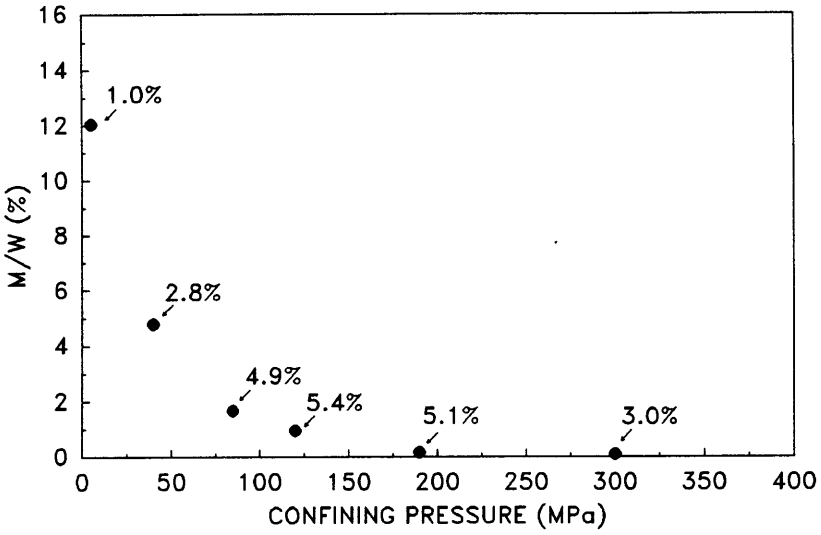
16
14
12
10
8
6
4
2
0
M/W (%)
1.0%
2.8%
4.9%
5.4%
5.1%
3.0%
0
50
100
150
200
250
300
350
400
CONFINING PRESSURE (MPa)

Figure 8

Chapter 4
Effect of Grain Size on Brittle and Semibrittle Strength: Implications for Micromechanical Modelling of Failure in Compression

INTRODUCTION

Grain size is one of the most important microstructural parameters affecting the mechanical properties of rocks. During deformation at high temperatures, diffusional creep and grain boundary sliding may be favored in fine-grained rocks whose coarser-grained counterparts deform by dislocation creep [e.g., *Schmid et al.*, 1977, 1987]. In addition, it is well established both experimentally and theoretically that in the diffusional creep/grain boundary sliding regime, fine-grained aggregates are weaker than coarser-grained aggregates [e.g., *Poirier*, 1985].

Conversely, the effect of grain size on the strength and rheology of rocks at low temperatures is less well known. An inverse relationship between the plastic yield stress and grain size is well established in metals deformed at low temperatures (i.e., those at which processes such as dislocation climb and cross-slip are negligible) [e.g., *Hansen*, 1985]. Analyses based on the concept of grain boundaries as obstacles to slip lead to the "Hall-Petch" equation, which predicts that the flow stress depends inversely on the square root of the grain size [*Hall*, 1951; *Petch*, 1953]. *Olsson* [1974] and *Schrodt and Holder* [1983] suggested that the yield stress of marble deformed in compression in the semibrittle field followed a Hall-Petch relationship; however, these workers did not correlate their empirical results with any particular micromechanical process, nor did they consider the differences in rheology amongst the different marbles. In fact, their measured yield stresses depended upon pressure, indicating that there was a brittle component to the deformation.

In the brittle field, the uniaxial compressive fracture strength is inversely related to grain size in anhydrite [*Skinner*, 1959], limestone [*Brace*, 1961], and dolomite [*Brace*, 1964]; Brace concluded that his observations agreed qualitatively with the predictions of simple Griffith crack theory. In triaxial compression tests, *Handin and Hager* [1957] and *Hugman and Friedman* [1979] also observed a negative correlation between the grain size and fracture strength of limestone and dolomite. Failure in compression is now understood to be due to the stable growth, interaction, and coalescence of microcracks [e.g., *Paterson*, 1978; *Wong*, 1982; *Kranz*, 1983], rather than to the unstable propagation of a single critical flaw. Thus, an extension of simple Griffith crack theory to the case of compressive loading [*Griffith*, 1924; *McClintock and Walsh*, 1962] is inappropriate for modelling shear fracture in rocks. In recent years, a number of workers have modelled microcrack propagation and coalescence in compression using linear elastic fracture mechanics [e.g., *Horii and Nemat-Nasser*, 1985*a*, 1986; *Ashby and Hallam*, 1986; *Kemeny and Cook*, 1987]. These models have generally focussed on predicting the variation of fracture stress with confining pressure and have succeeded in reproducing some of the experimental observations of the hardening and softening behavior of rocks deformed in compression. The theoretical predictions depend critically on the length of the initial flaws present in the rock, and since the initial flaw size scales with grain size [e.g., *Nur and Simmons*, 1970], one expects intuitively that the models should predict a grain size effect. However, we are not aware of any attempts to compare the predictions of the models with the experimental observations of the grain size dependence of fracture strength.

There is also preliminary evidence that the confining pressure at the brittle to plastic transition depends upon grain size. *Hugman and Friedman* [1957] observed that coarser-grained aggregates of limestone and dolomite are more "ductile" than finer-grained aggregates. Likewise, Solnhofen limestone deforms by brittle fracture under confining pressures at which the coarser-grained Wombeyan marble is ductile [*Paterson*, 1958]. Is there

a systematic effect of grain size on the brittle to plastic transition pressure? If so, how is it related to the grain size dependence of the brittle fracture and plastic yield stresses? Furthermore, what are the implications for the micromechanics of the brittle to plastic transition? Can the experimental results be used to evaluate the recently developed fracture mechanics models of brittle fracture and the brittle-plastic transition?

To address the above questions, we conducted a systematic series of triaxial tests on four calcite rocks whose average grain size ranged over four orders of magnitude. Calcite aggregates were chosen because of the relative ease in obtaining pure, non-porous samples with a wide range of grain sizes, and also because calcite aggregates undergo the brittle to plastic transition at moderate confining pressures and room temperature [*Scholz*, 1968; *Edmond and Paterson*, 1972; *Fredrich et al.*, 1989]. Dilatancy measurements and microstructural studies were performed on some samples to identify the active deformation mechanisms. The experimental results are compared with the theoretical predictions of micromechanical models for the failure of rock in compression.

EXPERIMENTAL PROCEDURES

Starting Material

The rocks studied are all of high purity, have grain sizes ranging from 1.7 mm (Wombeyan marble) to 6 μm (Solnhofen limestone), and, with the exception of Solnhofen limestone, have $< 1\%$ porosity (Table 1). Wombeyan marble is white in color; bulk chemical analysis indicates that it is 96% calcite [*Paterson*, 1958]. Grains are euhedral and most show twinning on at least one plane; fabric analysis indicates that the rock is isotropic [*Paterson*, 1958]. Carrara marble is white in color, more than 99% calcite [*Atkinson*, 1979], isotropic [*Ramez and Murrell*, 1964], and composed of equiaxed grains which are generally untwinned and have serrate boundaries. Saillon marble was obtained from a quarry in Wallis,

Switzerland; grains are slightly elongated, rarely show twinning, frequently show undulatory extinction, and have mildly serrate boundaries. *Schmid et al.* [1981] studied a marble collected from the same locality and concluded that the rock had a crystallographic preferred orientation. Optical and transmission electron microscopy suggest that the purity of this white marble approaches that of Carrara. The "massive" variety of Solnhofen limestone was used here; modal analysis indicates this rock is 97% calcite [*Wang*, 1966]. It is tan in color and isotropic [*Higgs et al.*, 1960]; grains are untwinned with serrate boundaries.

Although it is possible to synthesize a suite of starting materials which vary only in grain size by hot isostatic pressing, grain sizes would be constrained to 5-80 μm, since stresses due to the high thermal expansion anisotropy of calcite cause pervasive cracking upon quenching for larger grain sizes [*Olgaard*, 1985]. Thus, in order to encompass a wide range of grain size, the use of natural samples is necessary. We assume that any differences in the mechanical behavior due to the minor variations in microstructure noted above are second order. For example, Danby marble has a grain size close to that of Carrara marble; preliminary experiments indicate that the strength and rheological behavior of the two are similar [*J. Fredrich, unpublished work*, 1987-88]. The significant porosity of Solnhofen limestone may influence the mechanical behavior at high confining pressures [e.g., *Edmond and Paterson*, 1972]; this point is addressed further on.

Deformation Experiments

Precision ground cylindrical samples 15.88 mm in diameter and 38.10 mm in height were predried in vacuo at 40°C, jacketed with either two or three layers (each 0.76 mm thick) of polyolefin heat shrink tubing or thin (0.05 mm) copper foil, and deformed at a constant displacement rate of 8.9×10^{-5} cm/s in the conventional triaxial configuration at room temperature and confining pressures ranging from 5 to 450 MPa. The confining medium was petroleum ether (except for one test using argon gas). Samples were not vented to the

atmosphere. Load was measured with an external load cell, and displacement was measured with a differential transformer (DCDT) mounted between the moving piston and fixed lower platen. In some experiments, volumetric strain was measured with electric resistance strain gauges attached to the foils of copper jacketing. Additional details on the test procedure, data acquisition and reduction, and microscopy are given in *Fredrich et al.* [1989].

EXPERIMENTAL RESULTS

The mechanical axial stress-strain data are summarized in Table 2. The most extensive series of tests was performed on Carrara marble; detailed results were reported previously [*Fredrich et al.*, 1989], and only some of the experimental data for this rock are reproduced here. Because of the existence of a fabric in Saillon marble, a number of duplicate tests were performed on samples cored in different directions. The strength and rheological behavior did not show any statistically significant variation, and thus, we do not distinguish between the experimental results for the different orientations.

All of the rocks studied show a transition in mechanical behavior from work softening at low pressures to work hardening at high pressures (Figures 1*a-d*). Accompanying this transition is a change from failure along a macroscopic shear fault to homogeneously distributed deformation with no macroscopic evidence of cracking. At intermediate pressures where strength is nearly constant with strain, samples sometimes have numerous short, conjugate shear-oriented cracks visible on the sample surface. The rocks differ in the magnitude of differential stress supported at the same confining pressure and in the confining pressure at the transition from brittle fracture to semibrittle flow (Figure 2).

Brittle Field

When deformed uniaxially and at confining pressures of 5 and 10 MPa, all of the rocks exhibited work softening (Figure 1) and failed on a macroscopic shear fault. At constant confining pressure, the peak stress is inversely related to the square root of the grain size d; linear regression yields correlation coefficients of 0.99 (Figure 3*a*). Note that the uniaxial compressive strength and fracture strengths at confining pressures of 5 and 10 MPa are fit with lines of nearly identical slope.

At constant confining pressure, there is a clear progression with decreasing grain size in what may be loosely termed the "brittleness" of the deformation. For example, at a pressure of 5 MPa, the two finest-grained rocks, Solnhofen limestone and Saillon marble, failed dramatically (Figures 1*c* and 1*d*) with an audible acoustic emission. Narrow (<0.5 mm) macroscopic shear faults were formed, and a few axial cracks emanated from the fault, particularly in the Solnhofen (the finest-grained rock). Conversely, when deformed at the same pressure, Carrara and Wombeyan marbles exhibited stable work softening behavior (Figures 1*a* and 1*b*), with no audible acoustic emission. The faults were somewhat wider (>0.5 mm) than those in the Saillon and Solnhofen, and no axial cracks were visible. In Carrara marble, a macroscopic fault formed after the stress drop at 1% strain (Figure 1*a*, also see *Fredrich et al.* [1989]); however, the occurrence of a macroscopic fault in Wombeyan marble (the coarsest-grained rock) did not appear to be correlated to any particular feature of the post-peak deformation.

Since no attempts were made to control the post-peak behavior in any of the experiments, we cannot distinguish whether the Solnhofen and Saillon behavior at low confining pressures is class I or class II [*Wawersik and Fairhurst*, 1970]; however, it is clear that the post-peak behavior is significantly less stable than that of the coarser-grained marbles. Higher confining pressures increase significantly the stability of the post-peak deformation for the finer-grained marbles. The post-peak behavior of Saillon marble and Solnhofen limestone at pressures of 30

and 60 MPa (Figures 1*c* and 1*d*), respectively, is similar to that described above for Carrara and Wombeyan marbles at 5 MPa (Figures 1*a* and 1*b*).

Brittle-Ductile Transition and Semibrittle Flow

With increasing confining pressure, the calcite rocks undergo a transition from work softening to work hardening, which is associated with distributed deformation by both brittle microcracking and plastic flow mechanisms (i.e., twinning and dislocation glide); we refer to this as the brittle-semibrittle transition [see *Fredrich et al.*, 1989]. Samples deformed at a confining pressures slightly greater (i.e., tens of MPa) than those at the brittle-semibrittle transition show no barrelling and appear homogeneously deformed.

The confining pressure at which the brittle-semibrittle transition occurs depends inversely upon grain size: the transition pressure for the finest-grained rock is roughly three times that for the coarsest-grained rock (Figures 2 and 4). However, the ratio of the maximum applied axial stress to the confining pressure, $\lambda=\sigma_3/\sigma_1$, at the transition is a constant and equal to about 0.16 for the different calcitic rocks (Figure 2). Note that although the porosity of Solnhofen limestone is greater than those of the other calcite aggregates studied (Table 1), this does not influence the "type" of brittle-ductile transition [e.g., *Paterson*, 1978] which the rock undergoes. Data of *Edmond and Paterson* [1972] demonstrate unequivocally that the phenomenology of the brittle-ductile transition in Solnhofen is characteristic of that found in low-porosity calcite aggregates (and silicate rocks at elevated temperatures), rather than that observed in porous rocks.

In the semibrittle field, strength remains directly dependent upon confining pressure (although to a lesser degree than in the brittle field) and inversely dependent upon grain size (Figure 2). Since the rate of work hardening may depend upon grain size [e.g., *Hansen*, 1985], we take the macroscopic initial yield stress (σ_Y) as a measure of the grain size sensitivity of plastic flow; we define σ_Y as the differential stress at which the axial stress-

strain curve deviates from linearity. For Carrara marble deformed in the semibrittle field, the initial yield stress σ_Y is constant at confining pressures greater than 85 MPa and significantly lower than the differential stress at the onset of dilatancy (C') [*Fredrich et al.*, 1989]. Thus, the initial yielding in the semibrittle field is due to constant volume deformation mechanisms (e.g., twinning and dislocation glide). Microscopy also indicates that the initial yielding is associated with an increase in the density of twins [*Fredrich et al.*, 1989].

Limited measurements of dilatancy in Wombeyan and Saillon marbles suggest results analogous to those discussed above for Carrara marble. For Wombeyan marble deformed at 300 MPa, C' was 264 MPa, whereas σ_Y was 101 MPa. Likewise, for Saillon marble deformed at 190 MPa, C'= 275 MPa and σ_Y= 203 MPa. Defining a macroscopic initial "plastic" yield stress for Solnhofen limestone is problematic due to the occurrence of inelastic compaction during non-hydrostatic loading at confining pressures greater than 200 MPa [see also *Edmond and Paterson*, 1972]. We take the yield stress observed at a pressure of 85 MPa as a lower bound. The data are fit well by a straight line (with a correlation coefficient of 0.99) when plotted as a function of the inverse of the square root of grain size (Figure 3*b*). Neglecting the data point for Solnhofen limestone increases the linear regression slope slightly.

THEORETICAL BACKGROUND

Brittle Fracture

A number of theoretical studies of brittle failure in compression have focussed on the "sliding crack" (Figure 5*a*), which was first proposed by *Brace et al.* [1966] as a mechanism for the inelastic dilatancy of rock. Under non-hydrostatic compressive loading, when the shear traction along a "main crack" of length $2c$ exceeds the frictional resistance, slip along the main crack causes a "wing crack" to nucleate and grow. Several workers have developed models based on the sliding crack and attempted to simulate the experimentally observed

dilatant strains [*Holcomb*, 1978; *Kachanov*, 1982; *Moss and Gupta*, 1982; *Nemat-Nasser and Obata*, 1988]. *Stevens and Holcomb* [1980*a*,*b*] and *Costin* [1983] argued that the sliding crack model cannot account for all of the experimental observations and proposed alternative mechanisms such as elastic moduli mismatch. However, the elastic mismatch mechanism is difficult to analyze theoretically and models of shear failure that are based on this mechanism [*Costin*, 1985] are still semi-empirical. On the other hand, the sliding crack is well analyzed [*Horii and Nemat-Nasser*, 1985*a*, 1986; *Ashby and Hallam*; 1986], and thus we focus on these models in the interpretation of our experimental data (Figures 2-4). *Moss and Gupta* [1982] and *Nemat-Nasser and Obata* [1988] have addressed some of the criticisms of the sliding crack model, and *Nemat-Nasser* [1985] has pointed out that various mechanisms (including elastic mismatch) are expected to yield behavior which is qualitatively similar to that of the sliding crack.

Several groups have recently developed approximate analytic expressions for the mode I stress intensity factor K_1 at the tip of the wing crack [see a review by *Evans et al.*, 1989]. *Horii and Nemat-Nasser* [1986] consider a two-dimensional main crack of length $2c$ loaded by a remotely applied maximum compressive stress σ_1 and a lateral confining stress $\sigma_3=\lambda\sigma_1$ (Figure 5*a*). If the friction coefficient along the main crack surface is μ, then the most favorable orientation for the nucleation of the wing crack is $\tan(2\gamma)=1/\mu$. Assuming a cohesion $\tau_c=0$, then K_1 at the tip of a wing crack of length ℓ is given by

$$K_1/\sigma_1(\pi c)^{1/2}=$$

$$\{[(1-\lambda)(1+\mu^2)^{1/2}-(1+\lambda)\mu]/[\pi(L+L^*)^{1/2}]\}\sin\theta - (L^{1/2}/2)[(1+\lambda)-(1-\lambda)\cos2(\theta-\gamma)] \qquad (1)$$

where $L=\ell/c$ and $L^*=8/(3\pi^2)$. The first term represents the contribution of sliding on the main crack to the stress intensity factor, whereas the second term reflects that due to the far-field stresses. Propagation occurs when K_1 equals the mode I fracture toughness K_c. The angle between the wing crack and main crack is given by θ, and is determined by maximizing equation (1) with respect to θ. The wing crack grows along a curved path and ultimately turns

parallel to the applied maximum stress (i.e., $\theta=\gamma$). *Ashby and Hallam* [1986] considered this case and found

$$K_1/\sigma_1(\pi c)^{1/2}=$$

$$\{[(1-\lambda)(1+\mu^2)^{1/2}-(1+\lambda)\mu-(\lambda L\sqrt{3}/0.4)]/(1+L)^{3/2}\}\{(0.4L\sqrt{3})+[3(1+L)]^{-1/2}\} \quad (2)$$

Strictly speaking, we expect equation (2) to be valid only for $L>1$.

A key result is that for all-compressive loading, the stress intensity factor at the tip of the wing crack decreases as the crack grows; thus, the propagation behavior is stable [*Horii and Nemat-Nasser*, 1985*a*]. In the sliding crack model, work softening and instability must therefore result from crack interaction. A rigorous calculation by the same authors showed that the interaction effect may, in fact, result in unstable crack growth, which is assumed to correspond to the onset of shear localization. Unfortunately, their formulation is in terms of singular integral equations and thus did not yield closed-form solutions.

Ashby and Hallam [1986] derived an approximate analytic expression for crack interaction using beam theory. They found that crack interaction contributes to the stress intensity factor by an amount

$$K_1/\sigma_1(\pi c)^{1/2}=[2\epsilon_o(L+\alpha)/\pi]^{1/2}\{[1-8\epsilon_o\lambda(L+\alpha)^3][1-2\epsilon_o\lambda(L+\alpha)^3]\}^{1/2} \quad (3)$$

where $\alpha=2^{-1/2}$, $\epsilon_o=c^2N_A$, and N_A is the number of sliding cracks per unit area. In equation (3), the first term reflects the contribution of bending moments induced by the maximum compressive stress to the stress intensity factor, whereas the second term represents the crack-closing effect due to the lateral confining stress. The initial "damage" state is characterized by ϵ_o, which is the two-dimensional equivalent of the "crack density" parameter of *Budiansky and O'Connell* [1976]. The total stress intensity factor K_1 is found by summing equation (3) and either equation (1) or (2).

Brittle-Ductile Transition

Horii and Nemat-Nasser [1986] developed recently the first detailed micromechanical model of the brittle-ductile transition in compression. They analyzed the "blunting" effect of a line of dislocations colinear with both ends of a sliding crack (Figure 5*b*). In this model, sliding on the main crack can be accommodated either by the wedging open of wing cracks or by the glide of edge dislocations. Although the analysis is complicated, they found that whether the response of the rock was "brittle" or "ductile" depended upon only two parameters: the stress ratio $\lambda=\sigma_3/\sigma_1$, and a "ductility" parameter Δ defined as

$$\Delta=K_c/[\tau_y(\pi c)^{1/2}] \tag{4}$$

where τ_y is the "yield stress in shear". In the "brittle" mode, the initial inelastic response is dominated by wing crack growth, whereas in the "ductile" mode, the inelastic response is dominated by the growth of the plastic zones. Their model also predicts a "transitional" mode, in which the inelastic response is accommodated by both wing crack growth and plastic flow.

Due to the mathematical complexity, *Horii and Nemat-Nasser* [1986] considered only the behavior of an isolated flaw; their analysis does not include the potential enhancement of wing crack growth due to crack interaction. Thus, although their results cannot be used to calculate the peak stresses associated with the onset of unstable crack growth due to crack interaction (see above), the analysis should predict the conditions at which such interaction is necessarily impossible due to negligible wing crack growth. The limiting stress ratio above which the rock responds in a ductile mode depends on the ductility Δ. *Horii and Nemat-Nasser*'s [1986] results are not in analytic form; we therefore reproduce in Figure 6 a brittle-ductile transition map calculated by them assuming a flaw orientation $\gamma=45°$, a coefficient of friction $\mu=0.4$, and a cohesion $\tau_c=0$. The qualitative behavior is similar for a wide range in values of these parameters [*Horii and Nemat-Nasser*, 1986].

Comparison of Experimental Results and Theoretical Predictions

Choice of Material Parameters

Estimates of several parameters are needed in order to compare the experimental results to the theoretical predictions of the models discussed above (see equations (1-4)). The crack length $2c$ is probably the most critical parameter; unfortunately, it is also notoriously difficult to measure. The most fundamental problem lies in simply defining a crack. For example, microcracks in rocks are rarely straight; consequently, workers have adopted different definitions over how much a crack can vary its path and still be considered a single crack [cf. *Hadley*, 1976; *Kranz*, 1979]. The interpretation of interconnected cracks is similarly ambiguous. Furthermore, scanning electron microscopy (SEM) indicates that microcracks are sometimes "bridged" along small sections of their length [e.g., *Sprunt and Brace*, 1974; *Hadley*, 1976]; it is not clear whether or not these "bridges" should be considered as separating two different cracks.

Fortunately, what is most critical for the present work is simply the scaling of the initial crack length $2c$ with the grain size d. Microcracks in rocks are generally attributed to the internal stresses induced during unroofing by thermal expansion and elastic moduli anisotropy and mismatch [*Nur and Simmons*, 1970]. Theoretical analyses and microscopy of thermally induced cracking in rocks suggest that the lengths of such cracks scale with grain size [e.g., *Fredrich and Wong*, 1986]. Quantitative optical microscopy generally indicates an average crack length $0.2d < 2c < d$ [e.g., *Peng and Johnson*, 1972; *Simmons et al.*, 1975; *Chen et al.*, 1979; *Abdel-Gawad et al.*, 1987], whereas SEM studies usually show $2c \leq 0.2d$ [*Sprunt and Brace*, 1974; *Hadley*, 1976]. The latter estimates are probably lower since those workers considered cracks to terminate at "bridges". Our qualitative observations indicate that crack size scales with grain size (Figure 7); for the calculations below we generally assumed $2c = d$.

Determination of the crack density ϵ_o is also subject to the difficulties noted above, since $\epsilon_o = c^2 N_A$, where N_A is the number of sliding cracks per unit area. *Hadley* [1976] estimated $\epsilon_o = 0.25$ for an unstressed sample of Westerly granite. If we assume that the average flaw size is equal to the grain size (i.e., $2c = d$), then $\epsilon_o = 0.2$-0.5 corresponds roughly to 0.5-1.5 sliding cracks per grain area (assuming circular grains); we consider this a reasonable estimate (Figure 7).

Reasonable bounds for the coefficient of friction μ for calcite are 0.1-0.7 [e.g., *Horn and Deere*, 1962; *Paterson*, 1978]. In their model, *Horii and Nemat-Nasser* [1986] were not specific as to the interpretation of the fracture toughness K_c and the "yield stress in shear" τ_y. In the context of their discussion, we interpret these parameters to be single-crystal mineral properties whose values are therefore constant for the different calcite rocks. For the (1011) cleavage plane in calcite, K_c is 0.19-0.20 MPa $m^{1/2}$ [*Atkinson*, 1984], and the critical resolved shear stress for dislocation glide τ_y on the (1011) plane in calcite (the most easily activated slip system) is about 165 MPa at room temperature [*Turner et al.*, 1954; *Griggs et al.*, 1960].

Brittle Fracture

In this section, we compare the theoretical predictions of *Ashby and Hallam*'s [1986] model to the experimental observations of the effect of confining pressure and grain size on the brittle fracture stress. All of the calculations use *Ashby and Hallam*'s [1986] result for the crack interaction effect (equation (3)), and either *Horii and Nemat-Nasser*'s [1986] expression (equation (1)) or *Ashby and Hallam*'s result (equation (2)) for isolated wing crack growth.

Effect of confining pressure. In Figure 8 we show results for different values of the stress ratio $\lambda = \sigma_3/\sigma_1$ and crack density ϵ_o. The solid lines were calculated using equations (1) and (3), whereas the results in dotted lines are for equations (2) and (3). *Ashby and Hallam* [1986] showed results only for a stress ratio $\lambda = 0$ (i.e., uniaxial compression). For this case, the

model predicts unstable crack growth (i.e., work softening) for values of the crack density $\epsilon_o > 0$ (Figure 8*a*), in agreement with the earlier results of *Nemat-Nasser and Horii* [1982]. We performed some calculations to investigate the predicted effect of confining pressure on the brittle strength.

Shown in Figure 8*b* are the results for a crack density $\epsilon_o = 0.2$, coefficient of friction $\mu = 0.3$, and variable stress ratio λ. For a wide range in values of the crack density ϵ_o and coefficient of friction μ, *Ashby and Hallam*'s model predicts only stable crack growth for values of the stress ratio $\lambda > 0.015$. That is, a small amount of lateral confining pressure alone is sufficient to inhibit localization. However, our mechanical data and microstructural observations indicate that localization occurs for values of the stress ratio $\lambda \leq 0.16$ (Figures 1 and 2; Table 2). Furthermore, our microstructural analysis and dilatancy measurements indicate that the inhibition of localization in marble with increased confining pressure is due to the increased activity of plastic flow mechanisms, rather than due to the increased difficulties of crack propagation alone [*Fredrich et al.*, 1989].

It is clear from Figures 8*a* and 8*b* that *Ashby and Hallam*'s [1986] expression for isolated wing crack growth (equation (2)), which assumes $\theta = \gamma$, overestimates significantly the stress intensity factor K_1 for values of the normalized wing crack length $L < 1$. Additionally, *Horii and Nemat-Nasser*'s [1986] more accurate expression (equation (1)) predicts unstable crack growth for higher values of the stress ratio λ. Since we are generally interested in the crack growth behavior for small values of the normalized wing crack length L, only results based on equations (2) and (3) are shown for the remainder.

Effect of grain size. To calculate the theoretical predictions for the effect of the initial flaw size on the brittle fracture strength, we first compute the normalized peak axial stress, $\sigma_1(\pi c)^{1/2}/K_c$, observed prior to unstable crack growth for different values of the stress ratio λ, crack density ϵ_o, and coefficient of friction μ. As discussed previously, this peak axial stress is assumed to correspond to the onset of macroscopic work softening observed in triaxial

experiments (i.e., the fracture strength). It turns out that the normalized peak axial stress, $\sigma_1(\pi c)^{1/2}/K_c$, is linearly related to the normalized confining stress, $\sigma_3(\pi c)^{1/2}/K_c$, regardless of the stress ratio λ (an example is shown in Figure 9 for a crack density $\epsilon_o=0.2$ and coefficient of friction $\mu=0.5$). Therefore, if the confining pressure σ_3 is fixed, then the differential stress $(\sigma_1-\sigma_3)$ is proportional to $1/(2c)^{1/2}$ for a fixed K_c. In this manner, we calculate the slope of a plot of peak differential stress $(\sigma_1-\sigma_3)$ versus the inverse of the square root of the flaw size $2c$ for various values of the crack density ϵ_o and coefficient of friction μ (Figure 10). Since the model does not predict work softening for values of the stress ratio $\lambda>0.02$ (see Figures 8 and 9), these plots are valid only for $\lambda<0.02$.

The predicted (Figure 10) and experimentally observed (Figure 3*a*) slopes are comparable in magnitude for a wide range in the values of the crack density ϵ_o and coefficient of friction μ; however, it should be kept in mind that *Ashby and Hallam*'s model does not predict localization for the stress ratios observed in our experiments at confining pressures of 5 and 10 MPa (see prior discussion). The predicted slope is more sensitive to the crack density ϵ_o than to the coefficient of friction μ. Although a Hall-Petch relation would be approximately obeyed if the initial crack density ϵ_o in the different rocks varied slightly (i.e., say $0.2<\epsilon_o<0.5$), significant departures from a linear relationship would result if the initial crack density in the different rocks varied more substantially. For example, if the initial crack density in the different rocks ranged from one crack every six grains to three cracks every two grains (i.e., $0.05\leq\epsilon_o\leq0.5$), then correlation coefficients as low as 0.85 would be predicted (Figure 11). Note that the linear regression correlation coefficients for the experimental fracture data are all greater than 0.99. The model predicts that the effect of grain size on the fracture strength is independent of confining pressure (see Figures 9 and 10); our experimental data indicate that the Hall-Petch slope is nearly the same for the uniaxial compressive strength and the strength at confining pressures of 5 and 10 MPa.

Although *Ashby and Hallam*'s model predicts the experimentally observed Hall-Petch slopes reasonably well, it underestimates the experimentally determined uniaxial compressive strengths. In Figure 12 we compare the observed uniaxial strengths and the predicted strengths for a stress ratio $\lambda=0$ and different values of the ratio of initial flaw length to grain size ($2c/d$) and crack density ϵ_o; note that these predictions were calculated using the results shown in Figure 10 for a coefficient of friction $\mu=0.5$. As discussed above, qualitatively similar results are obtained for $\mu=0.1$. In general, the values of the ratio $2c/d$ which match best the experimentally observed Hall-Petch slope underestimate the observed uniaxial compressive strengths. Use of *Ashby and Hallam*'s expression for isolated wing crack growth (equation (2)), rather than *Horii and Nemat-Nasser*'s expression (equation (1)), results in even lower predicted strengths (see Figure 8).

Brittle-Ductile Transition

In this section we compare the predictions of *Horii and Nemat-Nasser*'s [1986] model for the brittle-ductile transition to the experimental data. Their model predicts that the stress ratio $\lambda=\sigma_3/\sigma_1$ at the brittle-ductile transition scales inversely with the ductility $\Delta=K_c/[\tau_y(\pi c)^{1/2}]$ (Figure 6). If the fracture toughness K_c and the yield stress in shear τ_y are interpreted as single-crystal mineral properties (see previous discussion), then the values of these parameters are constant for the different calcite rocks. Thus, if the initial flaw size scales with the grain size (see previous discussion), then the model predicts that the stress ratio λ at the transition should scale with the grain size d.

The experimental data, however, indicate that the stress ratio σ_3/σ_1 is nearly the same at the brittle-ductile transition for the different rocks (Figure 6). The model predicts that finer-grained rocks are more "ductile" than coarser-grained rocks, and that the two finest-grained rocks (Saillon marble and Solnhofen limestone) should deform ductilely, even under uniaxial compression (Figure 6). In fact, the experimental observations are exactly the opposite: the

finer-grained rocks are significantly more brittle than the coarser-grained rocks at low confining pressures (Figure 1, also see previous discussion).

DISCUSSION

Several inferences may be drawn from the above comparison of the experimental data and model predictions. In the following sections, we first discuss possible limitations in *Ashby and Hallam*'s [1986] model of brittle failure and compare our results with previous results by others. We then address possible reasons for the discrepancy between the experimental data and *Horii and Nemat-Nasser*'s [1986] model for the brittle-ductile transition. Finally, we consider the broad implications of our results.

Brittle Fracture

In *Ashby and Hallam*'s [1986] model, brittle cracking is the only mode for the inelastic deformation; the model predicts different crack propagation behavior for stress ratios $\lambda=0$ and $\lambda>0$ (Figure 8). Unstable crack growth is predicted for $\lambda=0$, and intervals of unstable crack growth are predicted for $0<\lambda<0.02$. However, only stable crack growth is predicted for $\lambda>0.02$; thus, a small amount of lateral confining pressure alone is predicted to be sufficient to inhibit localization. Our mechanical data indicate that in calcite rocks, localization occurs for stress ratios $\lambda\leq0.16$ (Figures 1 and 2, Table 2). Moreover, our microstructural analysis and dilatancy measurements indicate that the inhibition of localization in marble with increased confining pressure is due to the increased activity of plastic flow mechanisms, rather than due to the increased difficulty of crack propagation alone [*Fredrich et al.*, 1989]. This appears to be the case for low porosity crystalline rocks in general [see a review by *Evans et al.*, 1989]; at room temperature, non-porous silicate rocks fail by brittle fracture at confining pressures greater than 2 GPa [*Schock and Heard*, 1974; *Shimada et al.*,

1983]. *Tullis and Yund* [1987] have suggested an exception to this tendency: with increasing pressure, feldspar aggregates undergo a transition to non-localized deformation in the absence of dislocation activity.

A contributing factor to the model's overestimation of the role of confining pressure in inhibiting unstable crack propagation may be that frictional sliding on inclined microcracks is the only mechanism considered for microcrack initiation and propagation. In rocks, microcrack initiation and propagation are due to a variety of mechanisms [e.g., *Tapponier and Brace*, 1976], some of which are probably less sensitive to the effects of confining pressure than is the sliding crack (where frictional tractions on the crack, which scale with the normal stress, must be overcome in order for the wing cracks to initiate and grow).

An analysis of the crack interaction effect by *Horii and Nemat-Nasser* [1985*a*] is more rigorous than that of *Ashby and Hallam* [1986]; the former workers used the "method of pseudotractions" [*Horii and Nemat-Nasser*, 1985*b*] to derive the interaction effect for an array of aligned sliding cracks. However, their model has more free parameters: in addition to an "active" flaw size $2c$, which varies with confining pressure, the maximum and minimum flaw sizes, and the flaw spacing must also be specified. Their results are not in analytic form and, consequently were not used here. From the results presented in their paper, and assuming K_c=0.6 MPa $m^{1/2}$, we calculated that minimum and maximum flaw sizes of about $0.001d$ and $0.1d$ are required to fit the fracture strength data of *Wawersik and Brace* [1971] for Westerly granite. The "active" flaw size $2c$ ranged from $0.2d$ for stress ratios $\lambda < 0.03$, to $0.01d$ for $0.06 < \lambda < 0.16$. (Note that the sliding crack model requires the "active" flaw size to change with confining pressure in order to match the experimentally observed curvature of plots of peak stress versus confining pressure.) *Horii and Nemat-Nasser* [1985*a*] may be successful in modelling work softening behavior for stress ratios λ up to 0.16 simply because they analyze an intrinsically less stable crack configuration than *Ashby and Hallam*.

The fracture data (Table 2) clearly follow an inverse square root of grain size relation (Figure 3*a*). Thus, it is probably adequate to characterize the initial flaw population with a simple relation such as that used by *Ashby and Hallam* [1986]. In any case, complicated functions such as that used by *Horii and Nemat-Nasser* [1985*a*] (discussed above) would be difficult to specify a priori, especially since the "active" flaw size changes with confining pressure. Our data indicate that the dependence of fracture strength on grain size (i.e., the slope of the Hall-Petch relation) is the same for uniaxial compression, and for triaxial compression at confining pressures of 5 and 10 MPa; these data correspond to stress ratios λ ranging from 0 to 0.1. This observation would seem to preclude the "active" flaw size changing with confining pressure.

It is noteworthy that if the initial crack density ϵ_o in the different grain-sized aggregates varies substantially, then *Ashby and Hallam*'s [1986] simple model predicts significant departures from a linear Hall-Petch relation. For example, correlation coefficients of only 0.85 could result if the initial crack density varied from three cracks for every two grains to one crack for every six grains for the different aggregates (Figure 11). Although *Horii and Nemat-Nasser*'s [1985*a*] model predicts work softening behavior at stress ratios an order of magnitude greater than *Ashby and Hallam*'s [1986] model, the former seems even less likely to predict a near-perfect Hall-Petch relation for the different grain-sized aggregates, since the many additional parameters which are required to characterize the initial flaw population (see above) would have to be identical for the different rocks.

The above observations suggest to us that, in addition to constraining the initial crack size, grain size probably has a more fundamental effect on the fracture behavior. For example, the characteristic scale of the spatial heterogeneity of the local stress field should be significantly smaller in a fine-grained aggregate than in a coarse-grained aggregate. Such heterogeneity will clearly have strong effects on the crack propagation behavior, and may cause crack arrest at stages earlier than those predicted by the fracture mechanics models.

Effects such as these, however, would be difficult to model using a fracture mechanics approach. *Costin* [1985] includes such a scaling parameter in his model of rock failure.

Brittle-Ductile Transition

Our experimental data indicate that the stress ratio $\lambda=\sigma_3/\sigma_1$ at the brittle-ductile transition in the different calcitic rocks is a constant and equal to about 0.16 (Figure 2). Thus, *Horii and Nemat-Nasser*'s [1986] conclusion that the stress ratio λ at the brittle-ductile transition characterizes a material's "ductility" requires that the different calcitic rocks have the same "ductility". If it is assumed that the initial flaw size $2c$ is equal to (or some constant fraction of) the grain size d (Figure 7, see also previous discussion), then the ratio $(K_c/\tau_y)^2$ must scale with d in order for the different calcite rocks to have the same ductility. However, if the fracture toughness K_c and the "yield stress in shear" τ_y are interpreted as single-crystal mineral properties (i.e., constant for the different grain-sized aggregates), then the experimental data do not agree with the model (Figure 6).

The experimental data for the brittle-ductile transition require that either the yield stress in shear decrease or else the fracture toughness K_c increase with increasing grain size. Our mechanical data indicate that, in calcite aggregates, the "plastic" initial yield stress has an inverse square root dependence on the grain size d (Figures 3*a* and 3*b*). We cannot distinguish the relative contributions of twinning and dislocation glide to the plastic yield stress; both probably contribute to the observed grain size effect. At low temperatures, grain boundaries represent significant obstacles to dislocation glide and twin propagation due to the change in crystallographic orientation at the boundary. The case of a dislocation pile-up is well studied; analyses predict an inverse square root dependence of the plastic flow stress on the grain size (see Figure 3*b*) [*Hall*, 1951; *Petch*, 1953; see also *Hansen*, 1985]. Similarly, qualitative microstructural observations suggest an inverse relationship between grain size and twinning [e.g., *Schmid et al.*, 1987; *Takeshita et al.*, 1987; *Rutter and Rowe*, 1988]. It is difficult to

ascertain the effect of grain size on the fracture toughness K_c; we are not aware of any data for rocks and the data for ceramics are indeterminate [e.g., *Rice et al.*, 1980].

Thus, the brittle-ductile transition in polycrystalline aggregates is probably too complex to be characterized by *Horii and Nemat-Nasser*'s [1986] relatively simple model (Figure 5*b*). Our results imply that the structural complexity of polycrystalline aggregates influences significantly the nature of plastic flow and microcrack propagation. Specifically, our observations suggest that a grain size dependence of the "yield stress in shear" τ_y, and also possibly the fracture toughness K_c, must be considered in order to model the effect of grain size on the stress ratio λ at the brittle-ductile transition. Such considerations will also be necessary to model the brittle-ductile transition in silicate rocks at elevated temperatures, where crack-tip "blunting" and dislocation pile-ups are also expected to occur.

Implications

It is well established both experimentally and theoretically that fine-grained aggregates are weaker than coarse-grained aggregates when deformed in the diffusional creep/grain boundary sliding regime [e.g., *Poirier*, 1985]. Conversely, the effect of grain size on strength at low temperatures has received considerably less attention. Our experimental results indicate that the brittle fracture strength, semibrittle flow stress, and plastic yield stress of calcite aggregates at low temperatures are influenced significantly by grain size. Moreover, the qualitative nature of the dependence is similar in the different low-temperature deformational fields: fine-grained aggregates are stronger than coarse-grained aggregates. Thus, only in the deformational regime of diffusion-accommodated power-law creep may strength be considered to be independent of grain size.

It is well known that on a plot of strength versus confining pressure, the brittle-ductile transition in rocks is described by a linear relationship [*Byerlee*, 1968]. Although this relationship is generally observed in rocks [see a review of the experimental data by *Evans et*

al., 1989], the mechanical basis has never been well-founded. Our experimental results, coupled with *Horii and Nemat-Nasser*'s [1986] model (when interpreted in the appropriate context), provide insight into the physical basis for this relationship. Our observation that the stress ratio σ_3/σ_1 at the transition from brittle fracture to semibrittle flow is a constant for calcite aggregates (Figure 6) is, in fact, simply a restatement of *Byerlee*'s [1968] observation; the slope of the line bounding the transition in Figure 2 is the inverse of the stress ratio σ_3/σ_1. Since the coefficient of friction μ for different minerals is about the same [e.g., *Paterson*, 1978], *Horii and Nemat-Nasser*'s [1986] model suggests that rocks undergo the transition from brittle fracture to semibrittle flow at approximately the same stress ratio σ_3/σ_1 because the ductility of the different mineral aggregates does not vary greatly.

Conclusions

Our experimental data indicate that in calcite aggregates, the brittle fracture strength, "plastic" macroscopic yield stress at low temperatures, and brittle-ductile transition pressure depend inversely on the grain size d; our results agree qualitatively with those of previous workers who studied only individual aspects of the grain size effect [*Paterson*, 1958; *Brace*, 1961; *Olsson*, 1974; *Schrodt and Holder*, 1983]. Additionally, we find that the stress ratio $\lambda=\sigma_3/\sigma_1$ at the brittle-ductile transition is a constant independent of grain size, and equal to about 0.16 for calcite aggregates. The effect of grain size on both the brittle and plastic strengths is well described by empirical Hall-Petch relations, which express an inverse square root dependence of strength on grain size. Although the brittle fracture and low-temperature plastic flow strengths for other rocks are expected to follow $d^{-1/2}$ relations, we see no physical reason to suppose that the confining pressure at the transition from brittle fracture to semibrittle flow will depend inversely on grain size for all rocks. The only other data of which we are aware are those of *Paterson and Weaver* [1970] for MgO; they also found an inverse relationship between grain size and the brittle-ductile transition pressure. We expect

the qualitative nature of the trend to depend on the details of the grain size sensitivity in the brittle and plastic fields for each rock type.

We compared our experimental results to fracture mechanics models of brittle fracture and the brittle-ductile transition in compression. *Ashby and Hallam*'s [1986] model predicts that the presence of a small confining pressure alone is sufficient to inhibit work softening behavior and localization; however, our experimental results indicate that work softening and localization occur for stress ratios significantly higher than those predicted by the model. Moreover, we find that, in marble, the inhibition of localization with increased confining pressure is due to the increased activity of plastic flow mechanisms, rather than due to the increased difficulty of crack propagation alone [*Fredrich et al.*, 1989]. Non-porous rocks in general seem to follow the same trend: silicate rocks which do not deform plastically at room temperature exhibit shear localization at confining pressures greater than 2 GPa [*Schock and Heard*, 1974; *Shimada et al.*, 1983]. An exception is feldspar; with increasing pressure, non-porous aggregates appear to undergo a transition to non-localized deformation in the absence of crystal-plastic processes [*Tullis and Yund*, 1987].

The effect of grain size on fracture strength is typically rationalized by noting that, in rocks, the initial crack size $2c$ scales with the grain size d. With this premise, we calculated the theoretical predictions of *Ashby and Hallam*'s model for the effect of grain size on the fracture strength. In general, the values of the ratio $2c/d$ which match the experimentally determined Hall-Petch slope best underestimate significantly the experimentally observed strength in uniaxial compression. Additionally, their model predicts that significant departures from a linear Hall-Petch relation may occur if the initial crack density ϵ_0 ($=c^2N_A$, where N_A is the number of cracks per unit area) in the rocks differs substantially. That the experimental data follow a nearly perfect Hall-Petch relation at room pressure and confining pressures of 5 and 10 MPa suggests to us that, in addition to controlling the initial flaw size, grain size may have a more fundamental effect on brittle fracture. We suppose that the spatial heterogeneity

of the local stress field in rocks should scale inversely with the grain size, and that this may be a more likely cause for the observed grain size effect.

Comparison of our results with those of *Horii and Nemat-Nasser* [1985*a*] highlights some of the difficulties associated with the sliding crack model. *Horii and Nemat-Nasser* analyzed rigorously the interaction effect for an array of colinear sliding cracks and enjoyed considerable success in modelling experimental fracture data for Westerly granite. Thus, the theoretical crack growth behavior predicted by the sliding crack model is very sensitive to the geometrical details of the assumed flaw population. Likewise, *Kemeny and Cook* [1987] modelled axial splitting using the sliding crack and found that the predicted work softening behavior depended critically on whether axially aligned or parallel cracks were considered.

If the initial flaw size $2c$ scales with the grain size, and if the mode I fracture toughness K_c and yield stress in shear τ_y are interpreted as single-crystal mineral properties, then *Horii and Nemat-Nasser*'s [1986] model predicts that the stress ratio $\lambda=\sigma_3/\sigma_1$ at the brittle-ductile transition scales with the grain size d. However, the experimental data do not corroborate the model unless the ratio $(K_c/\tau_y)^2$ scales with d; this implies that the structural complexity of polycrystalline aggregates influences significantly the nature of plastic flow and crack propagation. Our experimental data indicate that the macroscopic initial "plastic" yield stress in marble depends upon grain size; this effect may be rationalized by noting that grain boundaries may act as obstacles to dislocation glide and twin propagation; the effect of grain size on the fracture toughness is less certain. Nevertheless, such considerations are probably necessary in order to model the brittle-ductile transition in polycrystalline aggregates. The stress ratio σ_3/σ_1 at the brittle-ductile transition is apparently a constant for many different rock types [e.g., *Byerlee*, 1968]; we suggest that the physical basis for this relationship is that the ductility of most mineral aggregates falls within a small range.

NOTATION

c one-half the initial flaw length, m.

C' differential stress at onset of dilatancy, MPa.

d grain size, m.

K_1 mode I stress intensity factor, MPa $m^{1/2}$.

K_c mode I fracture toughness, MPa $m^{1/2}$.

ℓ wing crack length, m.

L wing crack length normalized by one-half the initial flaw length, dimensionless.

N_A number of sliding cracks per unit area, m^{-2}.

γ angle between sliding crack and maximum applied stress, degrees.

Δ ductility parameter, dimensionless.

ϵ_o crack density parameter, dimensionless.

θ angle between sliding crack and wing crack, degrees.

λ ratio of minimum to maximum principle applied stress, dimensionless.

μ coefficient of friction on sliding crack, dimensionless.

σ_1 maximum principle applied stress, MPa.

σ_3 minimum principle applied stress, MPa.

σ_Y macroscopic initial yield stress, MPa.

τ_c cohesion along sliding crack surface, MPa.

τ_y yield stress in shear, MPa.

REFERENCES

Abdel-Gawad, M., J. Bulau, and B. Tittman, Quantitative characterization of microcracks at elevated pressure, *J. Geophys. Res.*, *92*, 12,911-12,916, 1987.

Ashby, M. F., and S. D. Hallam, The failure of brittle solids containing small cracks under compressive stress states, *Acta Metall.*, *34*, 497-510, 1986.

Atkinson, B. K., Fracture toughness of Tennessee sandstone and Carrara marble using the double torsion testing method, *Int. J. Rock Mech. Min. Sci. Geomech. Abstr.*, *16*, 49-53, 1979.

Atkinson, B. K., Subcritical crack growth in geological materials, *J. Geophys. Res.*, *89*, 4077-4114, 1984.

Brace, W. F., Dependence of fracture strength of rocks on grain size, *Proc. Symp. Rock Mechanics*, *4th*, Penn. State Univ. Min. Ind. Exp. Sta. Bull, *No. 76*, 99-103, 1961.

Brace, W. F., Brittle fracture of rocks, in *State of Stress in the Earth's Crust*, edited by W. R. Judd, pp. 111-174, Elsevier, New York, 1964.

Brace, W. F., B. W. Paulding, and C. H. Scholz, Dilatancy in the fracture of crystalline rocks, *J. Geophys. Res.*, *71*, 3939-3953, 1966.

Byerlee, J. D., Brittle-ductile transition in rocks, *J. Geophys. Res.*, *73*, 4741-4750, 1968.

Budiansky, B., and R. J. O'Connell, Elastic moduli of a cracked solid, *Int. J. Solids Struct.*, *12*, 81-97, 1976.

Chen, R., X.-x. Yao, H.-s. Xie, Studies of the fracture of gabbro, *Int. J. Rock Mech. Geomech. Abstr.*, 16, 187-193, 1979.

Costin, L. S., Damage mechanics in the post-failure regime, *Mech. Mat.*, 4, 149-160, 1985.

Edmond, J. M., and M. S. Paterson, Volume changes during the deformation of rocks at high pressures, *Int. J. Rock Mech. Min. Sci. Geomech. Abstr.*, *9*, 161-182, 1972.

Evans, B., and C. Goetze, The temperature variation of hardness of olivine and its implication for polycrystalline yield stress, *J. Geophys. Res.*, *84*, 5505-5524, 1979.

Evans, B., J. T. Fredrich, and T.-f. Wong, The brittle-ductile transition in rocks: Recent experimental and theoretical progress, in *The Heard Volume*, *Geophys. Monogr. Ser.*, edited by A. Duba, W. B. Durham, J. Handin, J. Logan, and H. Wang, AGU, Washington, D.C., in press, 1989.

Fredrich, J. T., and T.-f. Wong, Micromechanics of thermally induced cracking in three crustal rocks, *J. Geophys. Res.*, *91*, 12,743-12,764, 1986.

Fredrich, J. T., B. Evans, and T.-f. Wong, Micromechanics of the brittle to plastic transition in Carrara marble, *J. Geophys. Res.*, *94*, 4129-4145, 1989.

Griffith, A. A., The theory of rupture, in *Proc. 1st Int. Congr. Appl. Mech.*, edited by C. B. Biezeno and J. M. Burgers, pp. 54-63, Delft, J. Waltman, Jr., 1924.

Griggs, D. T., F. J. Turner, and H. C. Heard, Deformation of rocks at 500° to 800°C, in *Rock Deformation*, edited by D. T. Griggs and J. Handin, *Mem. Geol. Soc. Am.*, *79*, 39-104, 1960.

Hadley, K., Comparison of calculated and observed crack densities and seismic velocities of Westerly granite, *J. Geophys. Res.*, *81*, 3484-3494, 1976.

Hall, E. O., The deformation and aging of mild steel, III, Discussion of results, *Proc. Phys. Soc. London*, *64B*, 747-753, 1951.

Handin, J., and R. V. Hager, Experimental deformation of sedimentary rocks under confining pressure: Tests at room temperature on dry samples, *Bull. Amer. Ass. Petrol. Geol.*, *41*, 1-50, 1957.

Hansen, N., Polycrystalline Strengthening, *Metall. Trans.*, *16A*, 2167-2190, 1985.

Higgs, D. V., M. Friedman, and J. E. Gebhart, Petrofabric analysis by means of the X-ray diffractometer, in *Rock Deformation*, edited by D. T. Griggs and J. Handin, *Mem. Geol. Soc. Am.*, *79*, pp. 275-292, 1960.

Horn, H. M., and D. U. Deere, Frictional characteristics of minerals, *Geotechnique*, *12*, 319-335, 1962.

Holcomb, D. J., A quantitative model of dilatancy in dry rock and its application to Westerly granite, *J. Geophys. Res.*, *83*, 4941-4950, 1978.

Holcomb, D. J., and J. L. Stevens, The reversible Griffith crack: A viable model for dilatancy, *J. Geophys. Res.*, *85*, 7101-7107, 1980.

Horii, H., and S. Nemat-Nasser, Compression-induced microcrack growth in brittle solids: axial splitting and shear failure, *J. Geophys. Res.*, *90*, 3105-3125, 1985*a*.

Horii, H., and S. Nemat-Nasser, Elastic fields of interacting inhomogeneities, *Int. J. Solids Struct.*, *7*, 731-745, 1985*b*.

Horii, H., and S. Nemat-Nasser, Brittle failure in compression: splitting, faulting, and brittle-ductile transition, *Phil. Trans. Roy. Soc. Lond. A*, *319*, 337-374, 1986.

Hugman, R. H. H., and M. Friedman, Effects of texture and composition on mechanical behavior of experimentally deformed carbonate rocks, *Bull. Am. Ass. Petrol. Geol.*, *63*, 1478-1489, 1979.

Kachanov, M. L., A microcrack model of rock inelasticity, part I, Frictional sliding on microcracks, *Mech. Mat.*, *1*, 19-27, 1982.

Kemeny, J. M., and N. G. W. Cook, Crack models for the failure of rocks in compression, *Proc. Int. Conf. on Const. Laws for Eng. Mat.*, *2*, 879-887, 1987.

Kranz, R. L., Crack growth and development during creep of Barre granite, *Int. J. Rock Mech. Min. Sci. Geomech. Abstr.*, *16*, 23-35, 1979.

Kranz, R. L., Microcracking in rocks, a review, *Tectonophysics*, *100*, 449-480, 1983.

McClintock, F. A., and J. B. Walsh, Friction on Griffith cracks in rocks under pressure, *Proc. U.S. Nat. Congr. Appl. Mech.*, *4th*, *Vol. II*, American Society of Mechanical Engineers, 1015-1021, 1962.

Moss, W. C., and Y. M. Gupta, A constitutive model describing dilatancy and cracking in brittle rocks, *J. Geophys. Res.*, *87*, 2985-2998, 1982.

Nemat-Nasser, S., Discussion of "Geometric probability approach to the characterization and analysis of microcracking in rocks", by Teng-fong Wong, *Mech. Mat.*, *4*, 277-281, 1985.

Nemat-Nasser, S., and H. Horii, Compression-induced nonplanar crack extension with application to splitting, exfoliation, and rockburst, *J. Geophys. Res.*, *87*, 6905-6821, 1982.

Nemat-Nasser, S., and M. Obata, A microcrack model of dilatancy in brittle materials, *J. Appl. Mech.*, *55*, 24-35, 1988.

Nur, A., and Simmons, G., The origin of small cracks in igneous rocks, *Int. J. Rock Mech. Min. Sci.*, *7*, 307-314, 1970.

Olgaard, D. L., Grain growth and mechanical processes in two-phased synthetic marbles and natural fault gouge, Ph.D. thesis, Massachusetts Institute of Technology, Cambridge, 1985.

Olsson, W. A., Grain size dependence of yield stress in marble, *J. Geophys. Res.*, *79*, 4859-4862, 1974.

Paterson, M. S., Experimental deformation and faulting in Wombeyan marble, *Geol. Soc. Am. Bull.*, *69*, 465-476, 1958.

Paterson, M. S., *Experimental Rock Deformation - the Brittle Field*, 254 pp., Springer-Verlag, New York, 1978.

Paterson, M. S., and C. W. Weaver, Deformation of polycrystalline MgO under pressure, *J. Am. Ceram. Soc.*, 463-471, 1970.

Peng, S. S., and A. M. Johnson, Crack growth and faulting in cylindrical specimens of Chelmsford granite, *Int. J. Rock. Mech. Min. Sci. Geomech. Abstr.*, *9*, 37-86, 1972.

Petch, N. J., The cleavage strength of polycrystals, *J. Iron Steel Inst.*, *174*, 25-28, 1953.

Poirier, J. P., *Creep of Crystals*, 260 pp., Cambridge University Press, 1985.

Ramez, M. R. H., and S. A. F. Murrell, A petrofabric analysis of Carrara marble, *Int. J. Rock Mech. Min. Sci. Geomech. Abstr.*, *1*, 217-229, 1964.

Rice, R. W., S. W. Freiman, and J. J. Mecholsky, The dependence of strength-controlling fracture energy on the flaw-size to grain-size ratio, *J. Am. Ceram. Soc.*, *63*, 129-136, 1980.

Rutter, E. H., and K. J. Rowe, Experimental calibration of a calcite twinning paleopiezometer and its application to nature, *Eos Trans. AGU*, *69*, 1463, 1988.

Schmid, S. M., J. N. Boland, and M. S. Paterson, Superplastic flow in finegrained limestone, *Tectonophysics*, *43*, 257-291, 1977.

Schmid, S. M., M. Casey, and J. Starkey, The microfabric of calcite tectonites from the Helvetic Nappes (Swiss Alps), in *Thrust and Nappe Tectonics*, p. 151-158, Geol. Soc. Lond., 1981.

Schmid, S. M., R. Pannozzo, and S. Bauer, Simple shear experiments on calcite rocks: Rheology and microfabric, *J. Struct. Geol.*, *9*, 747-778, 1987.

Schock, R. N., and H. C. Heard, Static mechanical properties and shock loading response of granite, *J. Geophys. Res.*, *79*, 1662-1666, 1974.

Schrodt, J. K., and J. T. Holder, Temperature and strain rate effects on micromechanical behavior in triaxially compressed marbles, *Proc. U.S. Symposium on Rock Mechanics*, *24th*, 449-468, 1983.

Scholz, C. H., Microfracturing and inelastic deformation of rock in compression, *J. Geophys. Res.*, *73*, 1417-1432, 1968.

Shimada, M., A. Cho, and H. Yukatake, Fracture strength of silicate rocks at high confining pressures and activity of acoustic emission, *Tectonophysics*, *121*, 153-173, 1986.

Simmons, G., T. Todd, and W. S. Baldridge, Toward a quantitative relationship between elastic properties and cracks in low porosity rocks, *Am. J. Sci.*, *275*, 318-345, 1975.

Sprunt, E. S., and W. F. Brace, Direct observation of microcavities in crystalline rocks, *Int. J. Rock Mech. Min. Sci. Geomech. Abstr.*, *11*, 139-150, 1974.

Stevens, J. L., and D. J. Holcomb, A theoretical investigation of the sliding crack model of dilatancy, *J. Geophys. Res.*, *85*, 7091-7100, 1980.

Skinner, W. J., Experiments on the compressive strength of anyhdrite, *Engineer*, *207*, 255-259, 288-292, 1959.

Takeshita, T., C. Tome, H.-R. Wenk, and U. F. Kocks, Single-crystal yield surface for trigonal lattices: Application to texture transitions in calcite polycrystals, *J. Geophys. Res.*, *92*, 12,917-12,930, 1987.

Tapponier, P., and W. F. Brace, Development of stress-induced microcracks in Westerly granite, *Int. J. Rock Mech. Min. Sci. Geomech. Abstr.*, *13*, 103-113, 1976.

Tullis, J., and R. A. Yund, Transition from cataclastic flow to dislocation creep of feldspar: Mechanisms and microstructures, *Geology*, *15*, 606-609, 1987.

Turner, F. J., D. T. Griggs, and H. C. Heard, Experimental deformation of calcite crystals, *Geol. Soc. Am. Bull.*, *65*, 883-894, 1954.

Underwood, E. E., *Quantitative Stereology*, Addison-Wesley, Reading, Mass., 1970.

Wang, C.-y., Velocity of compressional waves in limestones, marbles, and a single crystal of calcite to 20 kilobars, *J. Geophys. Res.*, *71*, 3543-3547, 1966.

Wawersik, W. R., and C. Fairhurst, A study of brittle rock fracture in laboratory compression experiments, *Int. J. Rock Mech. Min. Sci. Geomech. Abstr.*, *7*, 561-575, 1970.

Wawersik, W. R., and W. F. Brace, Post-failure behavior of a granite and diabase, *Rock Mech.*, *3*, 61-85, 1971.

Wong, T.-f., Micromechanics of faulting in Westerly granite, *Int. J. Rock Mech. Min. Sci. Geomech. Abstr., 19, 49-64, 1982.*

TABLE 1. Rocks Studied

Rock	P_L[a], mm^{-1}	d[b], mm	φ[c], %
Wombeyan marble	0.846±00.198	1.773±0.337	0.6
Carrara marble	6.700±01.107	0.230±0.041	0.7
Saillon marble	50.250±07.011	0.030±0.004	0.6
Solnhofen limestone	256.667±21.602	0.006±0.001	5.5

[a]Mean grain boundaries per unit length measured optically on thin sections using a linear intercept method. Test grid intercepted more than one hundred grain boundaries.

[b]Equivalent grain size assuming spherical, space-filling grains [see *Underwood*, 1974].

[c]Porosity calculated by comparing the observed density in air with the density of calcite.

TABLE 2. Mechanical Data

Sample	P_C, MPa	M^a	$(\sigma_1-\sigma_3)_{max}$, MPa	$\epsilon_1{}^b$, %	$\sigma_Y{}^c$, MPa	$\sigma_{2\%}{}^d$, MPa
WM1	30	C	118	2.73	76	117
WM2	10	S	84	2.98	65	68
WM3	20	S	106	3.23	67	91
WM4	120	H	245	3.03	76	234
WM5	5	S	75	2.99	60	42
WM6	300	H	350	4.67	101	283
WM7	atm	S	64	0.68	60	*
CM4	30	C	150	4.21	*	158
CM6	10	S	108	5.16	*	97
CM16	230	H	319	3.63	*	284
CM21	5	S	95	1.88	*	*
CM23	atm	S	84	0.45	58	*
CM25	85	H	249	4.91	110	220
CM27	120	H	293	5.34	110	244
CM29	190	H	333	5.14	112	265
CM30	300	H	329	3.00	130	296
CM31	40	C	173	2.81	88	172
CM33	450	H	320	2.20	*	312
SM1	50	S	228	3.03	202	208
SM2	30	S	223	3.01	199	183
SM3	30	S	237	2.28	218	141
SM4	70	C	288	3.00	*	282
SM5	50	C	229	3.00	181	229
SM6	50	S	235	2.17	197	230
SM7	30	S	225	2.22	180	152
SM8	70	H	276	3.00	189	267
SM9	5	S	200	0.84	196	*
SM10	190	H	331	2.26	202	320
SM11	300	H	351	2.80	181	332
SM15	5	S	195	0.79	191	*
SM16	190	H	325	1.25	203	*
SM17	atm	S	183	1.12	181	*
SM18	10	S	210	0.95	196	*
SL3	150	H	412	3.87	*	399
SL4	50	S	376	1.41	*	*
SL5	85	C	385	3.02	278	383
SL6	70	C	370	3.05	255	362
SL7	60	S	368	3.26	261	350
SL8[e]	300	H	413	3.15	178	376
SL9	10	S	323	1.30	268	*

(continued)

TABLE 2. Mechanical Data (continued)

Sample	P_C, MPa	M^a	$(\sigma_1-\sigma_3)_{max}$, MPa	$\epsilon_1{}^b$, %	$\sigma_Y{}^c$, MPa	$\sigma_{2\%}{}^d$, MPa
SL10	5	S	323	1.45	280	*
SL11	atm	S	320	1.65	287	*

[a]Macroscopic axial stress-strain behavior: H= hardening, S= softening, C= nearly continuous stress level.

[b]Total axial strain (elastic + permanent).

[c]Differential stress at the onset of nonlinearity in the axial stress-strain curve.

[d]Differential stress at 2% axial strain.

[e]Volumetric strain measurements indicated that initial yielding and subsequent inelastic deformation was at least partially accommodated by compaction.

FIGURE CAPTIONS

Figure 1. Axial stress-strain curves for samples of (*a*) Wombeyan marble, (*b*) Carrara marble, (*c*) Saillon marble, and (*d*) Solnhofen limestone deformed at the indicated confining pressures.

Figure 2. Peak applied axial stress σ_1 at the onset of work softening behavior (open symbols) and applied axial stress σ_1 at 2% strain (closed symbols) for samples of Wombeyan marble (WM), Carrara marble (CM), Saillon marble (SM), and Solnhofen limestone (SL) deformed in the brittle (b) and semibrittle (sb) fields as a function of the confining pressure, σ_3. The dotted line corresponds to a stress ratio $\lambda=\sigma_3/\sigma_1=0.16$ and delineates the boundary between the brittle and semibrittle fields.

Figure 3. (*a*) Uniaxial compressive fracture strength (squares), and fracture strength at confining pressures of 5 MPa (circles) and 10 MPa (triangles) plotted as a function of the inverse of the square root of the grain size d. Linear regression fits to the data are shown with dotted lines; the slope at room pressure, 5 MPa, and 10 MPa is 21.3, 20.5, and 19.7 MPa $mm^{1/2}$, respectively. (*b*) Macroscopic initial yield stress in the semibrittle field plotted as a function of the inverse of the square root of the grain size d. The linear regression fit yields a slope of 15.5 MPa $mm^{1/2}$. The correlation coefficients in (*a*) and (*b*) are all greater than 0.99.

Figure 4. Confining pressure at the transition from brittle fracture to semibrittle flow versus the inverse of the grain size d. Vertical error bars denote the upper and lower limits of brittle fracture and semibrittle flow, respectively (see Table 2).

Figure 5. (*a*) Sliding crack used to model brittle faulting. The maximum and minimum compressive stresses are denoted by σ_1 and σ_3. Sliding on the main crack of length $2c$ (oriented at an angle γ to σ_1) is accommodated by the wedging open of wing cracks of length ℓ (at an angle θ to the main crack). (*b*) Variation of the sliding crack used to model the brittle-ductile transition. Sliding on the main crack can be accommodated by either the wedging open of wing cracks, or else by the glide of edge dislocations colinear with the main crack.

Figure 6. Brittle-ductile diagram for an initial flaw orientation $\gamma=45°$, coefficient of friction $\mu=0.4$, and cohesion $\tau_c=0$; the qualitative behavior is similar for a wide range in values of γ, μ, and τ_c (after *Horii and Nemat-Nasser* [1986]). Also shown are the experimental data for the stress ratio $\lambda=\sigma_3/\sigma_1$ at the transition from brittle fracture to semibrittle flow; the ductility Δ for the different rocks was calculated assuming an initial flaw size $2c$ equal to the grain size d.

Figure 7. Reflected light optical micrographs of thick (> 1-2 mm) polished sections of (*a*) Wombeyan marble, (*b*) Carrara marble, (*c*) Saillon marble, and (*d*) Solnhofen limestone. In (*a*) twins are visible, and small pores are evident in (*d*). The faint straight lines in (*b*) and (*c*) are due to polishing, and in (*c*) and (*d*) cracks are indicated by the arrows. Note that the initial flaw size scales with grain size (micrographs are in order of decreasing grain size; see Table 1).

Figure 8. Wing crack propagation behavior plotted as normalized stress versus normalized wing crack length for (*a*) uniaxial compression ($\lambda=0$) and different initial crack densities ϵ_o and (*b*) variable stress ratios λ, as predicted using *Ashby and Hallam*'s [1986] result for the crack interaction effect (equation (3)). The solid lines were calculated using *Horii and Nemat-Nasser*'s [1986] result for wing crack growth (equation (1)), whereas the dotted lines are for *Ashby and Hallam*'s expression (equation (2)) that assumes $\gamma=\theta$. *Ashby and Hallam*'s expression overestimates significantly the stress intensity factor for normalized wing crack lengths $L<1$. The propagation behavior differs substantially for stress ratios $\lambda=0$ and $\lambda>0$. For a wide range in values of the crack density ϵ_o and coefficient of friction μ, the model predicts unstable crack growth (which presumably corresponds to the onset of macroscopic work softening and shear localization) only for $\lambda<0.015$.

Figure 9. Sample plot of normalized peak axial compressive stress at the onset of unstable crack growth versus the normalized confining pressure for an initial crack density $\epsilon_o=0.2$ and coefficient of friction $\mu=0.5$ (calculated using equations (2) and (3)). The theoretical

predictions fall on a straight line, regardless of the stress ratio λ. Note that the magnitude of λ is small (<0.02) for all of the calculations. Plots such as these were used to calculate the effect of initial flaw size on fracture strength.

Figure 10. Predictions of *Ashby and Hallam*'s [1986] model for the effect of initial flaw size on fracture strength. Shown are the predicted Hall-Petch slopes (i.e., the slope of a plot of peak stress (σ_1-σ_3) at the onset of unstable crack growth versus the inverse of the square root of the initial flaw size $2c$) in units of MPa $mm^{1/2}$ as a function of the initial crack density ϵ_o and coefficient of friction μ. Note that the calculations are based on plots like the sample shown in Figure 9. *Horii and Nemat-Nasser*'s [1986] estimate for isolated wing crack growth (equation (1)) was used to calculate the stress intensity factor K_1. The predicted slope of the Hall-Petch relation is more sensitive to the initial crack density ϵ_o than to the coefficient of friction μ on the sliding crack. The magnitude of the slope is comparable to the experimentally observed slope (see Figure 3*a*). Note that these results are valid only for values of the stress ratio $\lambda<0.02$.

Figure 11. Predicted uniaxial compressive strength as a function of the inverse square root of the grain size d for a coefficient of friction $\mu=0.5$, an initial flaw size $2c$ equal to the grain size d, and the indicated crack density ϵ_o. The linear regression fit shown with the dotted line yields a correlation coefficient of 0.85.

Figure 12. Comparison of theoretical predictions (closed symbols) and experimental data (open symbols) for the uniaxial (i.e., $\lambda=0$) compressive strength as a function of the inverse square root of the grain size d. Theoretical predictions are shown for an initial crack size $2c$ equal to the one, one-half, and one-tenth the grain size d, and are for a coefficient of friction $\mu=0.5$, and initial crack density ϵ_o equal to (*a*) 0.05, (*b*) 0.2, and (*c*) 0.5. Linear regression fits to the data are shown with the dotted lines. The results are qualitatively similar for $\mu=0.1$ (see Figure 10). The predictions are based on equations (1) and (3) (see Figure 10). The Hall-

Petch slopes predicted from equations (2) and (3) are qualitatively similar; however, the predicted strengths are lower (see Figure 8).

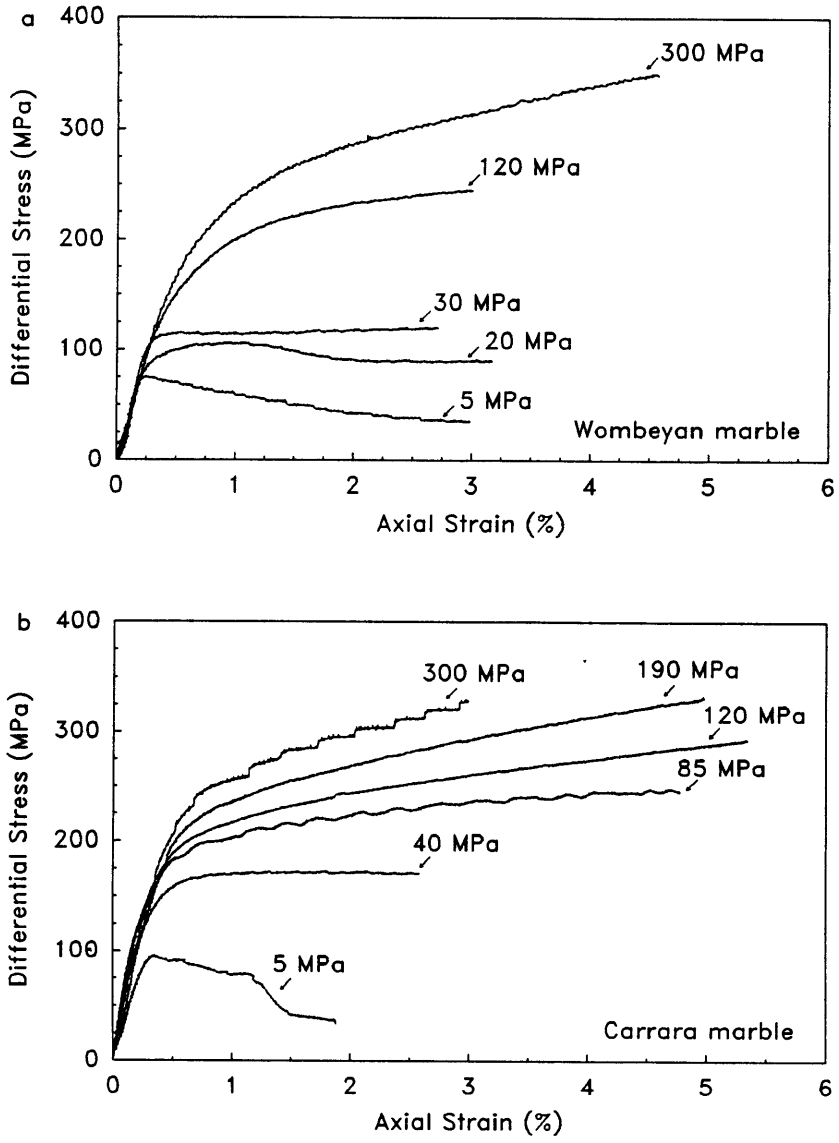
a
b
Differential Stress (MPa)
Axial Strain (%)
300 MPa
120 MPa
30 MPa
20 MPa
5 MPa
Wombeyan marble
190 MPa
85 MPa
40 MPa
Carrara marble
0
100
200
300
400
1
2
3
4
5
6

Figure 1*a*,*b*

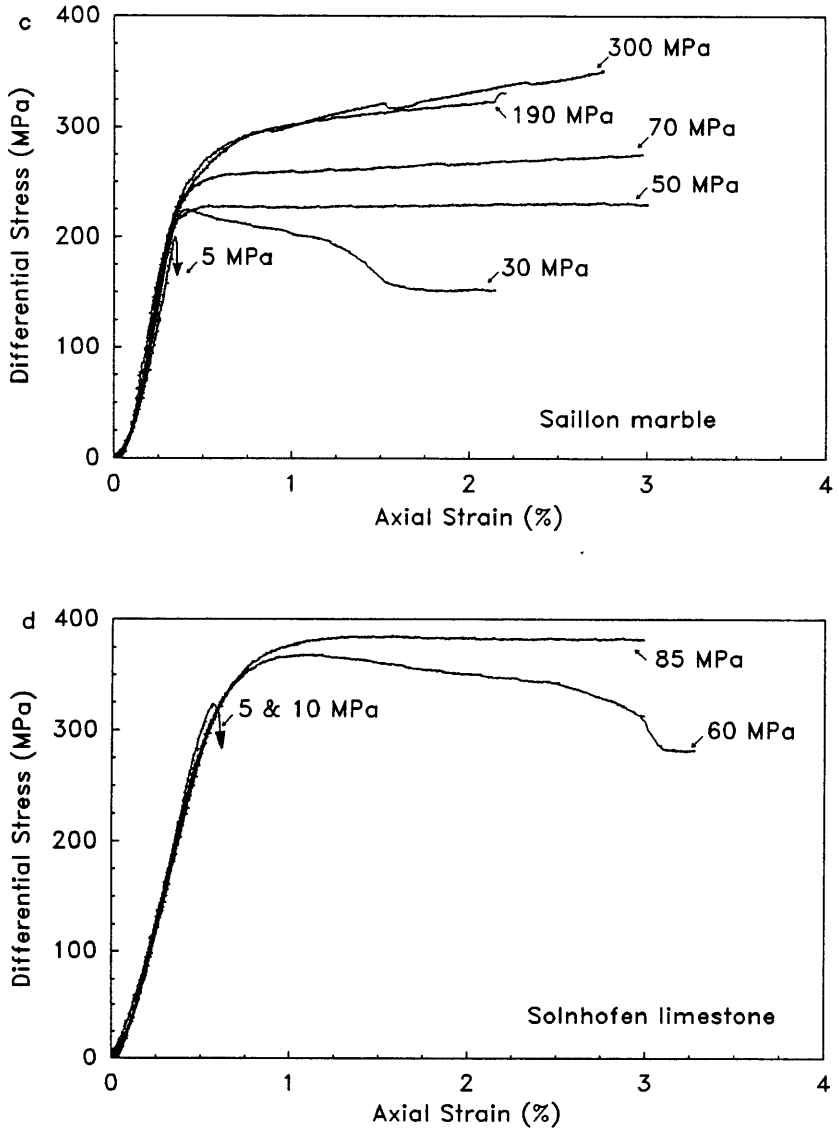
c
Differential Stress (MPa)
400
300
200
100
0
300 MPa
190 MPa
70 MPa
50 MPa
5 MPa
30 MPa
Saillon marble
0
1
2
3
4
Axial Strain (%)
d
Differential Stress (MPa)
400
300
200
100
0
85 MPa
5 & 10 MPa
60 MPa
Solnhofen limestone
0
1
2
3
4
Axial Strain (%)

Figure 1*c,d*

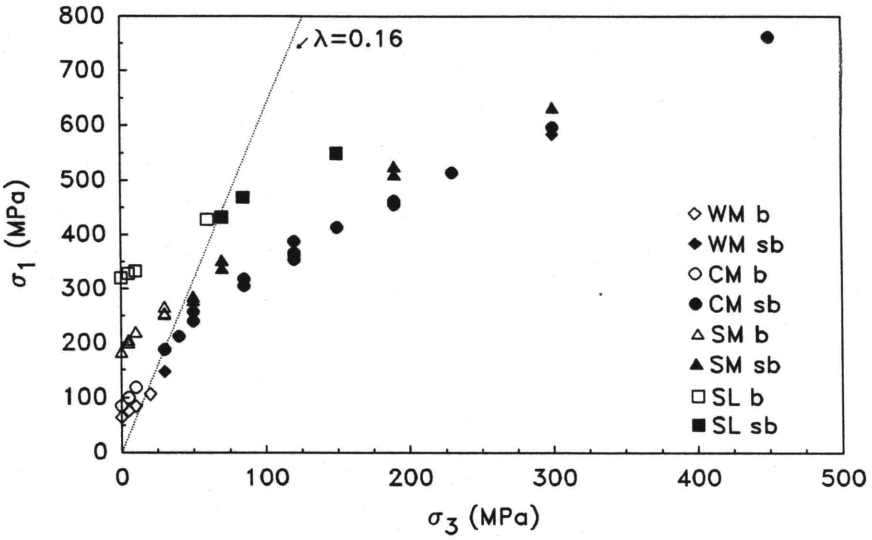
800
700
600
500
400
300
200
100
0
0
100
200
300
400
500
σ1 (MPa)
σ3 (MPa)
λ=0.16
WM b
WM sb
CM b
CM sb
SM b
SM sb
SL b
SL sb

Figure 2

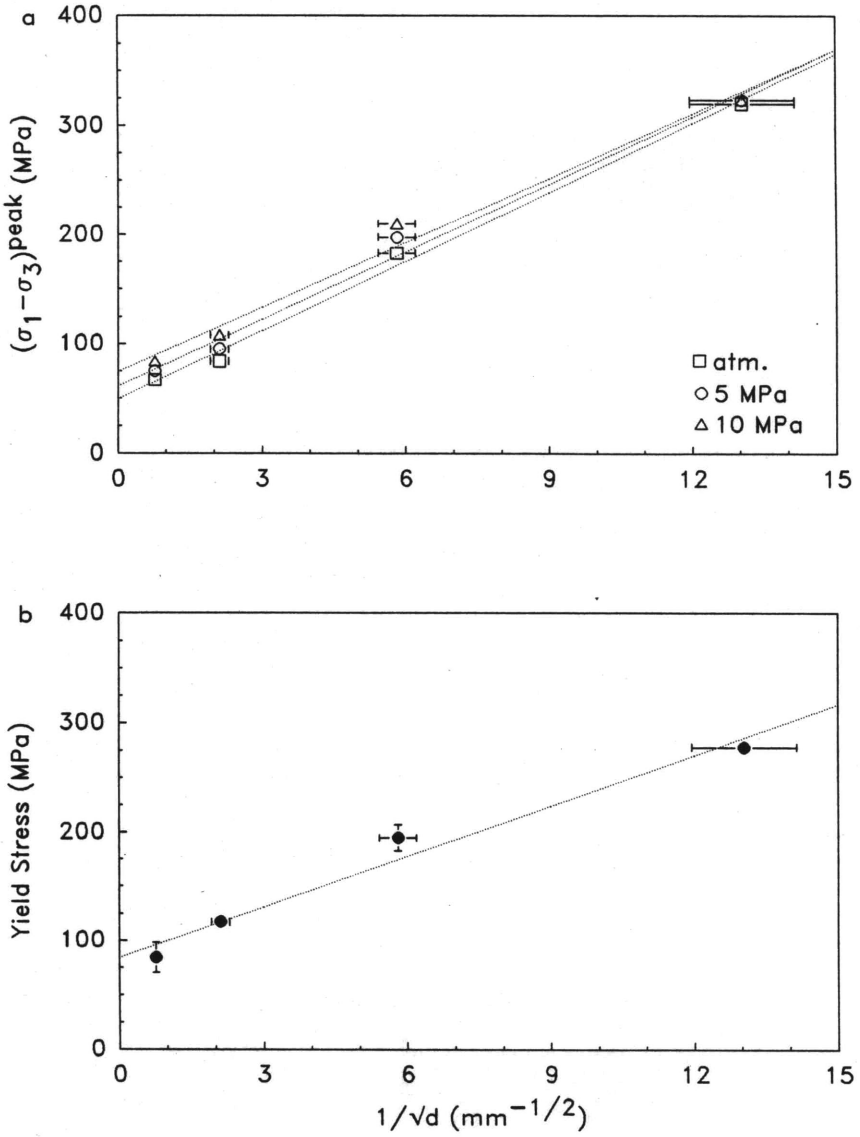
a
400
300
200
100
0
$(\sigma_1-\sigma_3)^{peak}$ (MPa)
0
3
6
9
12
15
□ atm.
○ 5 MPa
△ 10 MPa
b
400
300
200
100
0
Yield Stress (MPa)
0
3
6
9
12
15
1/√d ($mm^{-1/2}$)

Figure 3*a*,*b*

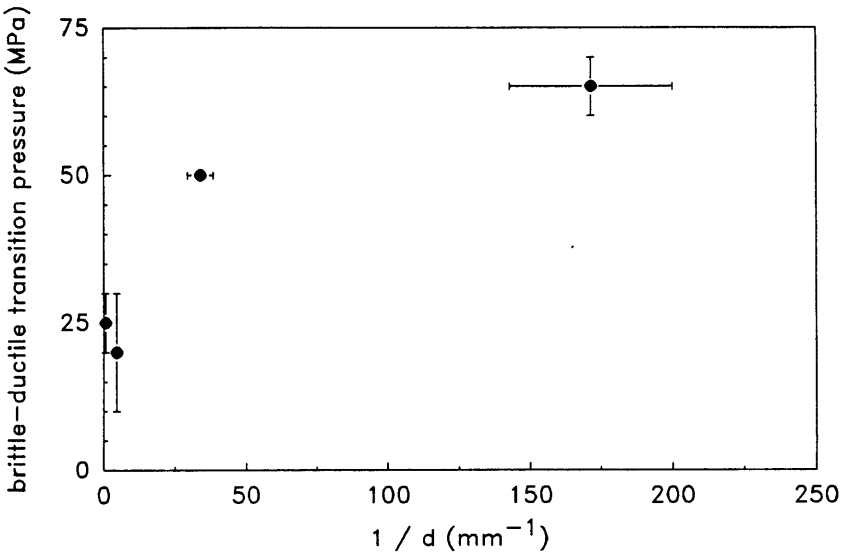
brittle–ductile transition pressure (MPa)
75
50
25
0
0
50
100
150
200
250
1 / d (mm^{-1})

Figure 4

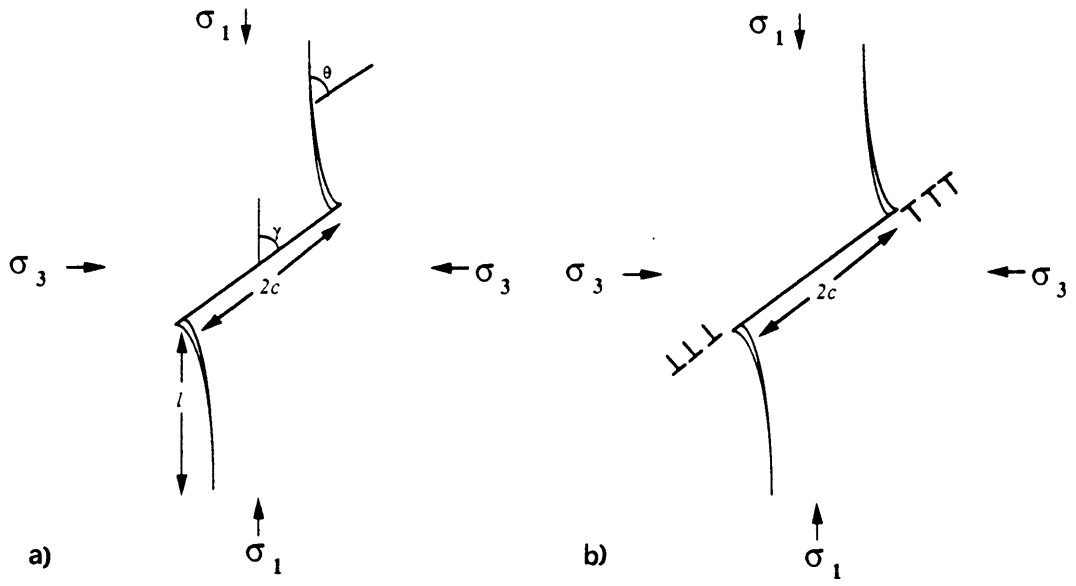

Figure 5*a,b*

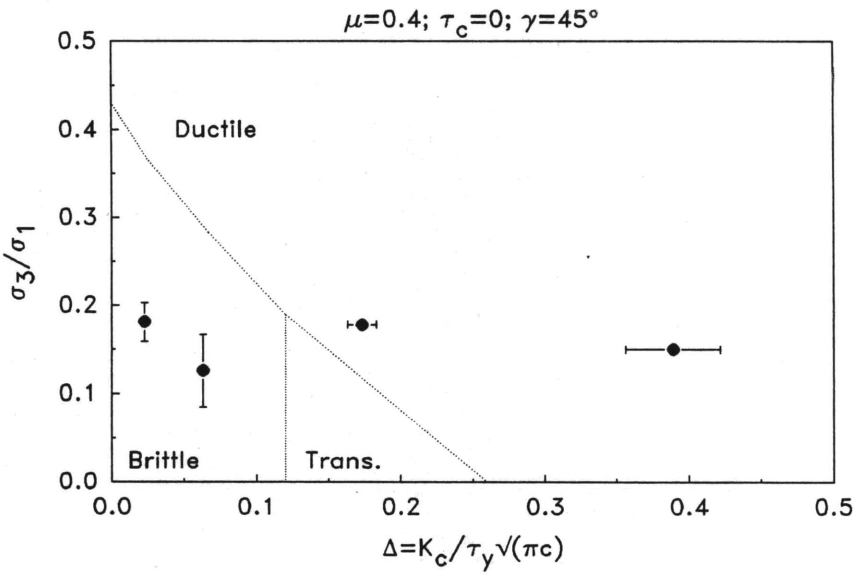
μ=0.4; τc=0; γ=45°
Ductile
Brittle
Trans.
σ3/σ1
Δ=Kc/τy√(πc)
0.0
0.1
0.2
0.3
0.4
0.5

Figure 6

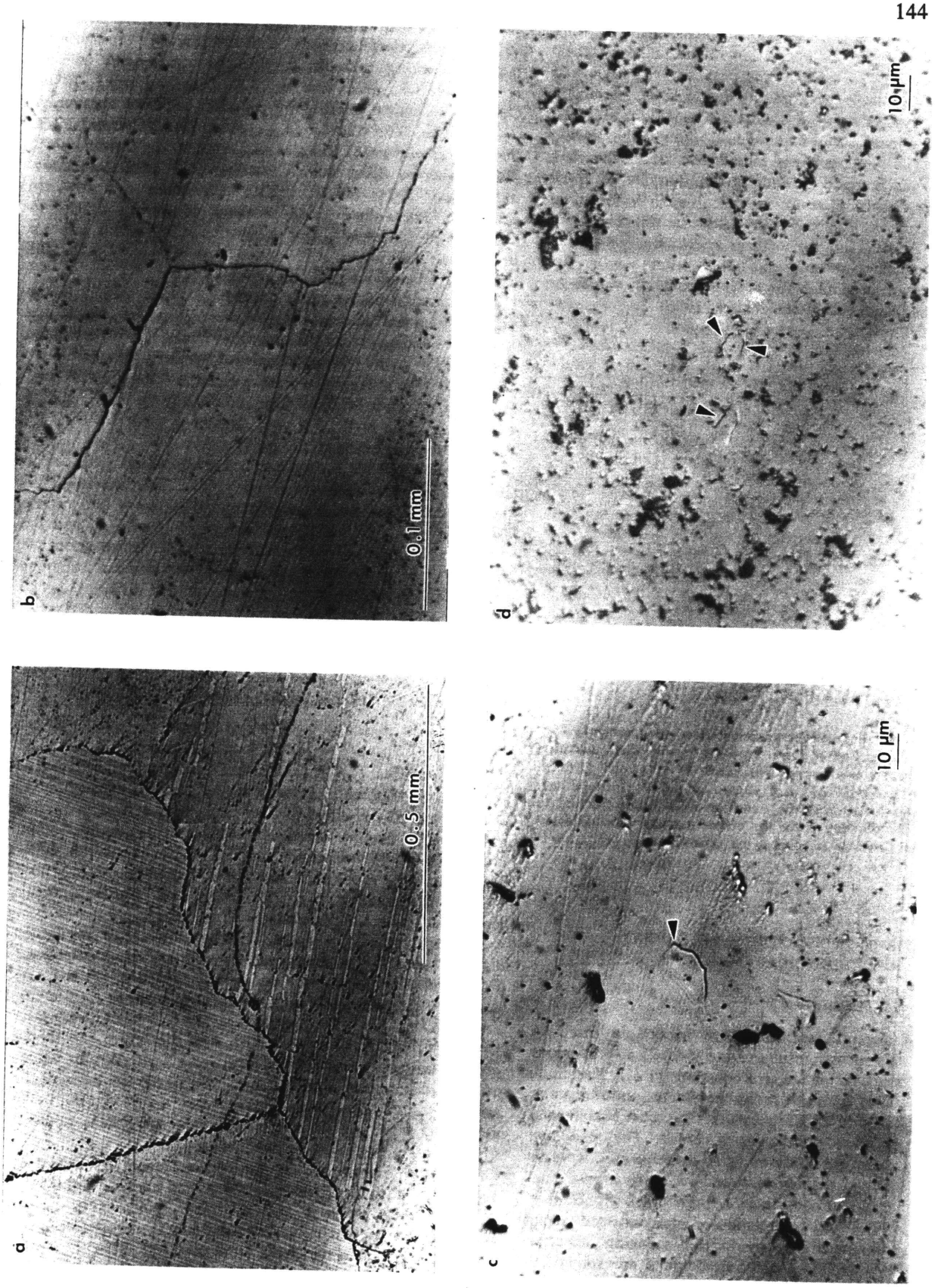

Figure 7

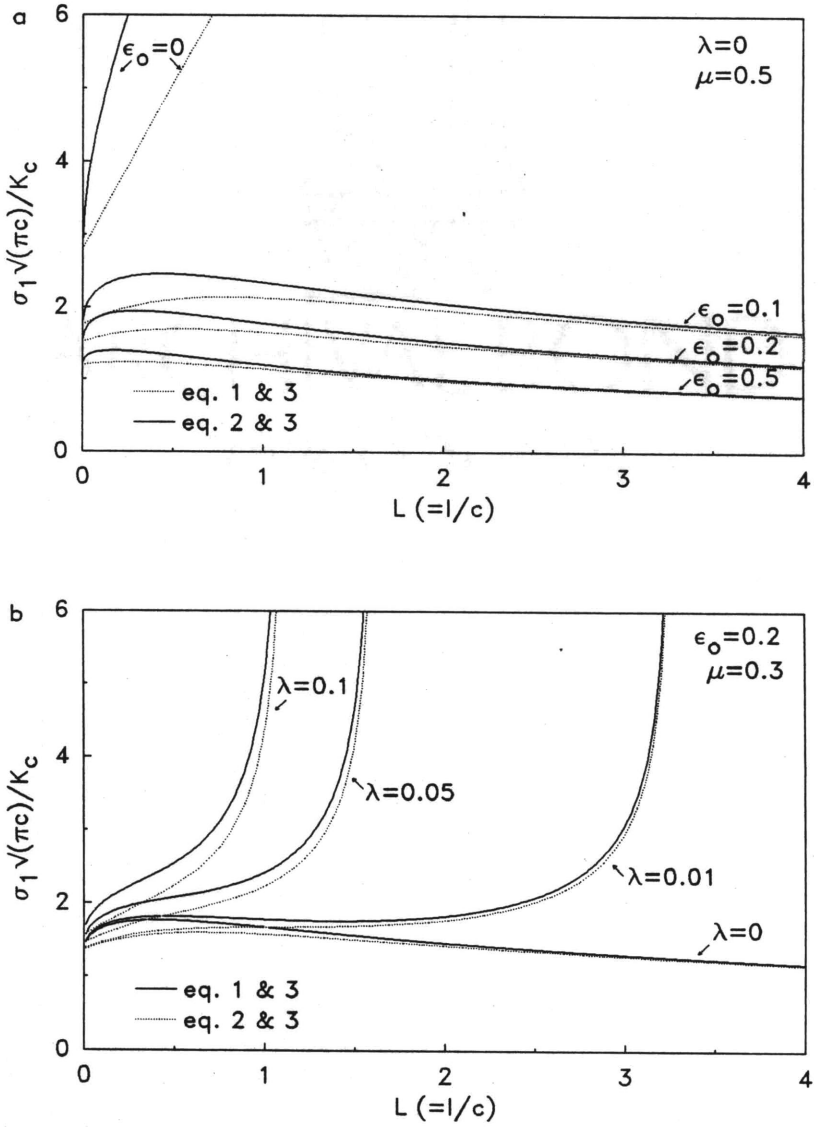
a
ϵ_o=0
λ=0
μ=0.5
ϵ_o=0.1
ϵ_o=0.2
ϵ_o=0.5
eq. 1 & 3
eq. 2 & 3
$\sigma_1\sqrt{(\pi c)}/K_c$
L (=l/c)
b
ϵ_o=0.2
μ=0.3
λ=0.1
λ=0.05
λ=0.01
λ=0
eq. 1 & 3
eq. 2 & 3
$\sigma_1\sqrt{(\pi c)}/K_c$
L (=l/c)

Figure 8*a,b*

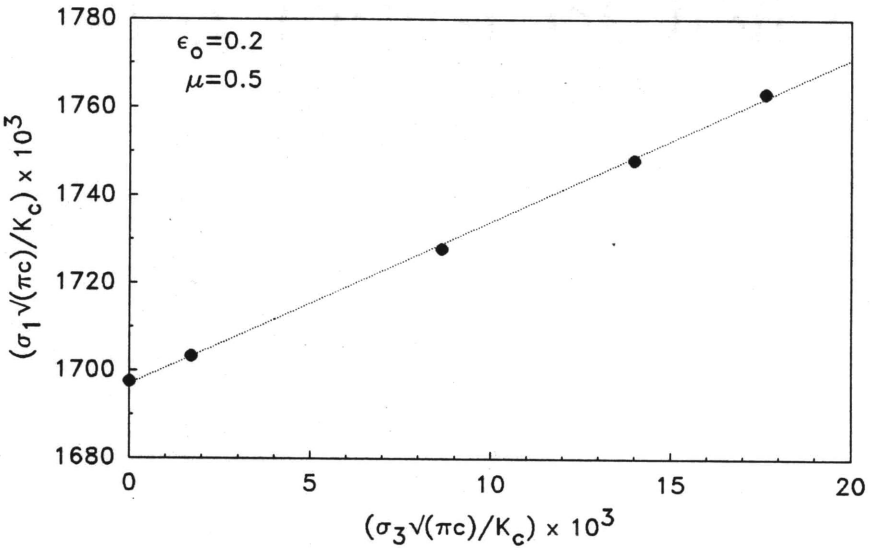
1780
1760
1740
1720
1700
1680
0
5
10
15
20
ϵ_o=0.2
μ=0.5
$(\sigma_1\sqrt{(\pi c)}/K_c) \times 10^3$
$(\sigma_3\sqrt{(\pi c)}/K_c) \times 10^3$

Figure 9

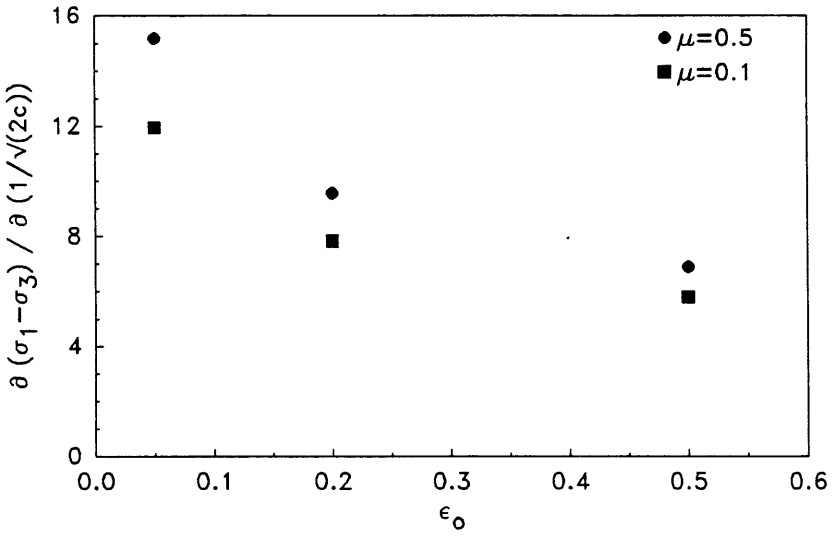
16
12
8
4
0
0.0
0.1
0.2
0.3
0.4
0.5
0.6
ϵ_o
$\partial(\sigma_1-\sigma_3) / \partial(1/\sqrt{(2c)})$
μ=0.5
μ=0.1

Figure 10

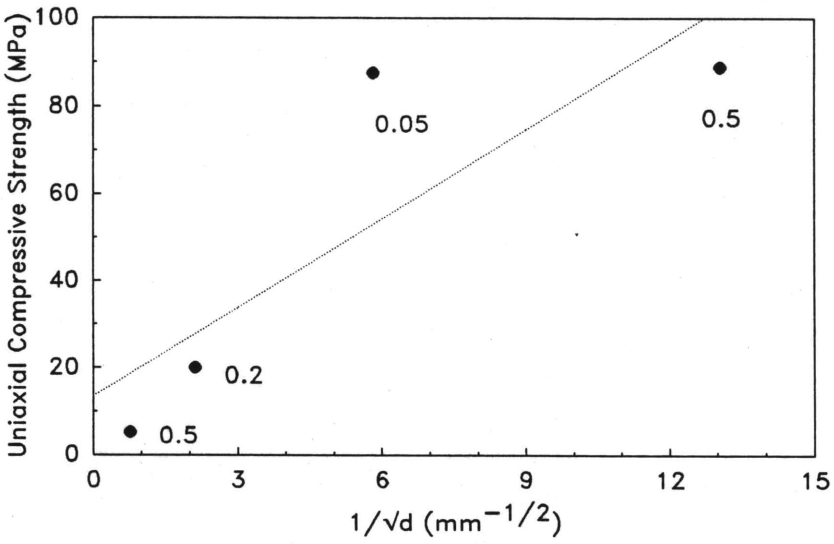
Uniaxial Compressive Strength (MPa)
100
80
60
40
20
0
0.05
0.5
0.2
0.5
0
3
6
9
12
15
1/√d (mm$^{-1/2}$)

Figure 11

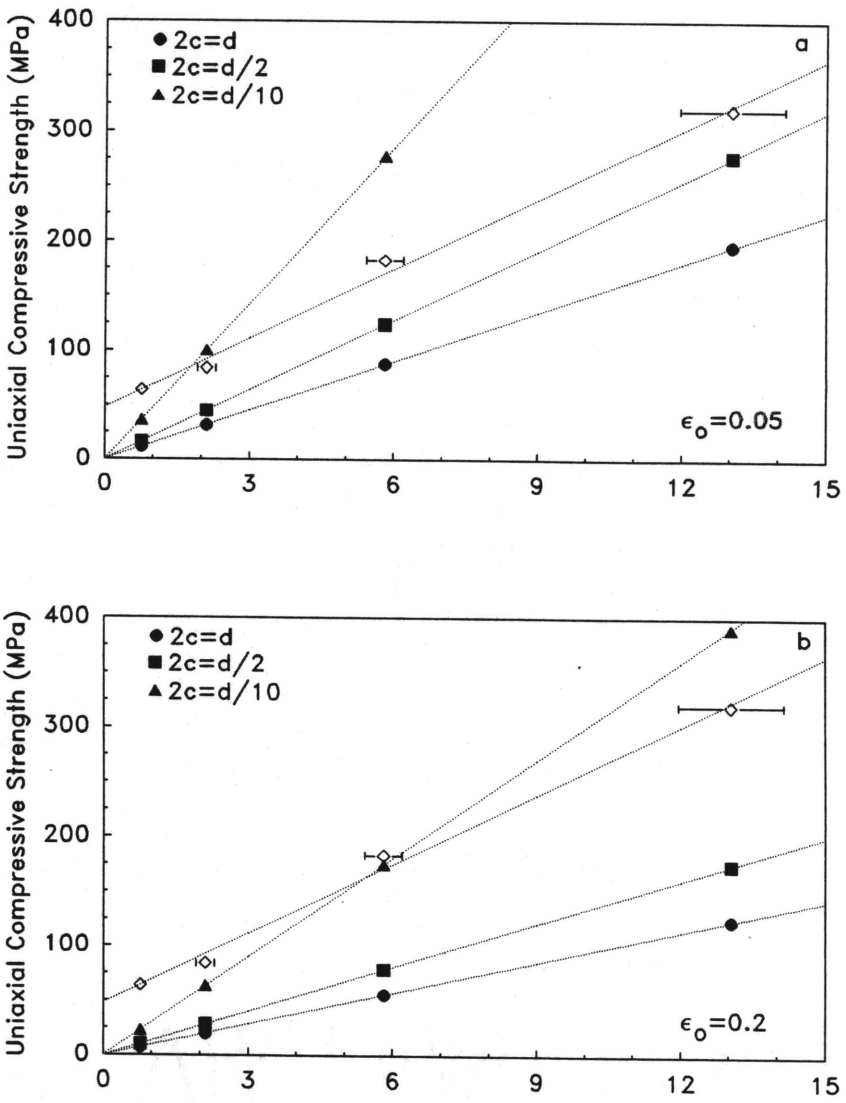
Uniaxial Compressive Strength (MPa)
400
300
200
100
0
0
3
6
9
12
15
● 2c=d
■ 2c=d/2
▲ 2c=d/10
a
ϵ_o=0.05
Uniaxial Compressive Strength (MPa)
400
300
200
100
0
0
3
6
9
12
15
● 2c=d
■ 2c=d/2
▲ 2c=d/10
b
ϵ_o=0.2

Figure 12*a,b*

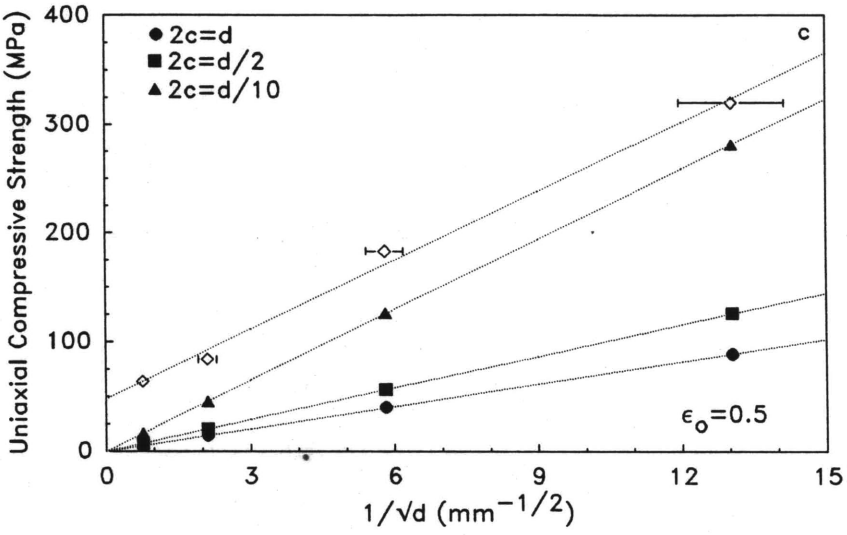
Uniaxial Compressive Strength (MPa)
400
300
200
100
0
● 2c=d
■ 2c=d/2
▲ 2c=d/10
c
ϵ_o=0.5
0
3
6
9
12
15
1/√d (mm$^{-1/2}$)

Figure 12*c*

Chapter 5
High Temperature Fracture and Flow of Maryland Diabase

INTRODUCTION

The lack of a constitutive relation for the semibrittle flow of silicate rocks is one of the most significant factors contributing to uncertainties in the rheology and strength of the lithosphere [e.g., *Carter and Tsenn*, 1987]. And although the room temperature deformation of carbonate rocks is to some extent analogous to the high temperature deformation of silicate rocks [e.g., *Evans et al.*, 1990], it is nevertheless of great interest to study directly the semibrittle deformation of silicate rocks. Specifically, at least two fundamental differences may exist between the semibrittle deformation of carbonate rocks (at room temperature) and silicate rocks (at high temperature). First, the high temperature deformation of silicate rocks depends critically on water content [e.g., *Paterson*, 1990]; and second, the micromechanisms of fracture and frictional slip may differ at high temperatures [e.g., *Paterson*, 1978], thus affecting the transition from brittle fracture to semibrittle flow.

Studies performed in solid-medium deformation apparatus indicate that water content significantly affects the transition from brittle fracture to semibrittle flow at confining pressures of 1000 to 1500 MPa [*Tullis and Yund*, 1980]. While microstructural observations suggest that the presence of water enhances dislocation glide and climb (see also *Tullis et al.* [1979], *Carter et al.* [1981], *Boland and Tullis* [1986], and *Tullis and Yund* [1989]), the extent of the mechanical weakening is less certain due to the use of sealed sample assemblies which render the effective confining pressure indeterminate.

Intriguing evidence suggesting that the micromechanisms of faulting at high temperatures may differ from those operative at low temperatures was presented by *Caristan* [1980, 1982]. He observed an inverse pressure dependence of rock strength at temperatures of 1000°C and associated it with unusual rheological behavior observed at the transition from brittle fracture

to semibrittle flow. Other observations of a "negative pressure effect" at confining pressures of 500-1500 MPa have been interpreted in the context of hydrolytic weakening [*Tullis et al.*, 1979; *Kronenberg and Tullis*, 1984].

Here we report the results of a study aimed at: (1) investigating the mechanisms of failure at high temperatures, and (2) establishing whether water content affects the mechanical strength at low confining pressures (100-400 MPa) in the vicinity of the brittle-plastic transition. Caristan's study utilized Maryland diabase, and since his experiments were performed in our laboratory, it seemed natural to use the same rock in the present study. The brittle-plastic transition in this rock has also been studied by *Kronenberg and Shelton* [1980].

Experimental Procedures

Sample Preparation, Microscopy, and Material Studied

Precision ground cylindrical samples 15.88 mm in diameter and 31.75 mm in height were vacuum impregnated with acetone, and then dried in vacuo at 92°C for 48 hours. For three experiments (FD16-18), samples were subjected to an additional heat treatment of 720°C for 20 hours. Copper foil was inserted in the furnace during the second stage in an attempt to maintain the oxygen fugacity at the Cu-Cu_2O buffer. The weight of samples subjected to the second heat treatment decreased by 0.02-0.03 wt%; we presume this represents H_2O lost via the decomposition of hydrous phases (see Table 1). The second heat treatment also induced a volume increase of 0.44-0.48% [e.g., see *Fredrich and Wong*, 1986]. Samples were kept in a desiccator prior to testing.

After testing, samples were impregnated with low viscosity epoxy in vacuo and cut in half along a plane parallel to the axis of the sample. Microscopy was performed on polished sections using a JEOL Superprobe equipped with backscattered and secondary electron

detectors and an energy dispersive x-ray analyzer (EDX), and on ion-milled ultra-thin samples using a JEOL 200-CX transmission electron microscope (TEM).

The modal analysis of Maryland diabase as determined by image processing of backscattered electrons is given in Table 1. The average grain size is 0.18 mm, and the porosity, to which cracks contribute a negligible amount, is 0.1% [*Brace et al.*, 1965].

Deformation Experiments

Experiments were performed in an internally heated, gas-medium, servo-controlled deformation apparatus at confining pressures of 100 to 400 MPa and temperatures of 800 to 900°C (Table 2). Confining pressure was measured with a Heise gage and maintained constant to within ± 4 MPa. Axial stress was supplied by a hydraulic loading system, measured with an external load cell, and transmitted to the sample through an alumina column with a diameter of 18.42 mm. Both the alumina column and sample were enclosed in thin-walled (0.3 mm) copper tubing; the oxygen fugacity was presumably maintained at the Cu-Cu_2O buffer. The annealed jacket was first swaged down upon a dummy column assembly in order to ensure an exact alignment of the sample with the loading column. The jacket allowed considerable slip to occur during stable faulting events; however, the rapid slip associated with unstable events frequently ruptured the jacket. Displacement was measured with a differential transformer (DCDT) mounted between the moving ram and fixed wall of the pressure vessel; the DCDT signal was compared to a control signal generated by a 12-bit D/A converter. The control signal was a ramp function which corresponded to a constant displacement rate of 10^{-5} in s^{-1}.

The molybdenum-wound internal furnace consisted of two separately controlled coils which were adjusted to yield temperature variations typically less than ± 10°C over the length of the sample (Table 2). The temperature profile of the furnace was determined using a hollow alumina column; calibrations to determine the optimum power settings for the two

coils were performed for each set of pressure and temperature conditions. During an experiment only the upper half of the alumina column was hollow; the control thermocouple was located within 3 mm of the top of the sample. Samples were thus "vented" to the atmosphere through the endplug.

In performing an experiment, a confining pressure of 100 or 200 MPa was first applied, and then the specimen was heated at a rate of about 12°C/minute until the desired temperature was reached. During the heating stage the confining pressure was gradually increased to the desired level. The assembly was allowed 25 minutes to equilibrate to the experimental conditions prior to the onset of axial loading. Temperature was typically maintained to within ± 1°C of the set point during the loading cycle. Power to the furnace was cut immediately after removal of the axial load; temperature dropped by more than 500°C in less than five minutes.

The load and displacement signals were sampled by a 12-bit A/D converter at 1/s with typical resolutions of 370 N and 0.01 mm. Axial stresses were calculated assuming zero volumetric strain and corrected for friction at the piston. (The strength of the copper jacket is negligible under the experimental conditions tested here.) The stiffness of the loading system was 0.11 GN m^{-1}; this was subtracted from the apparent displacement measured by the DCDT for calculation of axial strain. Although the machine stiffness was constant over the range of pressure and temperature considered here, it could vary by as much as 2% from run to run. Axial strains are referred to the initial sample length at atmospheric pressure.

RESULTS

Mechanical Data

Effect of pressure and temperature. The mechanical data are summarized in Table 2. At constant temperature, the axial stress-strain data show a transition in mechanical behavior as

the confining pressure is increased (Figure 1). At lower confining pressures, the samples exhibit work softening behavior and fail on a macroscopic shear fault. With the exception of FD10, samples deformed in the brittle field failed unstably with an audible acoustic emission. Samples deformed above the transition pressure exhibited extreme work hardening and showed no tendency to attain a steady-state flow stress over the range of strain in these experiments (see Table 2). For example, work hardening rates are an order of magnitude greater than those observed in marble [*Fredrich et al.*, 1989] deformed at room temperature in the semibrittle and plastic fields to comparable axial strains. At temperatures of 900°C, the transition occurs at pressures of 100-200 MPa (Figure 1*a*); whereas at 800°C, the transition occurs at pressures of 300-400 MPa (Figure 1*b*). The data are roughly consistent with *Kronenberg and Shelton*'s [1980] earlier work on the same rock.

In Figure 2 the yield stress, defined as the stress at which the axial stress-strain curve deviates from linearity, and the strength are plotted as a function of temperature and confining pressure. The data do not show a tendency towards decreasing strength with increasing confining pressure as was observed by *Caristan* [1980, 1982] for samples deformed at 1000°C in the same range of confining pressures.

Strength recovery. Two samples (FD5 and FD9) deformed at a confining pressure of 300 MPa and temperatures of 770 and 875°C exhibited stable work softening followed by an interval during which the strength first recovered and then exceeded that observed prior to softening (Figure 3). The modulus of the stress-strain curve during the recovered period was only slightly degraded in comparison to that observed prior to the softening event. FD5 exhibited one sequence of work softening followed by strength recovery and had a macroscopic fault running across the sample. FD9 displayed two periods of softening followed by recovery and, correspondingly, had two distinct faults traversing the sample length (Figure 4). Fiducial lines inscribed on the copper jackets indicated that slip had

occurred along the fault in FD5 and along both of the faults in FD9. Both samples retained coherency, even after the copper jacket was unpeeled.

Effect of second heat treatment. The mechanical behavior of samples subjected to a heat treatment at 720°C prior to testing (see previous description) differed markedly from their counterparts tested without the additional treatment (described above). Runs FD16 and FD17 were terminated prematurely because the loading capacity of the hydraulic system was exceeded. Nevertheless, two differences in sample behavior are apparent: the initial modulus of the stress-strain curve and the yield point of the heat-treated samples are greater than those of the untreated sample (Table 2). The mechanical behavior of two samples tested at 200 MPa and 900°C with (FD18) and without (FD2) the additional heat treatment are compared in Figure 5. Two differences are evident in addition to those just noted. Whereas the untreated sample deformed in a semibrittle mode, the treated sample failed violently along a shear fault. Furthermore, the fracture strength of the treated sample is more than 50% greater than the strength of the untreated sample at the same strain.

Microstructural Observations

Detailed studies of the deformation microstructures in Maryland diabase deformed in a solid-medium apparatus in the semibrittle field at temperatures of 800-1000°C and confining pressures of 500-1500 MPa have been reported by *Kronenberg and Shelton* [1980]. Limited observations of samples deformed in a gas-medium apparatus at confining pressures up to 400 MPa and temperatures of 1000°C were reported by *Caristan* [1980, 1982]. As noted previously, many of the experiments performed here ended in unstable failure. Consequently, our efforts were directed towards determining the stability of the phase assemblage and examining the structure of the faults formed in runs FD5 and FD9.

Partial melting. With the exception of FD16 and FD17, all of the samples listed in Table 2 were examined in a JEOL superprobe; features with dimensions less than 20 nanometers

were not resolvable. Glass (melt) was identified in all but three samples. Of these three samples, FD3 and FD9 were tested at the lowest confining pressure (100 MPa) and temperature (770°C), respectively, and FD18 was subjected to a second heat treatment. Note that microscopy indicated that glass was not present in the starting material.

Glass (melt) was identified in backscattered electron images by contrast (it appears slightly lighter than quartz) and EDX analysis; the minimum dimension required for reliable identification was about an order of magnitude greater than the resolution quoted above. When present, melt typically resided in pockets and channels which appeared to be isotropically distributed with respect to the macroscopic applied stress field and frequently contained remnant quartz cores (Figure 6). Quantitative microanalysis of the melt (Table 3) suggests that initial melting occurred close to the granite eutectic. Quantitative measurement of the melt fraction was impractical due to the small amounts of melt present. The most melt was observed in FD12; semi-quantitative analysis suggested a melt fraction of 1-2%. FD2, FD5, FD11, and FD15 had melt fractions estimated to approach 1%. Evidence that pyroxene participated in the partial melting was observed in runs FD11 and FD12. In FD4, FD8, and FD10, melt was restricted to zones on the order of 1μm thick surrounding quartz cores and was estimated to be less than 1%.

High temperature faults. The faults formed in samples FD5 and FD9 were examined in detail because of the unusual mechanical behavior with which they were associated (Figure 3). A significant amount of melt was visible along the fault in FD5. In some areas, discrete particles are connected by meniscuses (Figure 7*a*), the atomic number contrast of which is consistent with that of the melt (the meniscuses are too small for EDX analysis).

In contrast, scanning electron microscopy did not reveal melt along either of the faults formed in FD9. The structure of one of the faults is shown in Figures 7*b* and 7*c*. The 20-30 μm wide band of fine grained material containing angular particles is present along the entire length of the fault. The fine-grained material appears to form a continuous matrix and dilatant

cracks are visible above the large crack. The large crack repeatedly switches sides with respect to the band of fine-grained material and no shear displacement is evident along the crack. Thus, the crack apparently formed during quenching or unloading. The "smeared-out" appearance of pyroxene grains bordering the fault (Figure 7*d*) suggests that some of the shear displacement along the fault was accommodated by plastic deformation mechanisms. The second fault is similar in appearance (Figure 7*e*), although the band of fine-grained material is narrower and not present along the entire length of the fault.

To identify the material welding together the angular fragments, the faults formed in FD9 were examined in TEM. Selected area diffraction indicates that the angular particles (Figure 8*a*) reside in an amorphous material (Figure 8*b*). The spacing of the amorphous rings with respect to the diffraction pattern from the large angular fragment suggests that the amorphous material is a silicate glass.

DISCUSSION

Faulting at High Temperatures

Although brittle deformation of rocks has been studied extensively, few experimental studies of fracture have been performed at high temperatures. Our results suggest that, under certain conditions, the frictional behavior of faults at high temperatures may differ markedly from that observed at low temperatures. Specifically, the occurrence of small amounts of partial melt may alter the mechanical behavior significantly.

The periods of softening followed by recovery in experiments FD5 and FD9 (Figure 3) are consistent with either a mechanical effect (i.e., dilatancy hardening [*Brace and Martin*, 1968]) or a physical strengthening of the fault zone. For the reasons discussed below, we believe that both mechanical and physical processes along the fault zone may have contributed to the observed hardening.

Although our experiments were performed in nominally "drained" conditions, elevated pore pressures may nevertheless have developed due to the extremely low crack porosity of the rock. Indeed, the low level of differential stress at the onset of the softening events in experiments FD5 and FD9 suggests the existence of elevated pore pressures (cf. Figures 2*b* and 3). Locally elevated pore pressures in experiment FD5 could have been induced by the presence of a melt phase since dehydration-melt reactions proceed without the appearance of an H_2O fluid phase [e.g., *Thompson*, 1982]. No melt was observed in the bulk of sample FD9; thus, it is possible that the water released during the decomposition of biotite and other hydrous phases led to locally elevated pore pressures.

If the effective confining pressure were reduced due to elevated pore pressures, then localization could occur at the reduced stress levels observed (cf. Figures 2*b* and 3). An immediate effect of shear localization would be the introduction of a high permeability conduit to the atmosphere; thus, slip would tend to stabilize as the pore pressure dropped and the normal stress on the fault increased [*Brace and Martin*, 1968]. Microscopy also suggests the possibility that frictional heating elevated the temperature above the solidus in experiment FD9 (Figure 8). The apparent extreme plasticity of some grains adjacent to the fault zone (Figure 7*d*) also argues for the existence of transient temperature elevatations along the fault zone.

The level of recovery following the softening events suggests that physical healing of the fault zone also may have occurred. Experiment FD10 was performed under experimental conditions similar to those of FD5 and FD9; the stable sliding behavior exhibited is consistent with a coefficient of friction $\mu \approx 0.3$. Likewise, *Stesky et al.* [1974] found a coefficient of friction significantly less than 0.6 for faults in granite and gabbro at temperatures greater than 500-600°C. Thus, if it is assumed that the presence of the macroscopic fault resulted in the dissipation of elevated pore pressures, then the differential stress supported after the softening event in run FD5 should have induced frictional sliding on the fault for a coefficient of

friction $\mu \leq 0.65$. Similarly, the second faulting episode in run FD9 occurred at stress levels sufficient for slip on surfaces with frictional coefficients $\mu \leq 0.58$. We suppose that the high permeability of the fault zone may have induced degassing of the melt to the atmosphere, which would have increased the viscosity of the melt, and perhaps caused solidification and welding of the fault zone.

Effect of Water Content

Our results indicate that the imposition of a high temperature heat treatment prior to deformation increases the strength dramatically and retards the transition from brittle fracture to semibrittle flow in Maryland diabase. Similar observations for other silicate rocks deformed with varying water contents in the semibrittle and plastic fields [*Tullis et al.*, 1979; *Tullis and Yund*, 1980; *Carter et al.*, 1981; *Mainprice and Paterson*, 1984; *Kronenberg and Tullis*, 1984; *Boland and Tullis*, 1986; *M. S. Paterson*, personal communication, 1990] have been interpreted in the context of hydrolytic weakening.

Although the water fugacity was necessarily different during our experiments performed on samples with and without the additional heat treatment, we believe that our results can be explained by the presence of partial melt in the samples deformed without the second heat treatment. That the initial moduli of samples subjected to the additional heat treatment are markedly greater than those of the samples dried at 94°C (see Table 2) implies that even the small melt fractions present ($<$ 1-2%) significantly affected the deformation [e.g., *Goetze*, 1969]. (In fact, we are not aware of any other rationalization for the observed change in the Young's modulus). The conspicuous "S" shape of the stress-strain curve of the sample which contained melt also implies a visco-elastic rheology. Thus, we suggest that the presence of melt probably had a significant effect on the inelastic deformation [e.g., *Mainprice and Paterson*, 1984]. Estimates of the total weight percent of water dissolved in the melt (Table 3) are of the same order as the amount of water removed by the second heat treatment,

suggesting that any diffusive uptake of "water" by the feldspar or pyroxene grains must have been restricted to very small amounts.

Negative Pressure Effect

As stated earlier, part of the motivation for the present study was to verify and investigate the "negative pressure effect" observed by *Caristan* [1980, 1982]. His experiments on Maryland diabase were conducted at temperatures of 1000°C, strain rates ranging from 10^{-3} to 10^{-6}, and confining pressures up to 450 MPa. Caristan found that above a limiting confining pressure which depended upon the strain rate, rock strength decreased with pressure; he suggested that this inverse dependence was related to the transition from brittle fracture to semibrittle flow.

Our results are inconsistent with his conclusion. Specifically, the strengths of our samples deformed in the transitional field at temperatures of 800-900°C and pressures of 200-400 MPa display a positive pressure dependency (Figure 2); Caristan's samples deformed at the same strain rate and 1000°C show an inverse dependence at confining pressures greater than 150 MPa (see Figure 4 of *Caristan* [1982]). Since the experimental equipment and procedures employed in both studies are identical, we suspect that the only difference between Caristan's and our experiments is that the former probably contained a larger volume fraction of partial melt.

Earlier observations of a "negative pressure effect" in granite, aplite, albite, and quartzite deformed in a solid medium apparatus at temperatures of 800-900°C and confining pressures up to 1500 MPa by *Tullis et al.* [1979] and *Kronenberg and Tullis* [1984] were attributed to enhanced hydrolytic weakening at high pressures. However, *Kronenberg et al.* [1986] and others have shown that the previous evidence for a greatly enhanced diffusivity of water in quartz (the only mineral which has been studied in detail) at high pressures is invalid (see reviews by *Paterson* [1986, 1990]). Moreover, recent work by *Kronenberg and Wolf* [1990]

has shown that the intragranular water content in samples of quartzite deformed in the presence of excess water (and which exhibited the "negative pressure effect") did not increase with respect to that of the starting material.

Various workers have found that the strength of silicate rocks depends critically on water content at confining pressures of the order of 200-400 MPa [*Mainprice and Paterson*, 1984; *Boland and Tullis*, 1986; *M. S. Paterson*, personal communication, 1990]. As discussed above, the strengthening observed in our heat-treated samples is consistent with either a hydrolytic weakening phenomenon or a weakening effect due to partial melting, or possibly a combination of both. We note that small amounts of partial melt were also identified in some samples in the studies of *Mainprice and Paterson* [1984], *Kronenberg and Tullis* [1984], and *Boland and Tullis* [1986]. We believe that the possibility that the "negative pressure effect" observed by *Caristan* [1980, 1982] is either intrinsically or extrinsically related to the presence of partial melt cannot be ruled out at this time.

CONCLUSIONS

Several inferences regarding the semibrittle deformation of silicate rocks at high temperatures may be drawn from the results of our preliminary study. A few experiments suggest that, under certain conditions, the properties of high temperature faults may differ significantly from their low temperature counterparts. For example, data from one experiment suggests a low coefficient of friction at high temperatures ($\mu \approx 0.3$). Microscopy of another sample deformed within 100°C of the solidus suggests the possibility that frictional sliding may locally elevate temperatures to supra-solidus conditions and cause enhanced plasticity of grains in the vicinity of the fault. Two experiments illustrate dramatically the cyclic link between the physical and mechanical properties of fault zones. These experiments may also represent the first laboratory demonstration of in situ fault "healing".

The interpretation of some aspects of the present study are compromised by the occurrence of partial melt. Although the maximum melt fraction was less than 2%, comparison of the initial moduli of the stress-strain curves for samples with and without melt suggests that even small amounts may significantly affect the deformation. Thus, mechanical data for samples previously subjected to a high temperature heat-treatment are consistent with, although not evidence for, a hydrolytic weakening phenomenon.

Our experimental data do not confirm the "negative pressure effect" previously reported by *Caristan* [1980, 1982] in identical experiments performed on the same rock at 1000°C. Thus, our data indicate that the effect is not associated with the transition from brittle fracture to semibrittle flow. We surmise that his observations may be related to the higher melt fractions present in his experiments. Similarly, we believe that the possible effects of small amounts of partial melt on the strength of polycrystalline aggregates may be a neglected factor in the interpretation of many previous studies.

Our results argue persuasively for the use of synthetic aggregates in studies of the high temperature rheology of silicate rocks. For example, published modal analyses for Maryland diabase [*Brace et al.*, 1965; *Caristan*, 1980; *Kronenberg and Shelton*, 1980] did not lead us to believe that partial melting would occur at the experimental conditions employed here. Small amounts of partial melt induced by the occurrence of minor phases representing less than 3% of the bulk rock have similarly plagued other studies [e.g., *Mainprice and Paterson*, 1984; *Kronenberg and Tullis*, 1984; *Boland and Tullis*, 1986]. The decomposition of hydrous micas present in very small amounts in many natural rocks can lead to uncertainties in the pore pressure and also influence the water fugacity, thereby leading to considerable uncertainty in the interpretation of experimental data.

The role of water must indeed be regarded as one of the outstanding problems in rock deformation. Our results suggest that the basis for the weakening effect must be understood before constitutive relations for semibrittle flow can be realistically worked towards.

Although progress has recently been made towards constraining the effect of water on certain aspects of the deformation of single crystals [e.g., *Gerretsen et al.*, 1989; *McLaren et al.*, 1989], the role of water in the deformation of polycrystalline aggregates is still largely uncertain.

REFERENCES

Boland, J. N., and T. E. Tullis, Deformation behavior of wet and dry clinopyroxenite in the brittle to ductile transition region, in *Mineral and Rock Deformation: Laboratory Studies (The Paterson Volume)*, B. E. Hobbs and H. C. Heard (Eds.), *Geophys. Monogr. V. 36*, pp. 35-49, AGU, Washington, D.C., 1986.

Brace, W. F., A. S. Orange, and T. R. Madden, The effect of pressure on the electrical resistivity of water-saturated crystalline rocks, *J. Geophys. Res.*, *70*, 5669-5678, 1965.

Brace, W. F., and R. J. Martin, III, A test of the law of effective stress for crystalline rocks of low porosity, *Int. J. Rock Mech. Min. Sci.*, *5*, 415-426, 1968.

Caristan, Y., High temperature mechanical behavior of Maryland diabase, Ph.D. thesis, Massachusetts Institute of Technology, Cambridge, 1980.

Caristan, Y., The transition from high temperature creep to fracture in Maryland diabase, *J. Geophys. Res.*, *87*, 6781-6790, 1982.

Carter, N. L., D. A. Anderson, F. D. Hansen, and R. L. Kranz, Creep and creep rupture of granitic rocks, in *Mechanical Behavior of Crustal Rocks (The Handin Volume)*, N. L. Carter, M. Friedman, J. M. Logan, and D. W. Stearns (Eds.), *Geophys. Monogr. V. 24*, pp. 61-82, AGU, Washington, D.C., 1981.

Carter, N. L., and M. C. Tsenn, Flow properties of continental lithosphere, *Tectonophys.*, 136, 27-63, 1987.

Evans, B., J. T. Fredrich, and T.-f. Wong, The brittle-ductile transition in rocks: Recent experimental and theoretical progress, in *The Brittle-Ductile Transition in Rocks (The Heard Volume)*, A. Duba, B. Durham, J. Logan, and H. Wang (Eds.), *Geophys. Monogr. V. 56*, pp. 1-20, AGU, Washington, D.C., 1990.

Fredrich, J. T., and T.-f. Wong, Micromechanics of thermally induced cracking in three crustal rocks, *J. Geophys. Res.*, *91*, 12,743-12,764, 1986.

Fredrich, J. T., B. Evans, and T.-f. Wong, Micromechanics of the brittle to plastic transition in Carrara marble, *J. Geophys. Res.*, *94*, 4129-4145, 1989.

Gerretsen, J., M. S. Paterson, and A. C. McLaren, The uptake and solubility of water in quartz at elevated pressure and temperature, *Phys. Chem. Miner.*, *16*, 334-342, 1989.

Goetze, C., A brief summary of our present day understanding of the effect of volatiles and partial melt on the mechanical properties of the upper mantle, in *High Pressure Research Applications in Geophysics*, M. H. Manghnani and S. Akimoto (Eds.), pp. 3-23, Academic Press, New York, 1969.

Kronenberg, A. K., and G. L. Shelton, Deformation microstructures in experimentally deformed Maryland diabase, *J. Struct. Geol.*, *2*, 341-353, 1980.

Kronenberg, A. K., and J. Tullis, Flow strengths of quartz aggregates: grain size and pressure effects due to hydrolytic weakening, *J. Geophys. Res.*, *89*, 4281-4197, 1984.

Kronenberg, A. K., S. H. Kirby, R. D. Aines, and G. R. Rossman, Solubility and diffusional uptake of hydrogen in quartz at high water pressures: Implications for hydrolytic weakening, *J. Geophys. Res.*, *91*, 12723-12744, 1986.

Kronenberg, A. K., and G. W. Wolf, Fourier transform infrared spectroscopy determinations of intragranular water content in quartz-bearing rocks: Implications for hydrolytic weakening in the laboratory and within the earth, *Tectonophys.*, *172*, 255-271, 1990.

Mainprice, D. H., and M. S. Paterson, Experimental studies of the role of water in the plasticity of quartzites, *J. Geophys. Res.*, *89*, 4257-4269, 1984.

McLaren, A. C., J. D. FitzGerald, and J. Gerretsen, Dislocation nucleation and multiplication in synthetic quartz: relevance to water weakening, *Phys. Chem. Miner.*, *16*, 465-482, 1989.

Paterson, M. S., *Experimental Rock Deformation - The Brittle Field*, 254 pp., Springer-Verlag, New York, 1978.

Paterson, M. S., The thermodynamics of water in quartz, *Phys. Chem. Mineral.*, *13*, 245-255, 1986.

Paterson, M. S., The interaction of water with quartz and its influence on dislocation flow - an overview, in *Rheology of Solids and of the Earth*, S. Karato and M. Toriumi (Eds.), pp. 107-142, Oxford University Press, London, 1990.

Stesky, R. M., W. F. Brace, D. K. Riley, and P.-Y. F. Robin, Friction in faulted rock at high temperature and pressure, *Tectonophys.*, *23*, 177-203, 1974.

Thompson, A. B., Dehydration melting of pelitic rocks and the generation of H_2O-undersaturated granitic liquids, *Am. J. Sci.*, *282*, 1567-1595, 1982.

Tullis, J., G. L. Shelton, and R. A. Yund, Pressure dependence of rock strength: Implications for hydrolytic weakening, *Bull. Mineral.*, *102*, 110-114, 1979.

Tullis, J., and R. A. Yund, Hydrolytic weakening of experimentally deformed Westerly granite and Hale albite rock, *J. Struct. Geol.*, *2*, 439-451, 1980.

Tullis, J., and R. A. Yund, Hydrolytic weakening of quartz aggregates: The effects of water and pressure on recovery, *Geophys. Res. Lett.*, *16*, 1343-1346, 1989.

TABLE 1. Composition of Maryland Diabase

Phase	Percent
plagioclase	61.9±10.5
clinopyroxene	33.7±11.9
quartz	1.4±1.0
mica	≈1-2
opaques	≈1

TABLE 2. Mechanical Data

Sample[a]	P_C, MPa	T, °C	$(\sigma_1-\sigma_3)_{max}$, MPa	ϵ_1[b], %	σ_Y[c], MPa	M[d], GPa
FD2(1)	200	877±10	574	3.74	259	30.0
FD3(2)	100	892±8	380	1.12	359	49.4
FD4(2)	202	793±7	579	1.65	345	48.5
FD5(3)	301	875±25	712	2.42	329	44.7
FD8(4)	200	836±10	318	0.60	*	54.5
FD9(3)	305	770±8	603	2.68	465	63.5
FD10(2)	307	814±6	555	3.98	385	49.4
FD11(1)	405	818±4	714	2.07	363	53.1
FD12(1)	304	908±5	643	3.05	283	35.5
FD15(1)	404	909±4	735	2.54	304	50.0
FD16(4,5)	408	818±4	669	1.09	419	80.5
FD17(4,5)	405	818±4	674	1.10	608	72.0
FD18(2,5)	202	899±8	787	2.82	398	58.9

[a]Remarks: (1) semibrittle flow; (2) brittle fracture; (3) strength recovered; (4) experiment terminated prematurely; (5) sample underwent second heat treatment prior to testing.

[b]Total axial strain (elastic + permanent).

[c]Differential stress at the onset of nonlinearity in the axial stress-strain curve.

[d]Initial modulus of the stress-strain curve, uncertainty is less than 8%.

TABLE 3. Glass Composition*

Oxide	Weight Percent
MgO	0.16
Al_2O_3	13.73
SiO_2	74.75
CaO	1.17
$Ti0_2$	0.04
FeO	1.17
Na_2O	1.77
K_2O	4.91

*Volatile content estimated at 1-2%. Composition varied slightly from area to area.

FIGURE CAPTIONS

Figure 1. Axial stress-strain behavior observed at the indicated confining pressures and temperatures of approximately (*a*) 900°C and (*b*) 800°C. The transition to semibrittle flow occurs at higher confining pressures at lower temperatures and is associated with extreme work hardening. Data plotted are from experiments (*a*) FD3, FD2, FD12, and FD15; and (*b*) FD4, FD10, and FD11 (see Table 2 for details).

Figure 2. (*a*) Macroscopic yield stress and (*b*) strength as a function of temperature and confining pressure. In (*b*), open symbols denote the fracture strength and closed symbols the semibrittle strength observed at axial strains of 2.0%. Data for experiments FD5 and FD9 are not shown (see text). Note that neither data set exhibits convincing evidence for a negative pressure dependency.

Figure 3. Unusual stress-strain behavior observed in experiments (*a*) FD5 and (*b*) FD9. Whereas a single macroscopic shear fault was observed in sample FD5, two shear faults were present in sample FD9. Note that although the temperature control during experiment FD5 was inferior, experiment FD9 was well controlled in all respects (see Table 2).

Figure 4. Photograph of sample FD9. Displacement of the fiducial lines on the copper jacket indicated that slip had occurred along both shear faults.

Figure 5. Comparison of the mechanical behavior observed at a confining pressure of 200 MPa and temperature of 900°C for two samples tested with (FD18) and without (FD2) a second heat treatment at 720#C prior to deformation. The treated sample is stronger than the untreated sample and failed violently on a shear fault. Also note that the Young's modulus and yield stress of the treated sample are significantly greater than those of the untreated sample.

Figure 6. Backscattered electron micrograph illustrating the typical habit of the melt (sample FD11). Quartz is the darkest phase present, while pyroxene appears the brightest. The light gray phase is plagioclase. The melt resides primarily in pockets or channels which

show no evidence of a preferred orientation. Note the quartz core within most of the melt pockets (an example is indicated with the arrow). The lobate southern boundary of the large pyroxene grain in the upper right suggests that pyroxene participated in the partial melting during this particular run (see Table 2). The scale bar is 100 μm.

Figure 7. Backscattered electron micrographs illustrating the structure of the faults formed in experiments FD5 and FD9. (*a*) A significant amount of melt is visible along the fault formed in FD5. Note that some of the individual particles in the fault zone are connected by meniscuses (two examples are indicated with arrows). (*b*) Low and (*c*) high magnification views of one of the faults formed in FD9. The 20-30 μm wide band of fine grained material defines the fault zone and appears to form a continuous matrix around the angular particles. The large crack apparently formed during quenching or unloading. (*d*) Some pyroxene grains bordering the fault apparently deformed quite plastically. (*e*) Low magnification view of the other fault observed in FD9. Although less well defined, the structure is similar to that observed in (*b*) and (*c*). The scale bars are 10 μm in Figures 7*a*, 7*c*, and 7*d*, and 100 μm in Figures 7*b* and 7*e*.

Figure 8. (*a*) Bright-field transmission electron micrograph of one of the fault zones formed in experiment FD9 and (*b*) the selected area diffraction pattern from the region on the right containing the large rectangular fragment. The diffraction pattern from this region and many others indicates that the angular particles reside in an amorphous material. The horizontal dimension of the micrograph in (*a*) is about 7 μm.

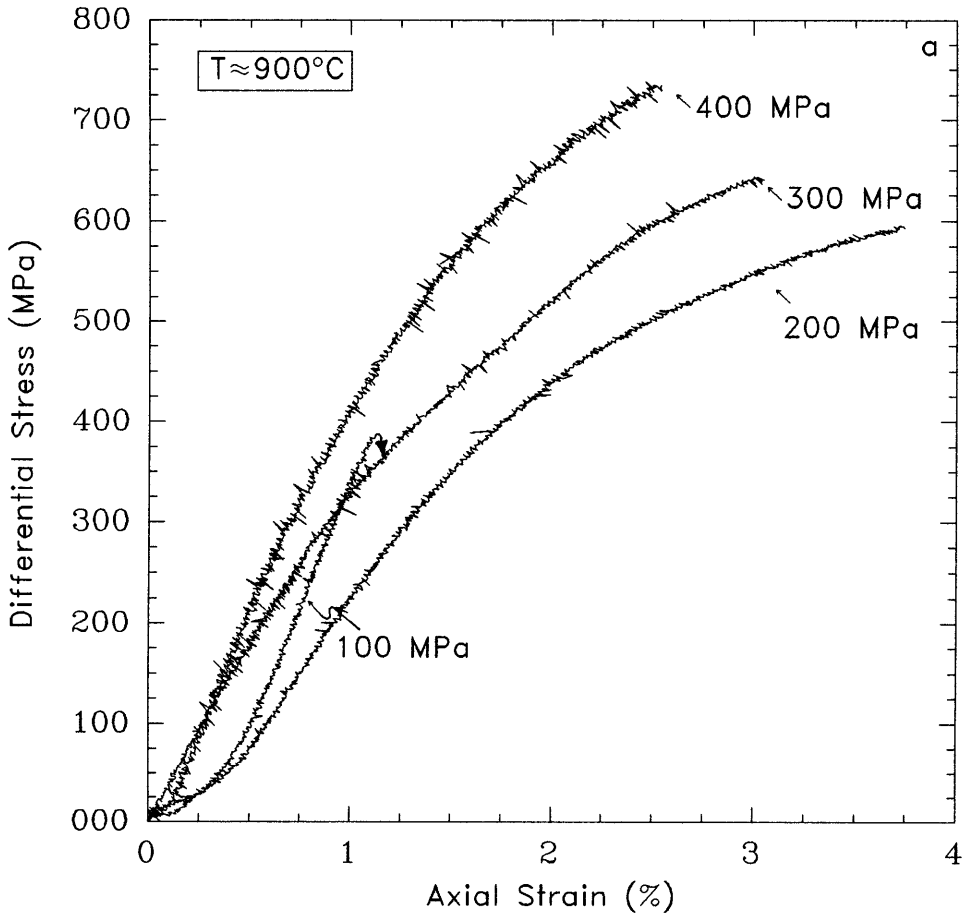
800
700
600
500
400
300
200
100
000
0
1
2
3
4
Differential Stress (MPa)
Axial Strain (%)
T≈900°C
a
400 MPa
300 MPa
200 MPa
100 MPa

Figure 1*a*

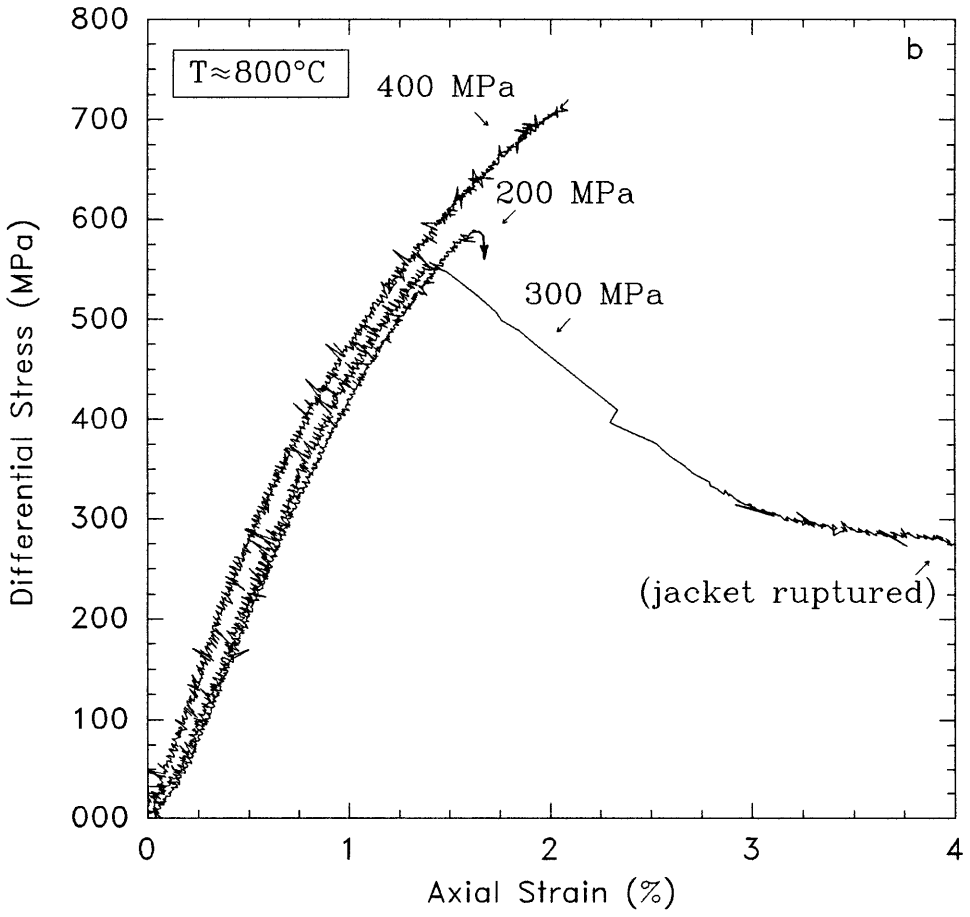
800
700
600
500
400
300
200
100
000
Differential Stress (MPa)
T≈800°C
400 MPa
200 MPa
300 MPa
(jacket ruptured)
b
0
1
2
3
4
Axial Strain (%)

Figure 1*b*

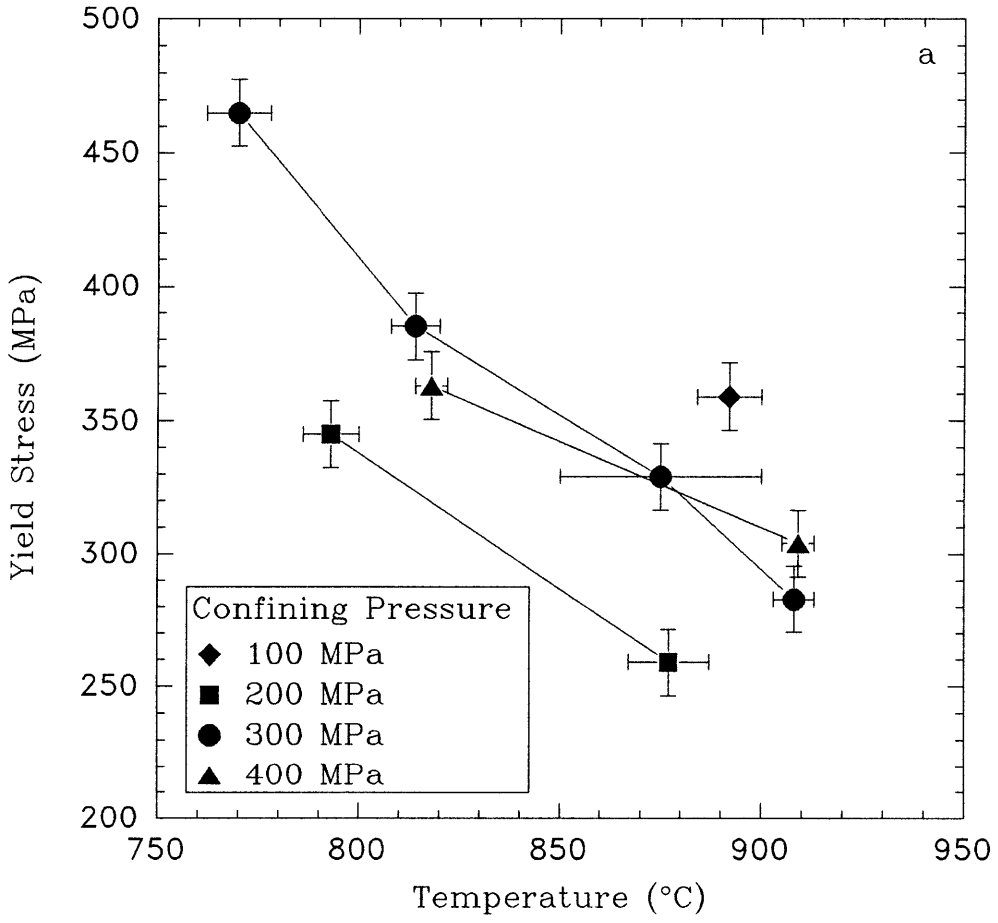
a
Yield Stress (MPa)
Temperature (°C)
500
450
400
350
300
250
200
750
800
850
900
950
Confining Pressure
100 MPa
200 MPa
300 MPa
400 MPa

Figure 2*a*

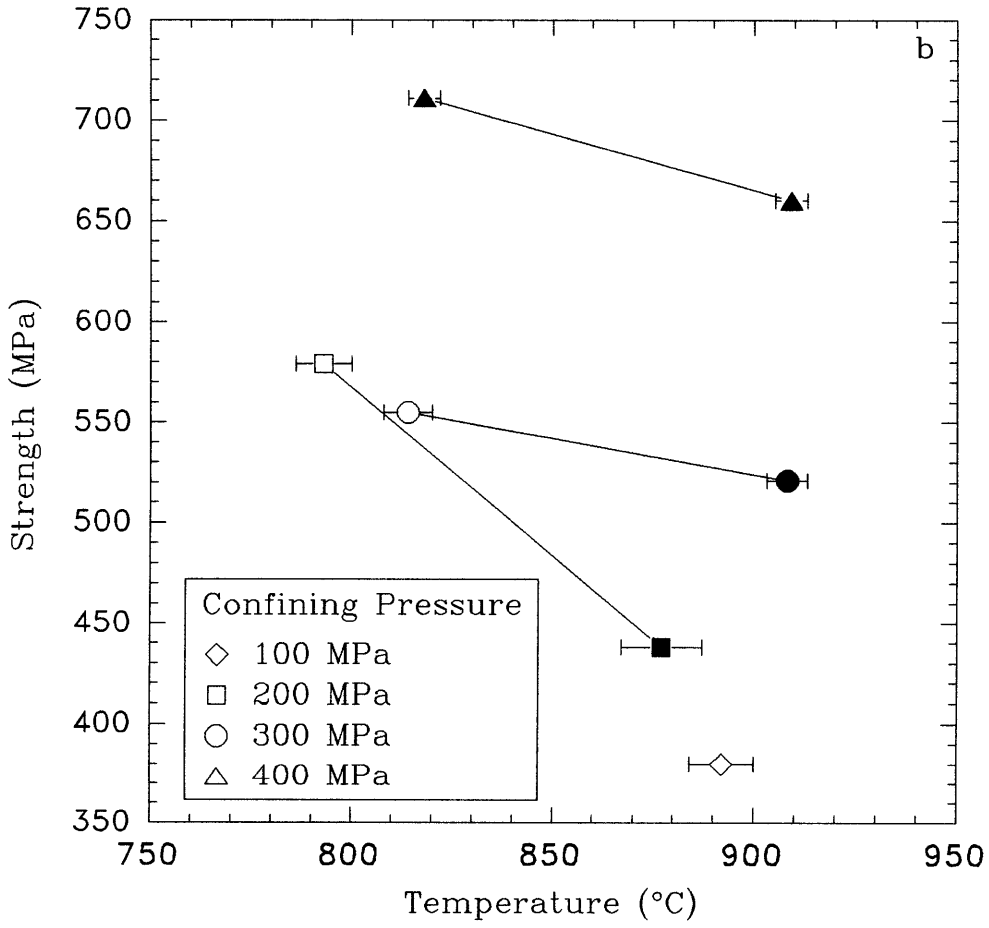
b
Strength (MPa)
750
700
650
600
550
500
450
400
350
750
800
850
900
950
Temperature (°C)
Confining Pressure
100 MPa
200 MPa
300 MPa
400 MPa

Figure 2*b*

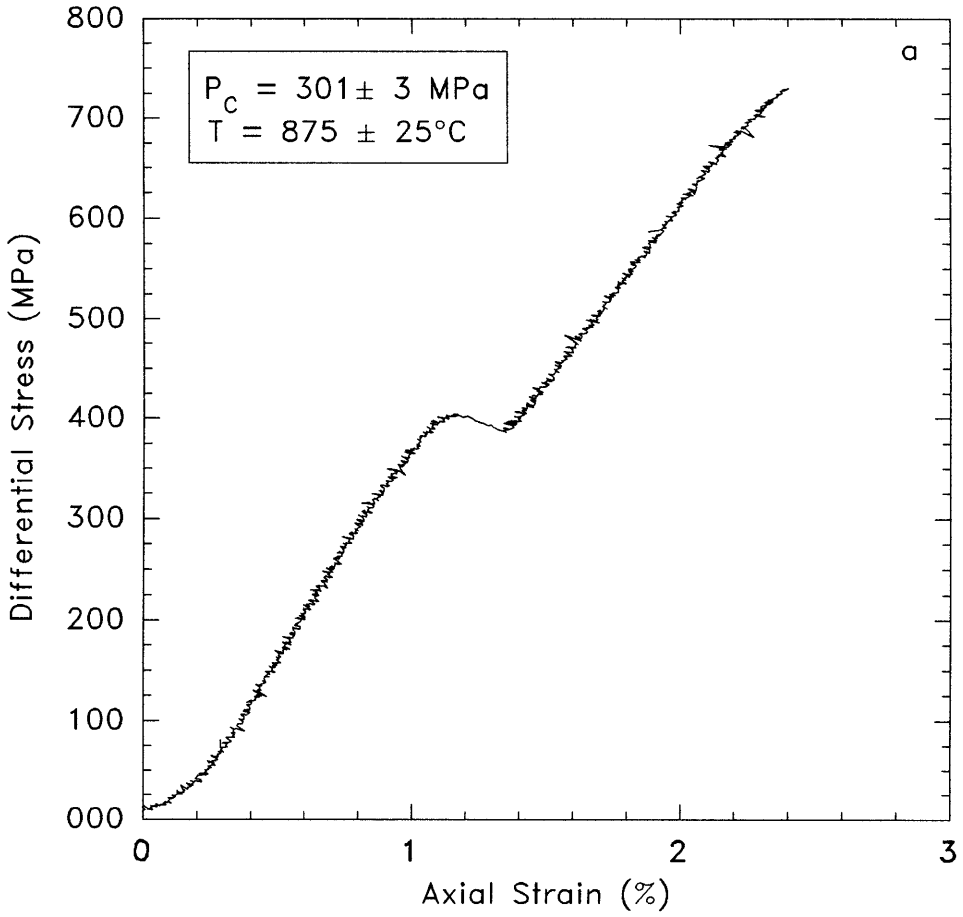
800
700
600
500
400
300
200
100
000
Differential Stress (MPa)
P_C = 301± 3 MPa
T = 875 ± 25°C
a
0
1
2
3
Axial Strain (%)

Figure 3*a*

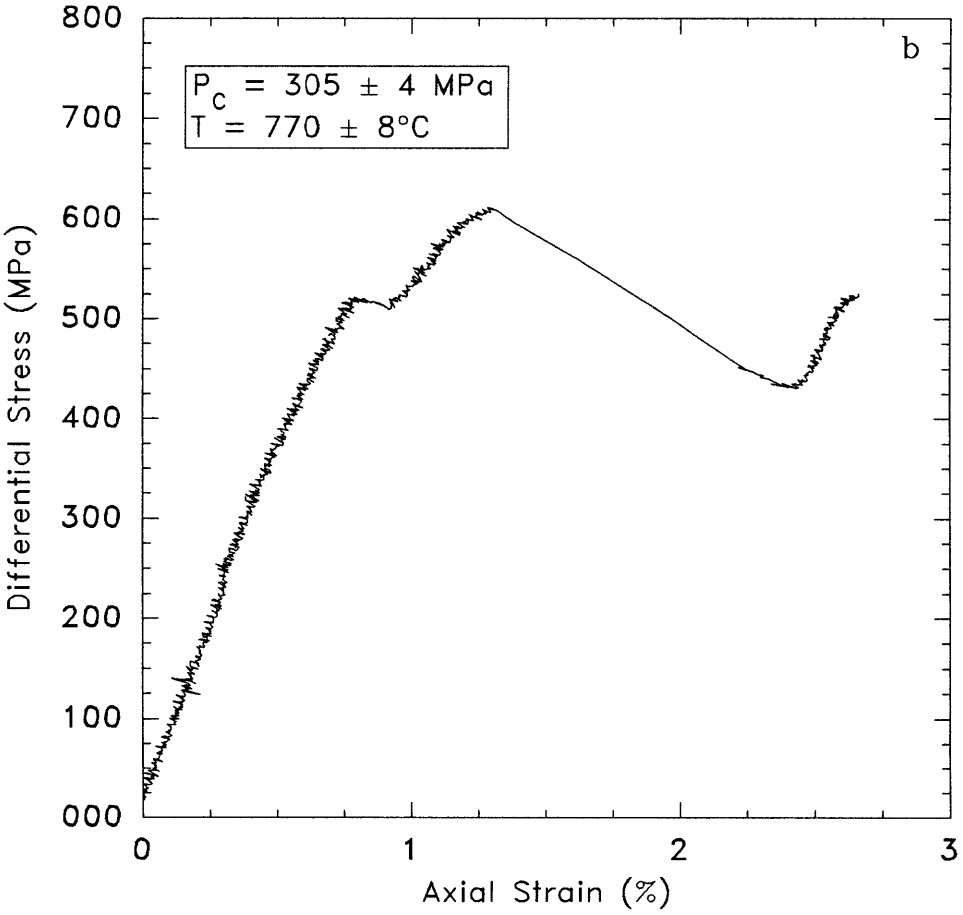
800
700
600
500
400
300
200
100
000
Differential Stress (MPa)
0
1
2
3
Axial Strain (%)
P_C = 305 ± 4 MPa
T = 770 ± 8°C
b

Figure 3*b*

Figure 4

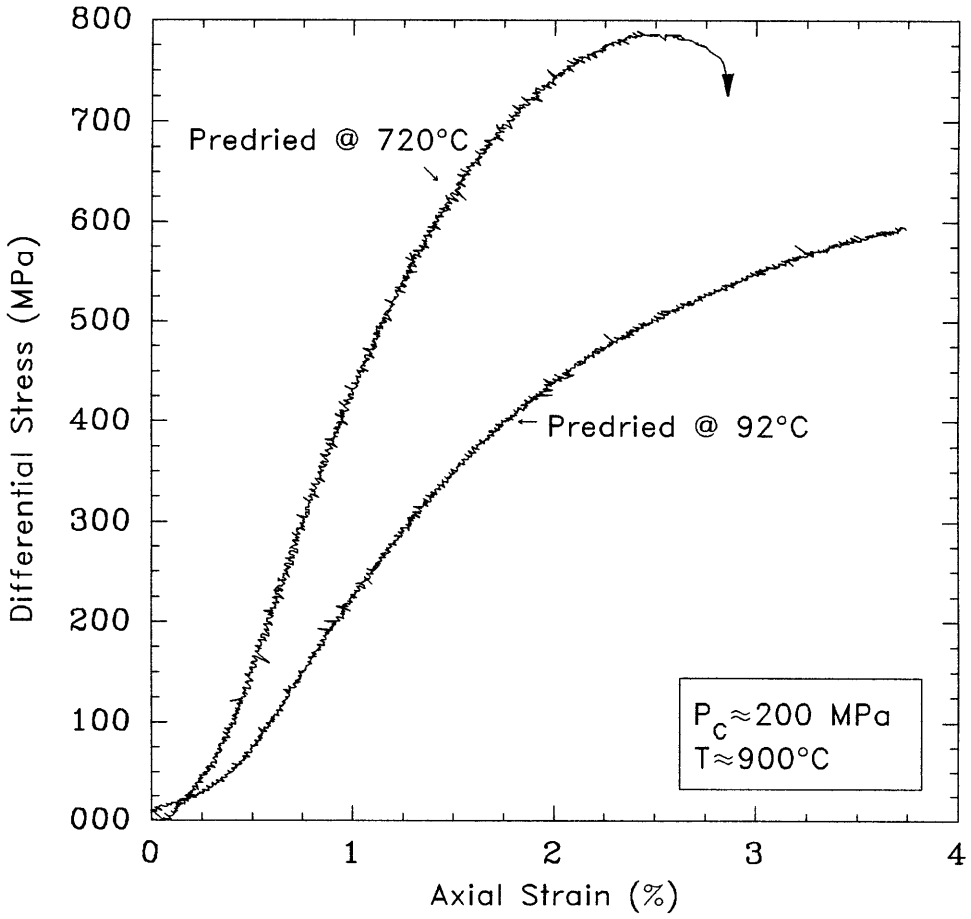
800
700
600
500
400
300
200
100
000
Differential Stress (MPa)
0
1
2
3
4
Axial Strain (%)
Predried @ 720°C
Predried @ 92°C
P_C≈200 MPa
T≈900°C

Figure 5

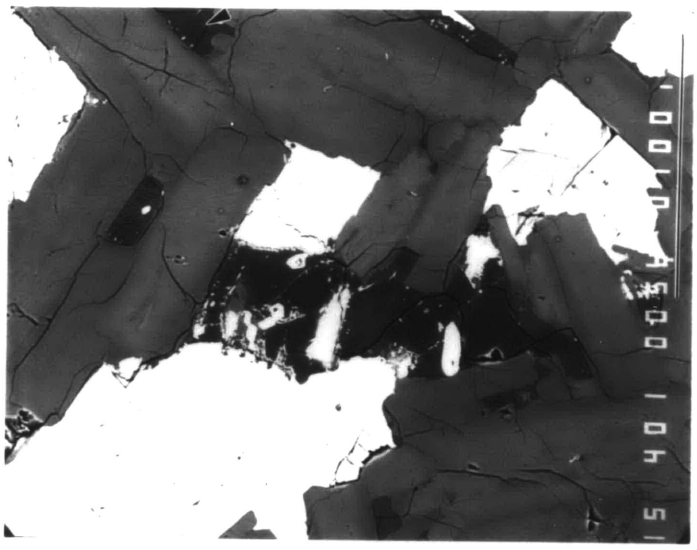

Figure 6

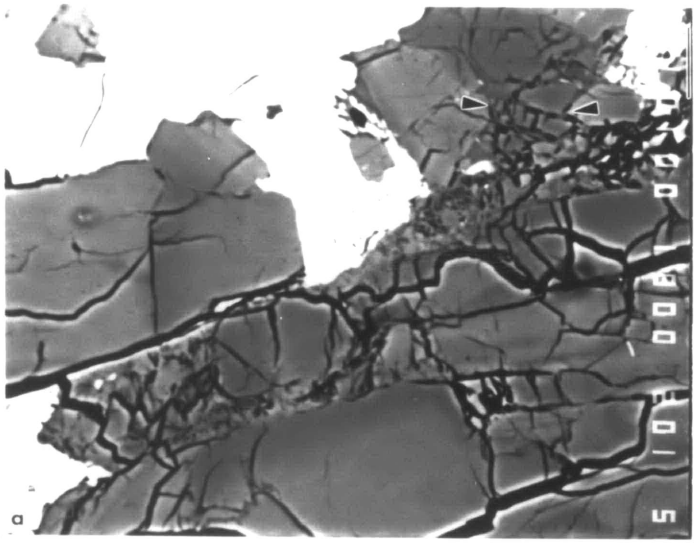

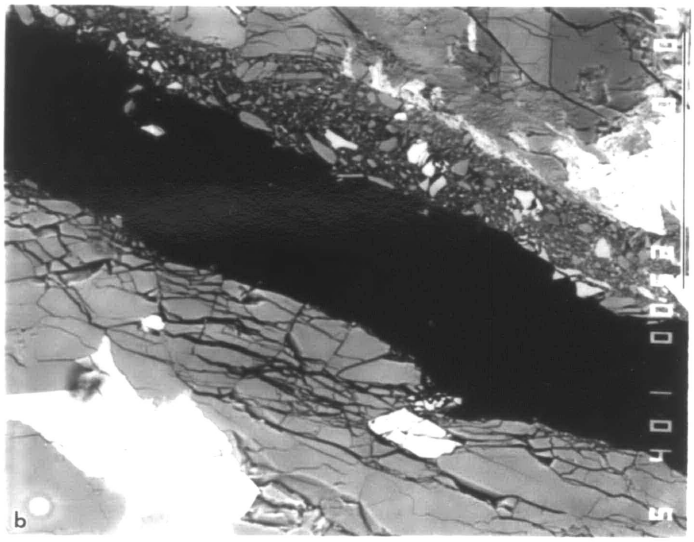

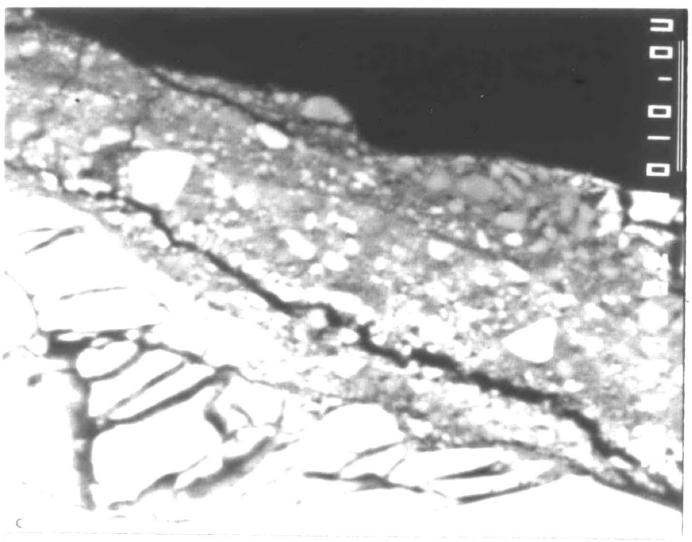

Figure 7a,b,c

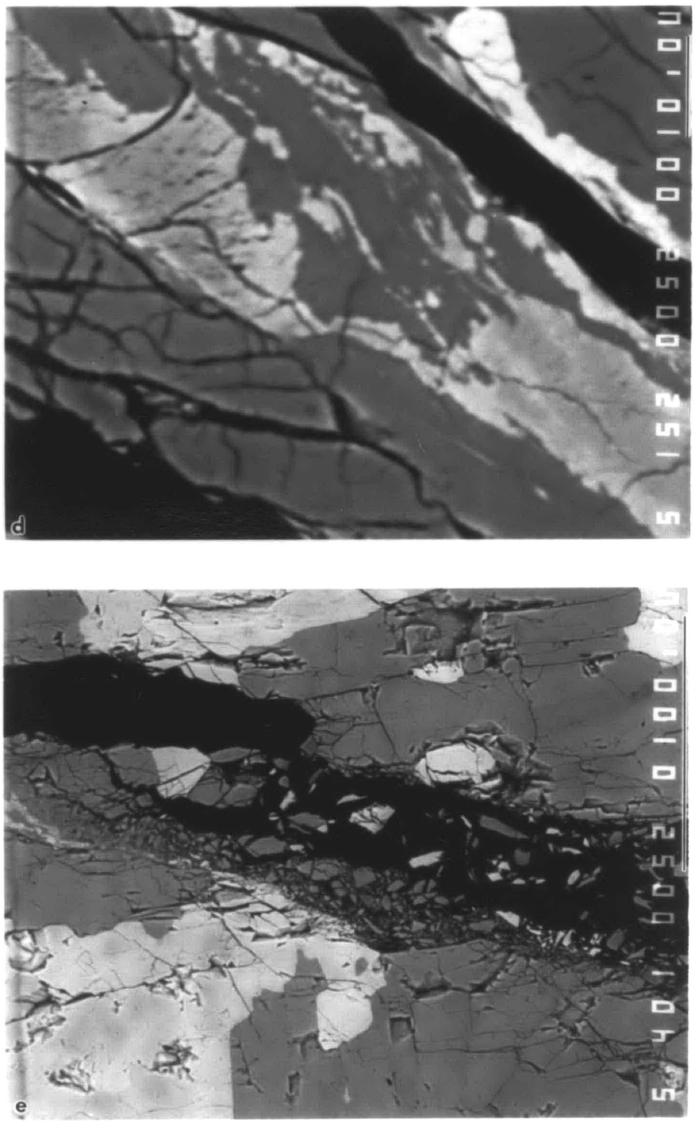

Figure 7d,e

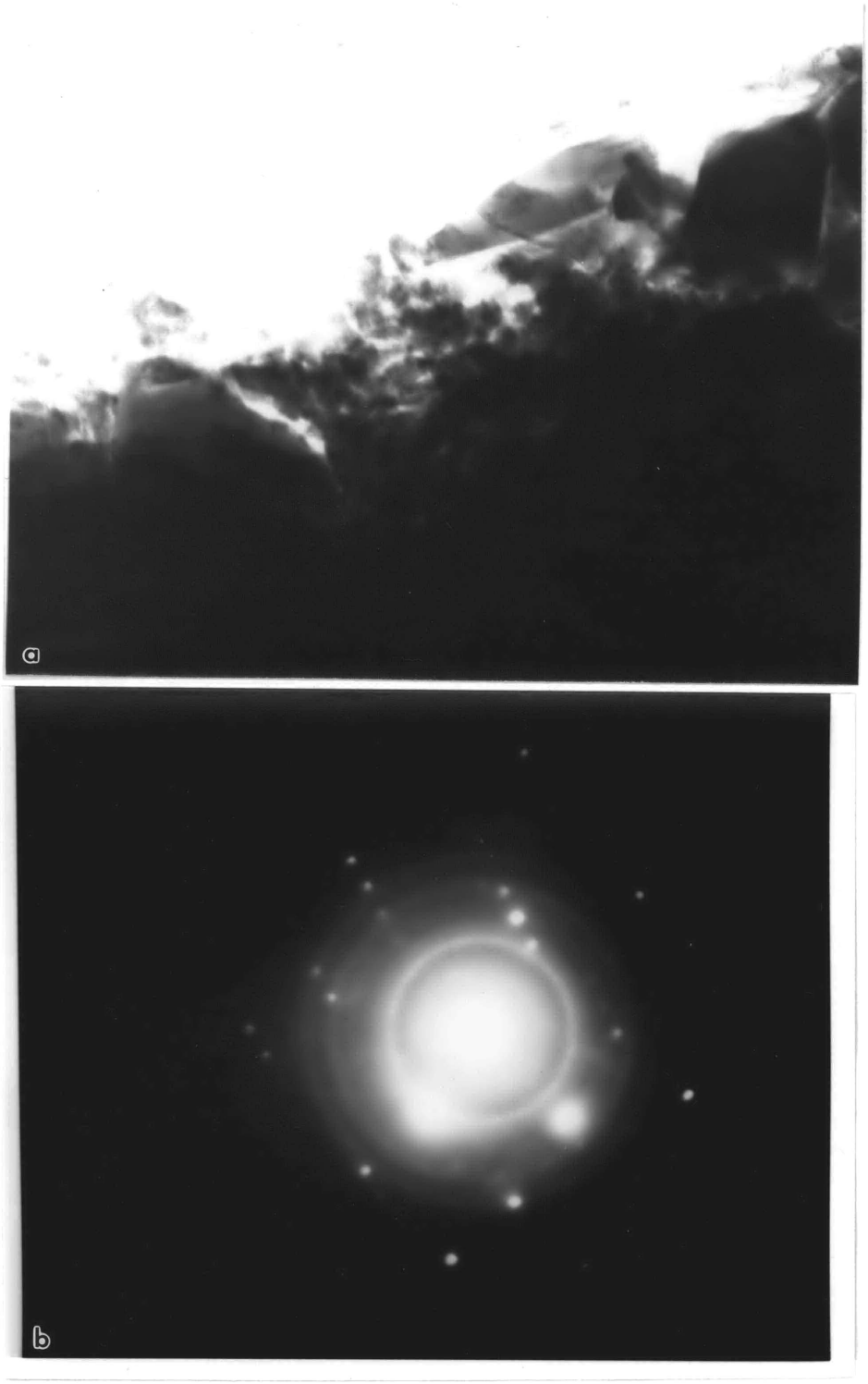

Figure 8*a,b*

Acknowledgements

Financial support for the graduate study which resulted in this thesis was provided by grants from the U.S. Geological Survey (contract 14-08-001-G1340) and National Science Foundation (contract EAR-8905711) to Professor Brian Evans.

I am indebted to Brian Evans for taking me on as a graduate student and for allowing me complete freedom to choose my thesis research. He was an constant source of insight, encouragement, and guidance during the past five years. His interminable optimism and enthusiasm for science have made working in the 7th floor rock mechanics group a pleasure. Special thanks are also owed for his managing to turn me into a runner.

Teng-fong Wong initially sparked my interest in the physical and mechanical properties of rocks. I thank him for his continued support and encouragement during the past five years. My thesis research has benefited considerably from interactions with him.

Much of this thesis benefitted from careful reviews by various individuals prior to publication. Bill Brace and John Logan provided useful comments on Chapter 2. John Rudnicki, Jan Tullis, Dave Kohlstedt, Bill Brace, and Ross Stein contributed thoughtful reviews of Chapter 3. Jan Tullis, Dave Olgaard, and an anonymous JGR reviewer supplied critical comments on Chapter 4.

Many other individuals supplied necessary assistance. Dave Olgaard kindly arranged delivery of a huge block of Carrara marble from Italy; he also supplied the Saillon marble. Mervyn Paterson generously donated the Wombeyan marble. Steve Recca provided vital assistance for the electron microprobe work in Chapter 5. Likewise, discussions with Tom Sisson and Tim Grove helped to ungarble my thoughts on phase stability and partial melting. Dave Kohlstedt kindly made available his unpublished data on Maryland diabase. Reid Cooper contributed some useful suggestions on the diabase experiments.

I thank Steve Hickman, Randy Hay, Yves Bernabe, and Georg Dresen for help and encouragement in the laboratory. Special thanks are due Derek Hirst for consistently turning my vague descriptions into working gadgets, and for always doing his best to repair equipment quickly. Thanks to Steve Recca and Rob McCaffrey for helping to solve various problems with my temperamental IBM PC-AT.

I thank the members of my thesis committee, Bill Brace, Brian Evans, Ted Madden, Jan Tullis, and Teng-fong Wong, for their constructive criticism and comments.

I thank my family, and in particular my mother, for their support and willingness to accept my seemingly permanent student status.

Most of all, I am grateful to my husband, Richard Fagioli, for his love and support during the past five years.